NASA TECHNICAL NOTE

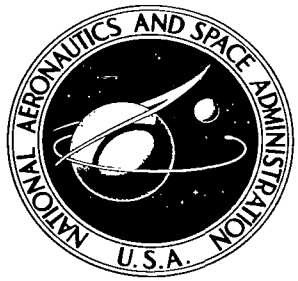

NASA TN D-5913

NASA TN D-5913

FIXED-BASE SIMULATION EVALUATION OF VARIOUS LOW-VISIBILITY LANDING SYSTEMS FOR HELICOPTERS

by Paul S. Rempfer, Lloyd E. Stevenson, and Joseph S. Koziol, Jr.

Electronics Research Center
Cambridge, Mass. 02139

NATIONAL AERONAUTICS AND SPACE ADMINISTRATION • WASHINGTON, D. C. • MARCH 1971

1. Report No.	2. Government Accession No.	3. Recipient's Catalog No.
NASA TN D-5913		

4. Title and Subtitle	5. Report Date
Fixed-Base Simulation Evaluation of Various Low-Visibility Landing Systems for Helicopters	April 1971
	6. Performing Organization Code
7. Author(s) P. Rempfer, L. Stevenson, and J. Koziol, Jr.	8. Performing Organization Report No. C-119
9. Performing Organization Name and Address	10. Work Unit No.
Electronics Research Center Cambridge, Mass.	11. Contract or Grant No. 125-06-10-13-25
	13. Type of Report and Period Covered
12. Sponsoring Agency Name and Address	Technical Note
National Aeronautics and Space Administration	14. Sponsoring Agency Code

15. Supplementary Notes

16. Abstract A fixed-base simulation evaluation of various low-visibility landing systems for helicopters has been made. The low-visibility mission consisted of a straight-in glide slope and localizer approach with a flare and deceleration maneuver at the end. The landing systems consisted of a fully automatic system and six manual systems. The manual systems consisted of three flight control modes each being flown with a flight director indicator and then with raw data displays. The three flight control modes were an attitude command mode with an unaugmented vertical axis, an attitude command mode with rate of descent command in the vertical axis, and a three-axis velocity command mode. The landing systems and the helicopter were simulated on a hybrid computer. The landing systems were all digital. A series of six subjects consisting of two engineers and four instrument-rated pilots flew each of the modes for the landing mission. Performance data were recorded by the digital computer and analog recorders. The relative performances of the modes are presented.

17. Key Words	18. Distribution Statement
.Helicopters .Low-Visibility Landing Systems .All Weather Landing Systems	Unclassified — Unlimited

19. Security Classif. (of this report)	20. Security Classif. (of this page)	21. No. of Pages	22. Price*
Unclassified	Unclassified	118	$3.00

*For sale by the National Technical Information Service, Springfield, Virginia 22151

FIXED-BASE SIMULATION EVALUATION OF VARIOUS LOW-VISIBILITY LANDING SYSTEMS FOR HELICOPTERS

By P.S. Rempfer, L.E. Stevenson, and J.S. Koziol, Jr.
Electronics Research Center

SUMMARY

A fixed-base simulation evaluation of various low-visibility landing systems for helicopters has been made. The low-visibility mission consisted of a straight-in glide slope and localizer approach with a flare and deceleration maneuver at the end. The landing systems consisted of a fully automatic system and six manual systems. The manual systems consisted of three flight control modes each being flown with a flight director indicator and then with raw data displays. The three flight control modes were an attitude command mode with an unaugmented vertical axis, an attitude command mode with rate of descent command in the vertical axis, and a three-axis velocity command mode. The landing systems and the helicopter were simulated on a hybrid computer. The landing systems were all digital. A series of six subjects consisting of two engineers and four instrument-rated pilots flew each of the modes for the landing mission. Performance data was recorded by the digital computer and analog recorders. The relative performance of the modes are presented.

The results indicate that all modes are acceptable for the mission prior to flare and deceleration. When flare and deceleration are considered, the simplest attitude command mode becomes unacceptable both with a flight director indicator and with raw data displayed. This is due primarily to the fact that this mode had no augmentation in the vertical axis and the coupled dynamics between pitch and power became difficult to control through the flare and deceleration maneuver. When augmentation in the vertical axis was added to provide a rate of descent command system with altitude hold capability, the system became acceptable both with the flight director indicator and with raw data displays.

INTRODUCTION

The majority of helicopters flying today do so with no electronic controls or, at most, with limited authority attitude rate stabilizing systems. Although these vehicles demand a high pilot workload they have been very successfully used under VFR conditions and under IFR conditions in cruise flight. Low-speed flight under IFR has been carried out by the military to some degree but it is generally agreed that advanced systems in con-

trols, displays, and navigation aids are required before the full range of IFR helicopter operation can be realized. Recognizing this, research and development of advanced IFR helicopter systems was initiated about ten years ago by the military and civilian agencies in the U.S. and abroad. The approach taken by the different agencies varied, resulting in a variety of control/display systems. For example, Langley Research Center has done work on a variety of displays with attitude rate stabilized vehicles (ref. 1) and on full authority attitude command control with flight director indicator displays (ref. 2). The British Royal Aircraft Establishment has studied flight director display with attitude rate stabilized vehicles (ref. 3). The Air Force Flight Dynamics Laboratory has worked with an attitude command control system with augmentation in the vertical axis to give rate of descent command/attitude hold (ref. 4). The U.S. Army Transportation Research Command is also considering a three-axis translational velocity command control system (ref. 5). Before commercial helicopter operations are able to include low-speed low-visibility missions, one of these types of advocated systems must be selected. The criteria for selection will involve trade-off studies among cost, system reliability, mission reliability, and most certainly system performance.

The objective of this investigation is to present performance data on a number of low-visibility landing systems to be used in making these required trade-off studies. The low-visibility landing mission which was considered is shown in Figure 1. A conventional localizer intercept is made at approximately 800 ft of altitude and the helicopter is decelerated to 42 knots range rate. The glide path is intercepted and followed at 42 knots range rate. At 150 ft of altitude a combined flare and deceleration is made to 50 ft of altitude and 10 knots range rate. This condition is held while tracking the localizer until at 100 ft of range-to-go visual contact is assumed to have occurred.

In order to study a number of landing system concepts, a flexible digital multi-mode landing system was developed. This system allowed the pilot to select any one of a variety of landing systems. These landing systems consisted of a fully automatic system and six manual systems. The manual systems consisted of three flight control modes each being flown with a flight director indicator and then with raw data displays. The three control modes were an attitude command mode with unaugmented vertical axis, an attitude command mode with rate of descent command and a three-axis translational velocity command mode.

The helicopter along with the landing system was simulated on a hybrid computer. The helicopter simulated was the CH-46C helicopter stationed at NASA Langley Research Center. This

vehicle was chosen since it was available for possible flight test of the landing system. The pilot interface was provided with a single seat fixed base cockpit. The digital multi-mode landing system was simulated on the digital portion of the hybrid computer. The functional layout of the simulation is shown in Figure 2.

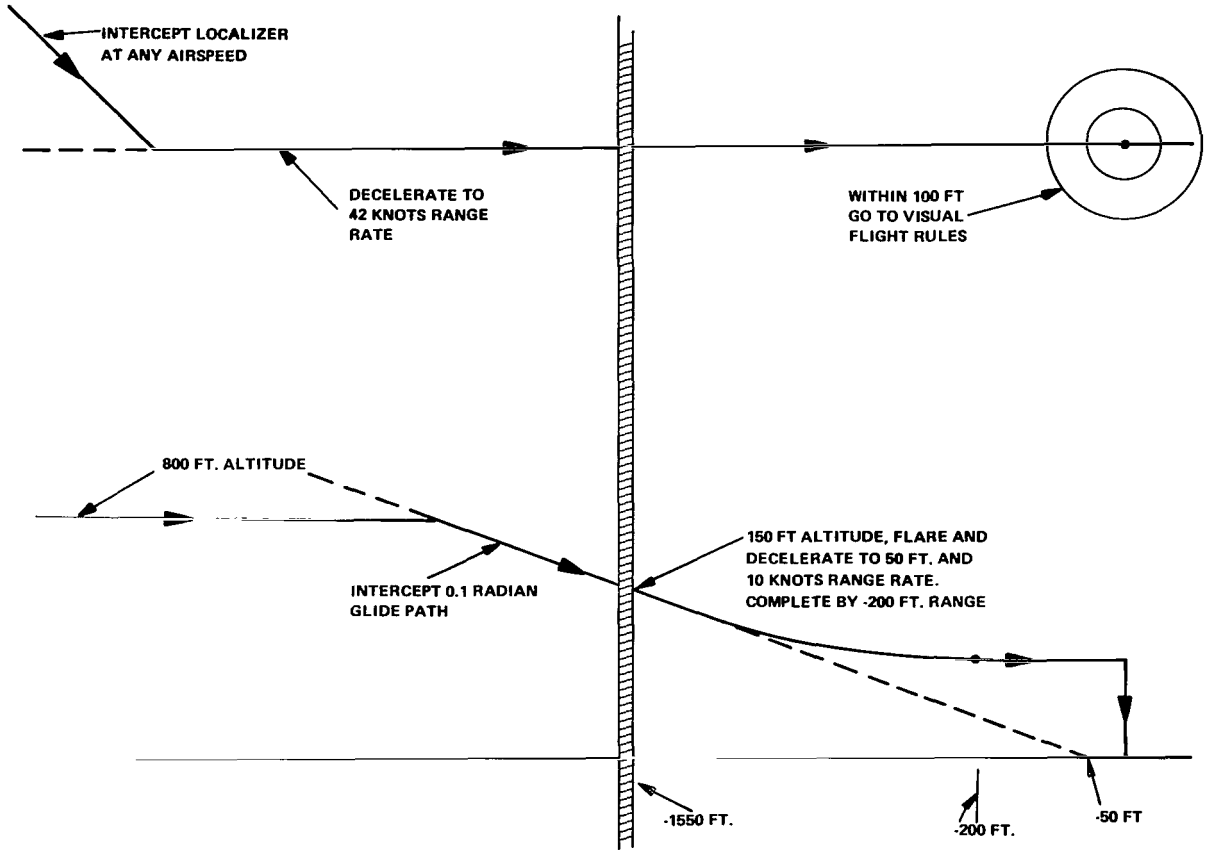

Figure 1.- Mission profile

The fixed-base simulator studies were conducted using both instrument-rated pilots and engineers with simulator experience. The low-visibility mission was flown several times for each landing system by each subject. The resulting data are presented in this report along with some preliminary conclusions.

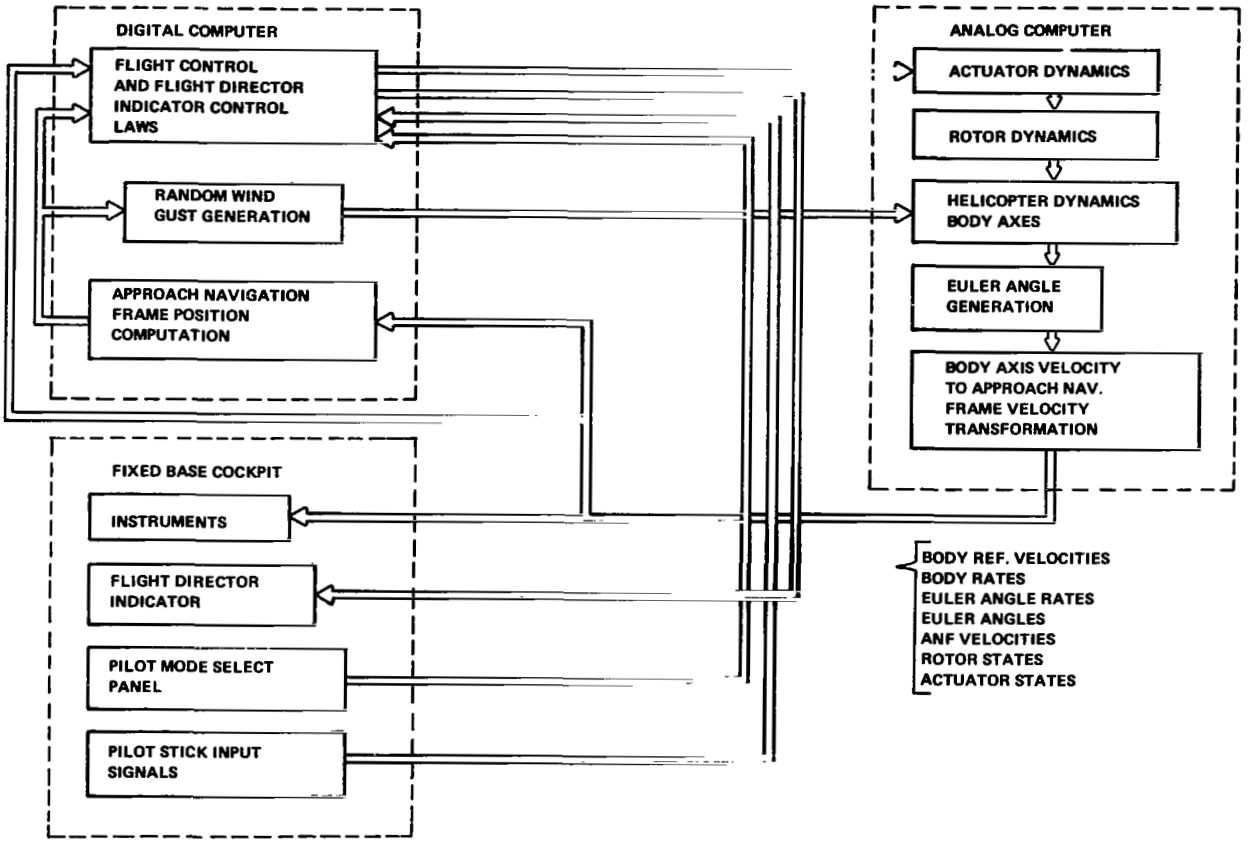

Figure 2.- Hybrid computer simulation

The report is organized such that the reader may get an overview by reading the Introduction, Results, and Conclusions. The details of the low-visibility mission and its selection are presented in the Low-Visibility Mission Section. The details of the multi-mode landing system and a tutorial discussion of its synthesis are presented in the System Description Section. The details of the hybrid simulation are presented in the Simulation Description Section. Finally, the experimental procedures used in making the tests and obtaining the data are detailed in the Experiment Section.

These studies were conducted at the Electronics Research Center in the period March, 1968 to January, 1970. Although the authors were the principal investigators, many people assisted in carrying out the effort. In addition to the NASA employees,

involved in these studies were the following: Messrs. Stanley Driban, Mannie Smith, Jay Haas, and Roger Brown of Service Technology Corporation were responsible for the hybrid programming and cockpit interface throughout the effort; mssrs. Joseph P. Tymczyszyn, Thomas Imrich, graduate students at M.I.T., and John Spencer of Bell Aerosystems acted as test subjects. The authors gratefully acknowledge the assistance of these people without whose help the effort would not have been possible.

SYMBOLS

A_c, A_e, A_a, A_r	Actuator output state in the vertical, pitch, roll, and yaw axes, respectively, inches
DCC, DEC, DAC, DRC	Control system input in the vertical, pitch, roll, and yaw axes, respectively, inches
DCP, DEP, DAP, DRP	Pilot inputs from collective stick, longitudinal center stick motion, lateral center stick motion, and pedals, respectively, inches
DCCBIAS	Reference control input in vertical axis, inches
DCR	Reference collective stick input, inches
DCRO	Reference collective stick input, inches
DER	Reference longitudinal stick input, inches
DERO	Reference longitudinal stick input, inches
DV2	Velocity command limit, ft/sec
DV4	Forward loop gain in altitude loop of guidance, sec^{-1}
DV5	Velocity command rate limit, ft/sec^2
DV10	Forward loop gain in altitude loop of FDI, sec^{-1}
E	Variable in performance index
ENOM	Nominal value of a variable in the performance index
EMAX	Maximum allowable excursion of a variable in the performance index from its nominal value

g	Acceleration of gravity at surface of the earth, ft/sec^2
$G\beta$	Forward loop gain in beta loop of yaw axis, sec^{-1}
$G\Phi$	Forward loop gain in roll loop of roll axis, in/radian
$G\Psi$	Forward loop gain in heading loop of yaw axis, sec^{-1}
GQ	Feedback gain on pitch rate, sec
GR	Forward loop gain in yaw rate loop of yaw axis, in/(radian/sec)
GS	Glide slope angle, radians
$G\Theta$	Forward loop gain in pitch loop of pitch axis, in/radian
GY	Forward loop gain in lateral position loop of roll axis, sec^{-1}
GZ	Forward loop gain for altitude loop of vertical axis, sec^{-1}
$GI\Phi$	Integral-by-pass gain in roll loop of roll axis, sec^{-1}
$GI\Theta$	Integral-by-pass gain in pitch loop of pitch axis, sec^{-1}
GVXI	Integral-by-pass gain in velocity loop of pitch axis, radians/ft
GVX	Forward loop gain in velocity loop of pitch axis, radians/(ft/sec)
GVY	Forward loop gain in velocity loop of roll axis, radians/(ft/sec)
GZD	Forward loop gain in velocity loop of vertical axis, in/(ft/sec)
G_{XA}, G_{YA}, G_{ZA}	Wind gusts along the X, Y, Z, body axes, respectively, ft/sec
GV1	Integral-by-pass gain in altitude loop of guidance, sec^{-1}

GV2	Forward loop gain in altitude loop of guidance, sec^{-1}
GCFR	Roll command to yaw crossfeed in yaw axis, sec^{-1}
GCFΨ	Roll command to yaw crossfeed in yaw axis of automatic mode, sec^{-1}
GLAATT	FDI input gain in roll loop of roll axis, volts/radian
GLOATT	FDI input gain in pitch loop of pitch axis, volts/radian
GVATT	FDI input gain in raw collective loop of vertical axis, volts/in
GVVEL	FDI input gain in velocity loop of vertical axis, volts/(ft/sec)
I_{xx}, I_{yy}, I_{zz}	Moment of inertial about the X, Y, Z, body axes, respectively, slug ft^2
I_{xy}	Product of inertia = $\int xy\ dm$, slug ft^2
J_{xy}	Product of inertia = $-\int xy\ dm$, slug ft^2
L, M, N	Applied moments about the X, Y, Z, body axes, respectively, ft-lbs
m	Mass of the helicopter, slugs
P, Q, R	Angular rate of helicopter along the X, Y, Z, body axes, respectively, radians/sec
RFDI	Range at initiation of deceleration, ft
RFDT	Range at termination of deceleration, ft
S	Laplace transform variable
SΦ	Stick sensitivity in roll loop of roll axis, radians/in
SΨ	Pedal sensitivity in heading loop of yaw axis, (radians/sec)/in
SZD	Collective stick sensitivity in velocity loop of vertical axis, (ft/sec)/in
SVX	Stick sensitivity in velocity loop of pitch axis, (ft/sec)/in

SVY	Stick sensitivity in course loop of roll axis, (radian/sec)/in
$S\Theta$	Stick sensitivity in pitch loop of pitch axis, radian/in
$S\beta$	Pedal sensitivity in beta loop of yaw axis, radian/in
TAS	Airspeed of the helicopter, ft/sec
TAST	Airspeed at which transition from turn coordination to heading hold in yaw axis takes place, ft/sec
$T\beta$	Lag time constant in beta loop of yaw axis, sec
t	Current time in wind noise generation, sec
TAU	Elapsed time since flare initiation, sec
TVZD	Total time of open loop flare, sec
TCFR	Lag time constant on roll command to yaw crossfeed, sec
$TCF\Psi$	Lag time constant in roll command to yaw crossfeed in automatic system, sec
TP	Roll rate feedback gain, sec
U, V, W	Inertial velocity of the helicopter along the X, Y, Z, ft/sec
VXCR	Reference forward velocity in velocity loop of the pitch axis, ft/sec
VXCRO	Reference forward velocity in velocity loop of FDI, ft/sec
VXCI	Velocity command at initiation of deceleration, ft/sec
VXCF	Velocity command at termination of deceleration,ft/sec
V_x, V_y, V_z	Inertial velocity of helicopter along the X, Y, Z, axes of the approach navigation frame, respectively, ft/sec
V_x^h, V_y^h, V_z^h	Inertial velocity of helicopter along the X, Y, Z, axes of the heading vertical frame, respectively, ft/sec
VLAI	FDI input to vertical command bar, volts
VEI	FDI input to vertical tab, volts

VLOI	FDI input to horizontal command bar, volts
VXCO	Initial velocity command in vertical axis for flare, ft/sec
VZGR	Vertical velocity reference in guidance, ft/sec
X, Y, Z	Position of the helicopter in the approach navigation frame when not subscripted, feet. When subscripted, these variables represent the applied forces along the X, Y, Z body axes, respectively, lbs
XFLI	Range at initiation of flare, feet
ZFLT	Altitude at initiation of flare, feet
ZR	Reference altitude in altitude loop of vertical axis, feet
ZRO	Reference altitude in altitude loop of FDI, feet
ZCGS	Glide slope altitude at current range, feet
α_n	Correlation time of noise process
β	Sideslip angle, radians
β_n	Noise process parameter
γ	Locke number
Γ	Noise process variable
δ_c, δ_e, δ_a, δ_r	Rotor output variables in the vertical, pitch, roll and yaw axes, respectively, inches
Δ_n	Noise sequence discretization interval
ζ_a	Actuator model damping ratio
ζ_n	White noise with spectral density of unity
η_n^n	White quassian random sequence with zero mean and unity variance
Ψ, Θ, Φ	Yaw, pitch, and roll Euler angles taken in that order from a local vertical frame to the helicopter body axes, radians
ΘR	Reference pitch attitude, radians

ξ	Course of helicopter, radians
ξR	Reference course of helicopter in course loop of roll axis, radians
Ξ	Noise process variable
ρ_n	Variance of noise process
σ_n	Noise process parameter
σ	Dummy variable of integration
τ	Correlation time
ΨR	Reference heading for heading loop of yaw axis, radians
ω_a	Actuator model natural frequency, rad/sec
Ω	Angular rate of the rotor, rad/sec
Δ ( )	Perturbation of ( )
VAR ( )	Variance of ( )
$\int$ ( )	Integral of ( )
Σ ( )	Summation of ( )
$\lvert$ ( ) $\rvert$	Absolute value of ( )
E ( )	Expected value of ( )
$\frac{d\ (\ )}{dt(\ )}$	Total time derivative of ( )
$\frac{\partial\ (*)}{\partial\ (\ )}$	Partial derivative of (*) with respect to ( )
$(\dot{\ })$	Total time derivative of ( )

Subscripts

p, q, r, u, v, w, δ	subscripts on X, Y, Z,; L, M, N, denote the partial derivative of the aerodynamic force of moment with respect to P, Q, R, U, V, W, δ_c, δ_e, δ_a, or δ_r, respectively. (i.e., stability and control derivatives).

A	subscript on X, Y, Z, denotes the force is due only to aerodynamics
TR	denotes the variable is a trim value in steady level flight
COM	denotes the variable is a command input
IC	denotes initial value or condition
AS	denotes velocity with respect to air mass rather than inertial

Axis Systems

Body Frame.- Origin is fixed as the normal center of gravity of the helicopter; X-axis is directed forward out the nose of the helicopter, and parallel to the water line; Z-axis is directed downward and perpendicular to the water line; Y-axis completes the orthogonal triad.

Approach Navigation Frame.- Origin is fixed at the runway touchdown point; X-axis is horizontal and directed in the direction of travel for an approach; Z-axis is vertical and directed downward; Y-axis completes the orthogonal triad.

Vertical Heading Frame.- Origin is fixed at the normal center of gravity of the helicopter; X-axis is the orthogonal projection of the body X-axis onto the local horizontal plane; Z-axis is vertical and directed downward; Y-axis completes the orthogonal triad.

LOW-VISIBILITY MISSION

The low-visibility mission which was considered consists of a straight-in approach and landing. The mission profile appears in Figure 1. The mission assumes visual contact with the desired touchdown point will occur before 100 ft of range-to-go at 50 ft of altitude. With landing lights available, this is virtually a zero visibility condition. A conventional localizer intercept is made at 800-ft of altitude. A 0.1 radian (6-degree) glide path is intercepted and tracked at 42-knots range rate. At 150 ft of altitude, a flare and deceleration maneuver is made to 50 ft altitude and 10 knots range rate. This condition is held with localizer track until visual contact is made.

This mission is conservative in that it is a simple extension of current fixed wing aircraft IFR operation. It requires

approximately 1500 ft of range without obstructions protruding above the height of the desired touchdown point. Such a mission could be flown into ports over a body of water, to the roofs of high buildings or, possibly, to ports built over freeways with the approach made along the freeway. Depending on the exact nature of the mission, either ILS-type equipment or approach radar could be used. Since the ILS-type equipment is the most constraining, it was chosen as the basic approach navigation source for this study. The profiles generated are compatible with a radar source of information.

The parameters of the mission trajectory were selected with the following considerations:

(a) A glide path of 0.1 radian was used based upon the material presented in reference 6. The glide path source is located 50 ft in front of the desired touchdown point so that the aircraft will fly over the source making it available for the next aircraft. During the simulation, the conventional fixed wing glide path sensitivity of ± .5 degrees full-scale was found to be too sensitive for this mission. A sensitivity of ± 2.0 degrees full-scale was found by experiment to be acceptable to within 1500 ft of range.

(b) The range rate along the glide path is 42 knots so that the aircraft will not exceed the 500 to 700 fpm rate of descent limit sited in reference 7. This range rate is also in keeping with the more recent studies of reference 2.

(c) The flare and deceleration are initiated at 150 ft of altitude. This altitude was selected based upon a tradeoff between the following:

(1) Hold maximum range rate as long as possible to get down quickly,

(2) Keep the range over which a radar altimeter might have to be used to a minimum,

(3) Stay within the 0.15-g deceleration limit recommended in reference 8.

(4) Keep any dipping below the desired final altitude to a minimum.

(d) The final altitude is 50 ft which is consistent with reference 2. This altitude might have to be adjusted for operational use.

(e) The final range rate was chosen at 10 knots. This is a modest rate from which visual takeover at 100 ft of range could be smoothly accomplished.

(f) The glide slope intercept altitude is 800 ft. This corresponds to a range of 8050 ft. From intercept to flare initiation is 6500 ft. At 42 knots, this gives the pilot just over the 1.5 minutes recommended in reference 6 to stabilize on the glide path before flare.

(g) The localizer source is located 1000 ft down range. During the simulation, the conventional fixed wing localizer sensitivity of ± 2.5 degrees full-scale was also found to be too sensitive for this mission. A sensitivity of ± 5.0 degrees full-scale was found by experiment to be acceptable. The combination of the resultant localizer sensitivity with the location of the localizer source gave full scale over the desired touchdown point of ± 100 ft assuring a pilot on scale of visual contact. At 10,000 ft-range, the localizer behaves very much like a standard ± 2.5-degree sensitivity localizer at the far end of a 10,000-ft runway.

(h) The range and range rate source are located with the localizer for convenience.

SYSTEM DESCRIPTION

In this section, the digital multi-mode landing system modes are defined; the block diagrams and gain values for each mode are presented, and the flight control system synthesis based upon linear analysis and simulation is shown. The flight director laws were synthesized with reference to the automatic mode.

Mode Definition

The digital flight control system was comprised of four flight control (FC) modes and three associated flight director indicator (FDI) modes. Each FC mode was a four-axis system controlling differential collective rotor pitch (DEC) for pitching moment, collective rotor pitch (DCC) for lift, lateral cyclic rotor pitch (DAC) for rolling moment, and lateral differential cyclic rotor pitch (DRC) for yawing moment. The DRC input is analagous to rudder input in fixed wing aircraft. Electro-hydraulic actuators of an Electric Input Servo System (EISS) served to force the required control linkages. Each FC mode

accepted four axes of pilot input. Each input device produced an electric signal and had artificial force feel. The inputs were longitudinal motion of center stick (DEP) normally to DEC, lateral motion of center stick (DAP) normally to DAC, pedal motion (DRP) normally to DRC, and collective stick motion (DCP) normally to DCC. The yaw axis for the FC modes varied with airspeed having a low-speed characteristic and a high-speed characteristic.

The FDI is shown in Figure 3. Each FDI mode was a three-axis system addressing the horizontal command bar (VLOI) for pitching motion commands, the vertical "tab" (VEI) for lift commands and the vertical command bar (VLAI) for rolling motion commands.

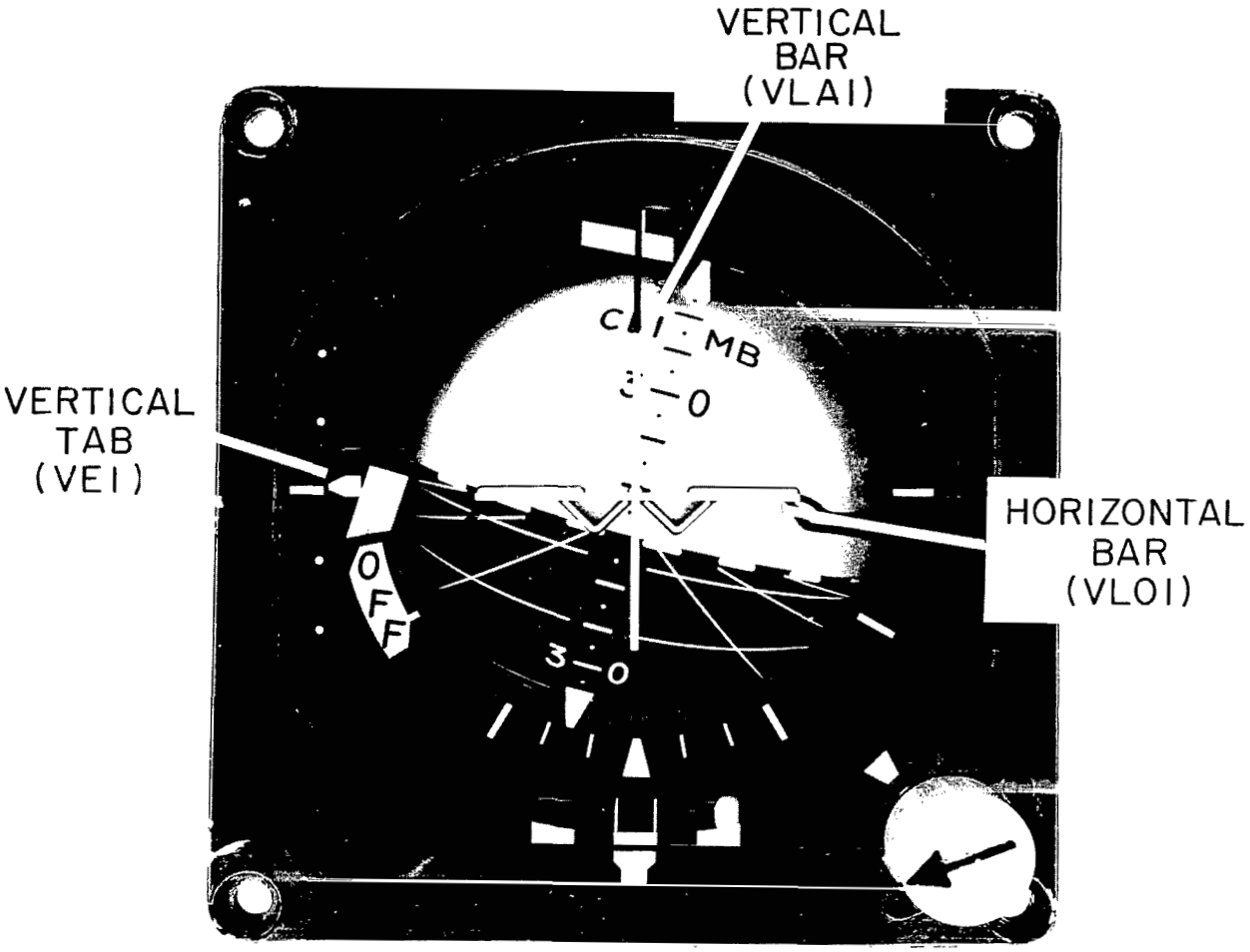

Figure 3.- Flight director indicator

The sense of the FDI commands, the pilot inputs, and EISS inputs are defined in the following tables.

PILOT INPUTS

DCP gradient is positive for stick down

DEP gradient is positive for stick back

DRP gradient is positive for right pedal in

DAP gradient is positive for stick right

EISS INPUTS

DCC positive gives an upward acceleration

DEC positive gives a pitch up acceleration

DRC positive gives a yaw right acceleration

DAC positive gives a roll right acceleration

FDI INPUTS

VEI positive moves the vertical tab down

VLOI positive moves horizontal bar down

VLAI positive moves vertical bar right

A definition of each of the FC modes and associated FDI modes follows, along with their block diagrams. These definitions were arrived at by considering the complexity of the sensors and computations which would be required to implement each mode in operation. Hypothesized sensors for each mode are presented in Appendix A.

In each manual mode, the pilots' command inputs from the center sticks and the pedals are passed through a dead zone to eliminate small amplitude noise and bias inputs. The dead-zone transfer function is shown in Figure 4. It is essentially a unity pass transfer function with threshold. It should be noted that added variables have been introduced into the various modes and given values when the particular mode is first entered. These references are implemented to prevent system transients when the

desired mode is initially entered or changed. Finally, in each of the flight control modes and flight director modes all integrators are initially set to zero when the particular mode is first entered.

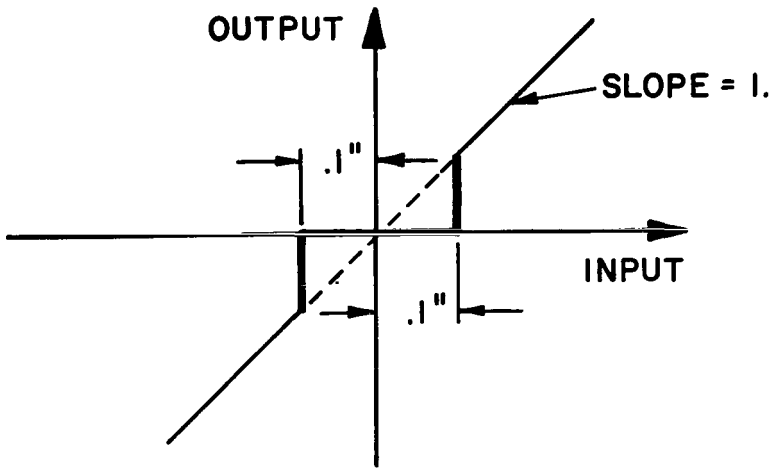

Figure 4.- Dead zone transfer function

Attitude Command Mode I.- This mode is basically an attitude command mode in roll and in pitch. The vertical axis is unaugmented and the rudder axis is a sideslip command system at high airspeeds and a heading rate command system at low airspeeds. The block diagrams are given in Figures 5 – 11. A precise definition of the control and FDI inputs follows.

DEP input is interpreted as a pitch attitude command. The helicopter responds by adopting and holding a pitch attitude proportional to the DEP input.

DAP input is interpreted as a roll attitude command. The helicopter responds by adopting and holding a roll attitude proportional to the DAP input.

DCP input is interpreted as a raw collective rotor pitch input. The helicopter is not augmented in this axis.

DRP input interpretation varies with airspeed. At low airspeeds the input is interpreted as a heading rate command. The helicopter responds by tracking a

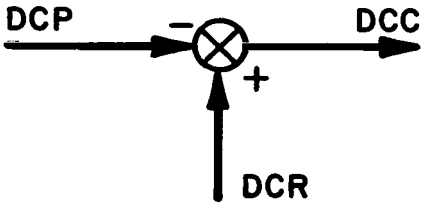

DCR = (DCP + DCC)(AT MODE ENGAGE)

Figure 5.- Vertical axis of Attitude Command Mode I

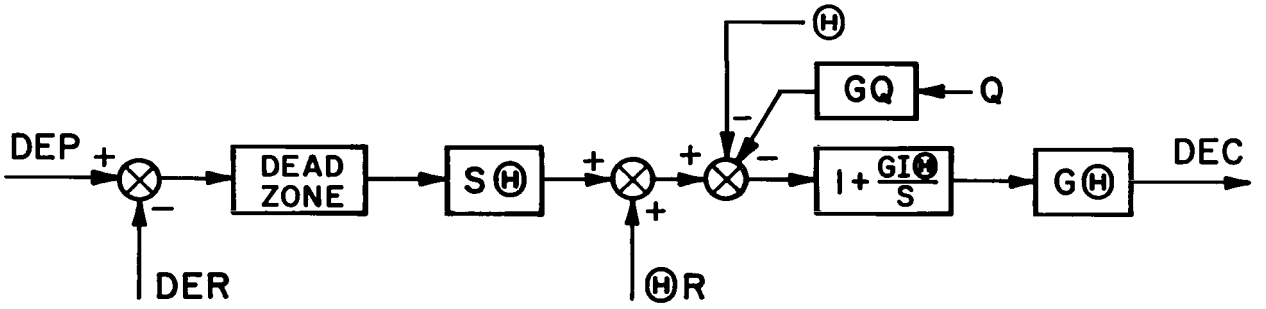

ⓗⒽR = (ⓗⒽ + DEC/GⓗⒽ)(AT MODE ENGAGE)

DER = DEP (AT MODE ENGAGE)

GQ = 0.5 SEC.

GⓗⒽ = 20. IN/RADIAN

GIⓗⒽ = 0.2 SEC.$^{-1}$

SⓗⒽ = 0.1 RADIAN/IN

Figure 6.- Pitch axis of Attitude Command Mode I

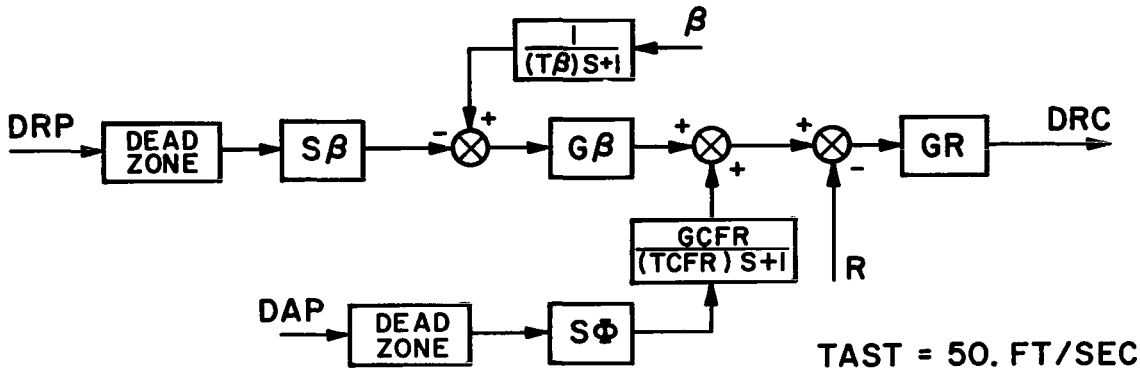

TAST = 50. FT/SEC
Tβ = 0.5 SEC
Sβ = -0.2 RAD/IN
Gβ = 0.3 SEC^{-1}
SΦ = 0.1 RAD/IN
GCFR = 0.3 SEC^{-1}
TCFR = 0.5 SEC
GR = 15. IN/(RAD/SEC)

Figure 7a.- Yaw axis of Attitude Command Mode I (TAS ≥ TAST)

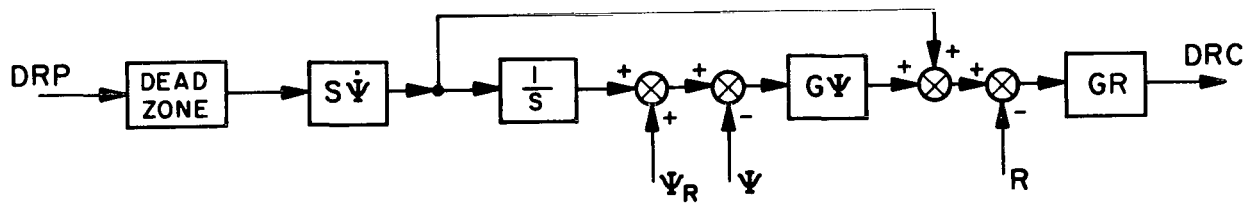

$\Psi_R = \Psi$ (AT MODE ENGAGE)

SΨ̇ = 0.2 (RAD/SEC)/IN
GΨ = 1.0 SEC^{-1}
GR = 15. IN/(RAD/SEC)
TAST = 50. FT/SEC

Figure 7b.- Yaw axis of Attitude Command Mode I (TAS < TAST)

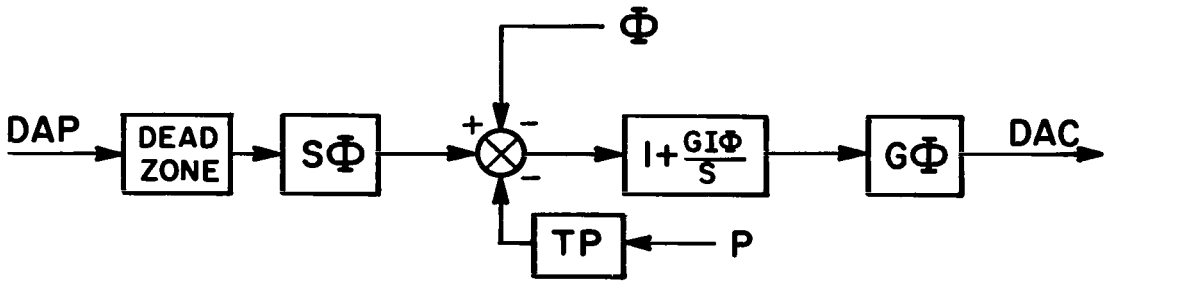

SΦ = 0.1 RAD/IN
TP = 0.5 SEC
GIΦ = 0.35 SEC^{-1}
GΦ = 15. IN/RAD

Figure 8.- Roll axis of Attitude Command Mode I

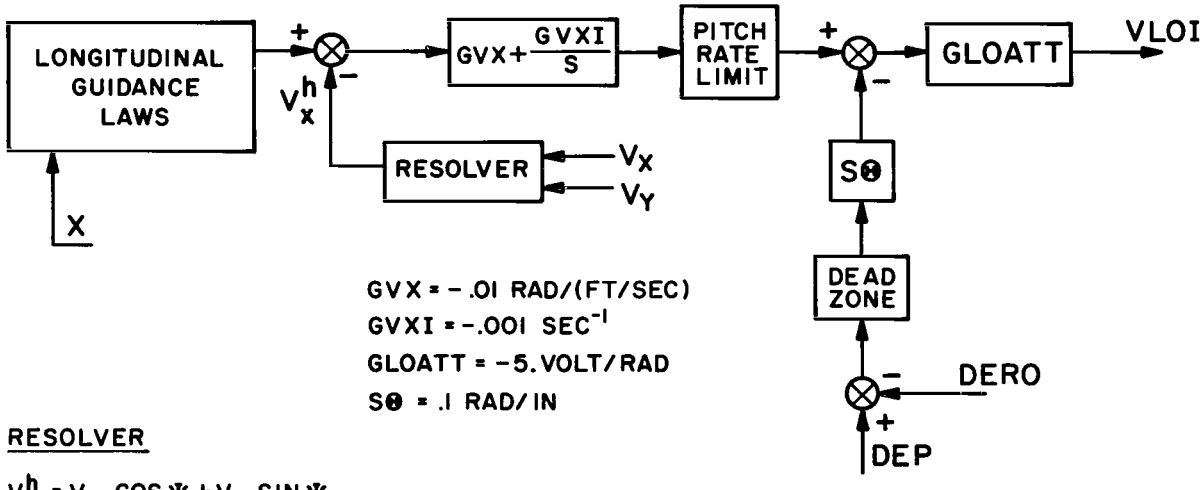

GVX = −.01 RAD/(FT/SEC)
GVXI = −.001 SEC^{-1}
GLOATT = −5. VOLT/RAD
SΘ = .1 RAD/IN

RESOLVER

$V_x^h = V_x \cos\Psi + V_y \sin\Psi$

DERO = DEP (AT MODE ENGAGE)
PITCH RATE LIMIT = ±0.1 RAD/SEC
VLOI FULL SCALE = ±2.6 VOLTS

Figure 9.- VLOI/FDI axis of Attitude Command Mode I

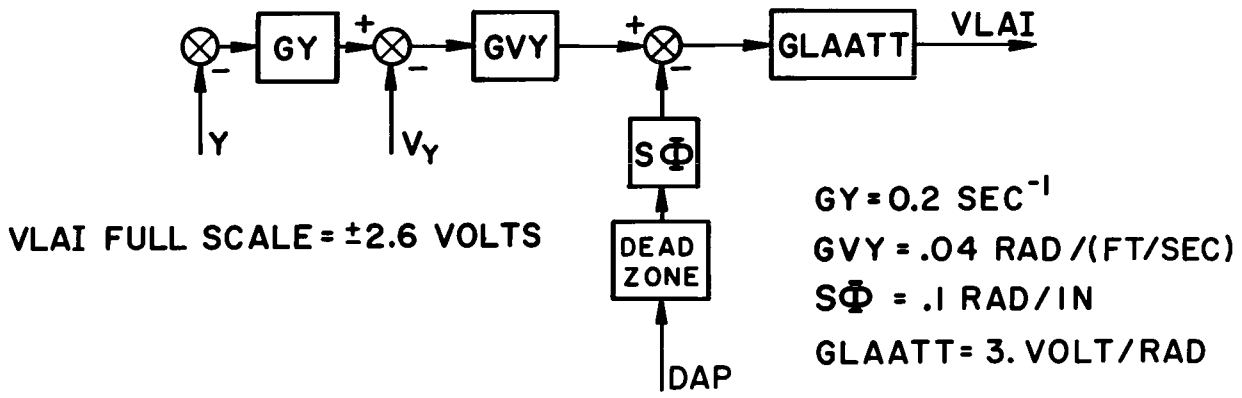

Figure 10.- VLAI/FDI axis of Attitude Command Mode I

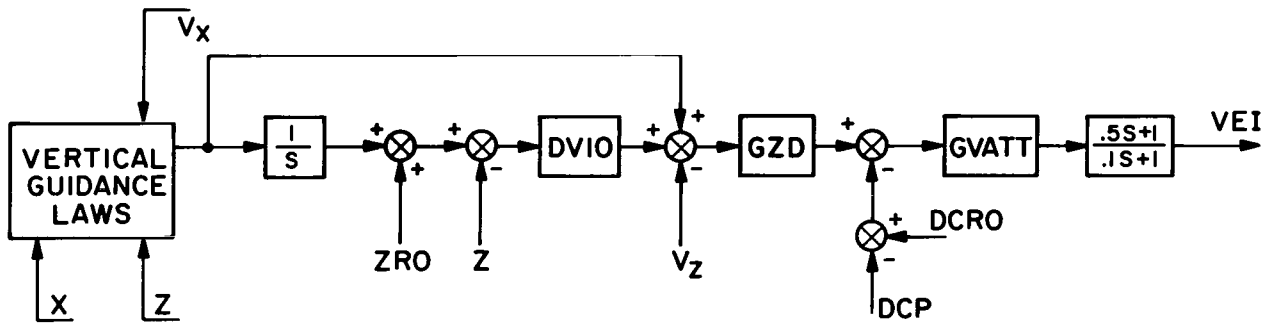

ZRO = Z (AT MODE ENGAGE)
DCRO = DCP (AT MODE ENGAGE)

VEI FULL SCALE = ±16.VOLTS

DVIO = 0.3 SEC^{-1}
GZD = -0.2 IN/(FT/SEC)
GVATT = -5. VOLT/IN

Figure 11.- VEI/FDI axis of Attitude Command Mode I

heading rate proportional to the DRP input. Zero input is heading hold. At high airspeed, the input is interpreted as a sideslip command. The helicopter responds by adopting and holding a sideslip angle proportional to the DRP input. Zero input provides for a coordinated turn. The airspeed value separating low and high speed is called the transition airspeed (TAST).

VLOI — output represents the error between the pitch attitude desired by the landing system outer loops and the current pilot-commanded pitch attitude.

VLAI — output represents the error between the roll attitude desired by the landing system outer loops and the current pilot-commanded roll attitude.

VEI — output represents the error between the collective rotor pitch desired by the landing system outer loops and the current pilot-commanded collective rotor pitch.

Attitude Command Mode II.- This mode is similar to the Attitude Command Mode I except that the vertical axis is a rate of descent command system with altitude hold capability. The block diagrams for the vertical axis are given in Figures 12 and 13. A precise definition of the control and FDI inputs for the vertical axis follows.

DCP — input is interpreted as a rate of descent command. The helicopter adopts and holds a rate of descent proportional to the DCP input. Zero input provides an altitude hold.

VEI — output represents the error between the rate of descent desired by the landing system outer loops and the current pilot-commanded rate of descent.

Velocity Command Mode.- In this mode the pilot controls his translational velocity with respect to the ground. The vertical axis and rudder axis are the same as in Attitude Command Mode II. Forward displacement of the center stick results in rate of change of the helicopters forward velocity. Lateral displacement of the center stick results in a rate of change of the helicopter's course along the ground. Due to the nature of the rudder axis this course change is accomplished with a coordinated turn at high airspeed and a sideslip maneuver at low airspeed. The block diagrams required by this mode are presented in Figures 14 to 17.

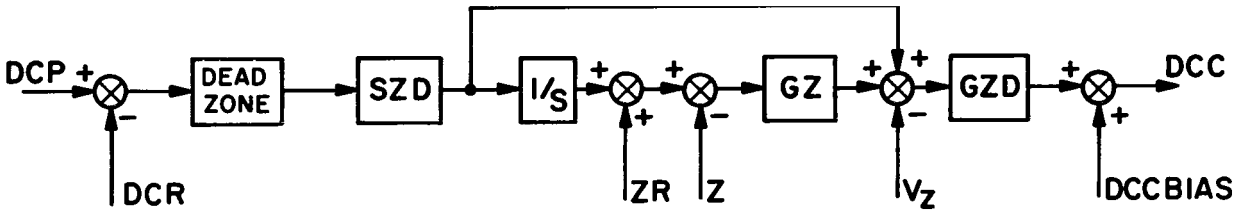

SZD = 8.(FT/SEC)/IN
GZ = 1.3 SEC^{-1}
GZD = -.2 IN/(FT/SEC)

DCCBIAS = DCC (AT MODE ENGAGE)

ZR = Z (AT MODE ENGAGE)

DCR = (DCP - V_Z/SZD) (AT MODE ENGAGE)

OUTPUT OF THE ALTITUDE INTEGRATOR RESET TO -150. FT AT FLARE INITIATION

Figure 12.- Vertical axis of Attitude Command Mode II

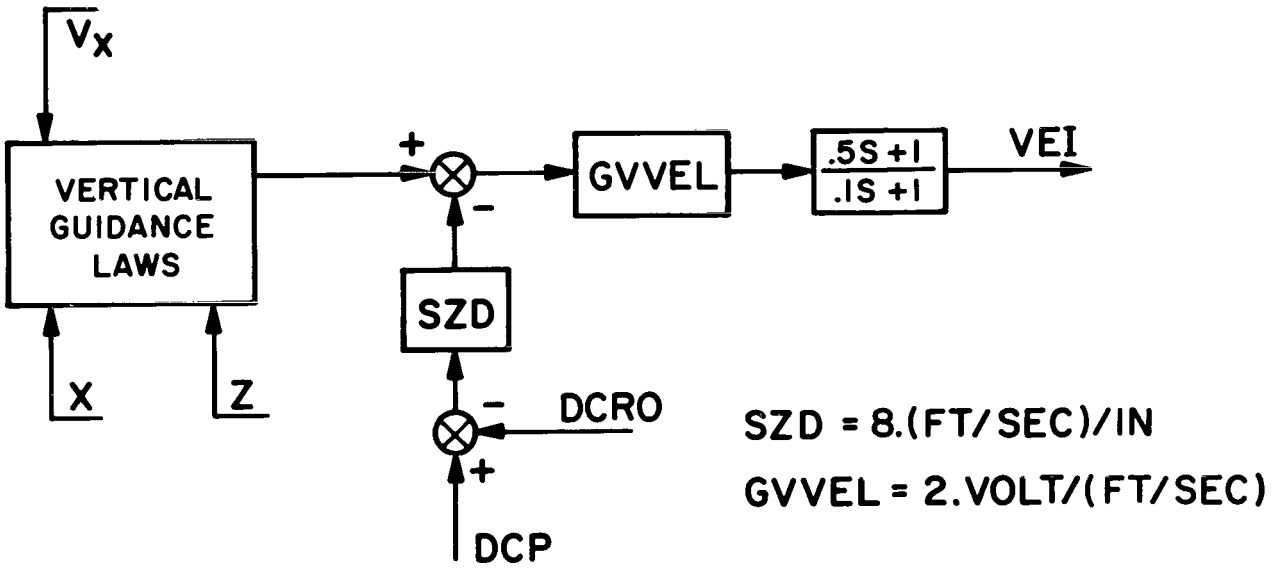

DCRO = (DCP - VZ/SZD) (AT MODE ENGAGE)

VEI FULL SCALE = ±16.VOLTS

Figure 13.- VEI/FDI axis of Attitude Command Mode II

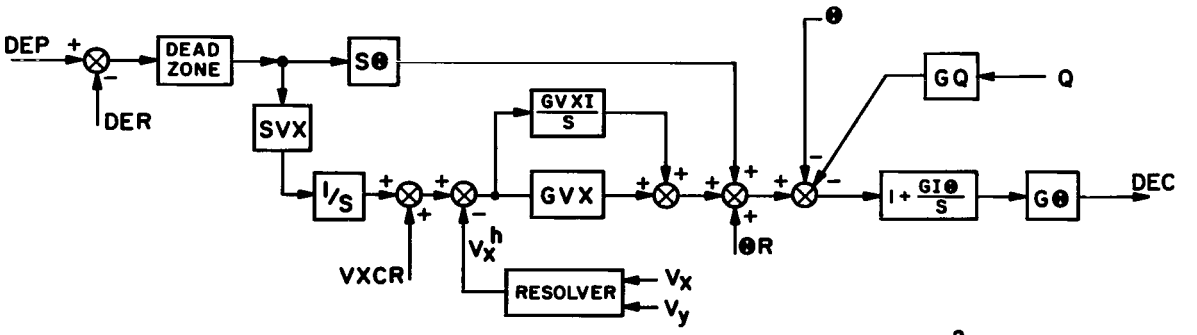

VXCR = $(V_X \cos\Psi + V_Y \sin\Psi)$ (AT MODE ENGAGE)
DER = DEP (AT MODE ENGAGE)
ΘR = (Θ + DEC/GΘ) (AT MODE ENGAGE)

RESOLVER:

$V_X^h = V_X \cos\Psi + V_Y \sin\Psi$

SVX = −3.0 (FT/SEC^2)/IN
GVX = −.01 RAD/(FT/SEC)
GVXI = −.001 SEC^{-1}
GQ = 0.5 SEC
GΘ = 20. IN/RAD
GIΘ = 0.2 SEC^{-1}
SΘ = 0.1 RAD/IN

Figure 14.- Pitch axis of Velocity Command Mode

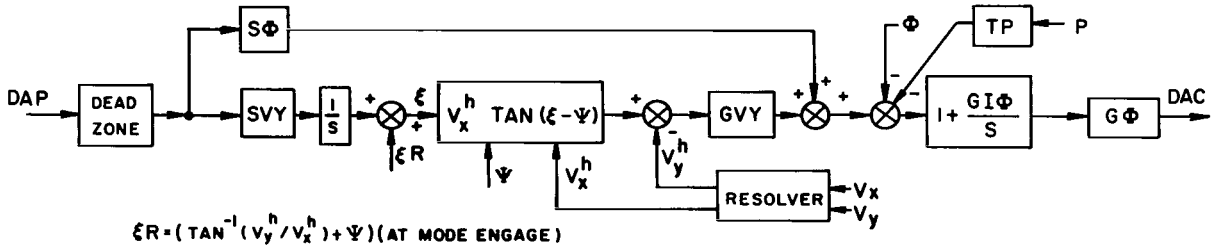

ξR = $(\tan^{-1}(V_y^h/V_x^h) + \Psi)$ (AT MODE ENGAGE)

$$SVY = \begin{cases} .04\ \frac{RAD/SEC}{IN} & ; V_x^h \geq 70.\ FT/SEC \\ .0133\ (2. + 70./V_x^h)\ \frac{RAD/SEC}{IN} & ; 10.FT/SEC < V_x^h < 70.FT/SEC \\ 0.\ \frac{RAD/SEC}{IN} & ; V_x^h \leq 10.\ FT/SEC \end{cases}$$

RESOLVER:

$V_x^h = (V_x \cos\Psi + V_y \sin\Psi)$

$V_y^h = (V_y \cos\Psi - V_x \sin\Psi)$

SΦ = 0.1 RAD/IN
GVY = .04 RAD/(FT/SEC)
TP = 0.5 SEC
GIΦ = 0.35 SEC^{-1}
GΦ = 15.0 IN/RAD

Figure 15.- Roll axis of Velocity Command Mode

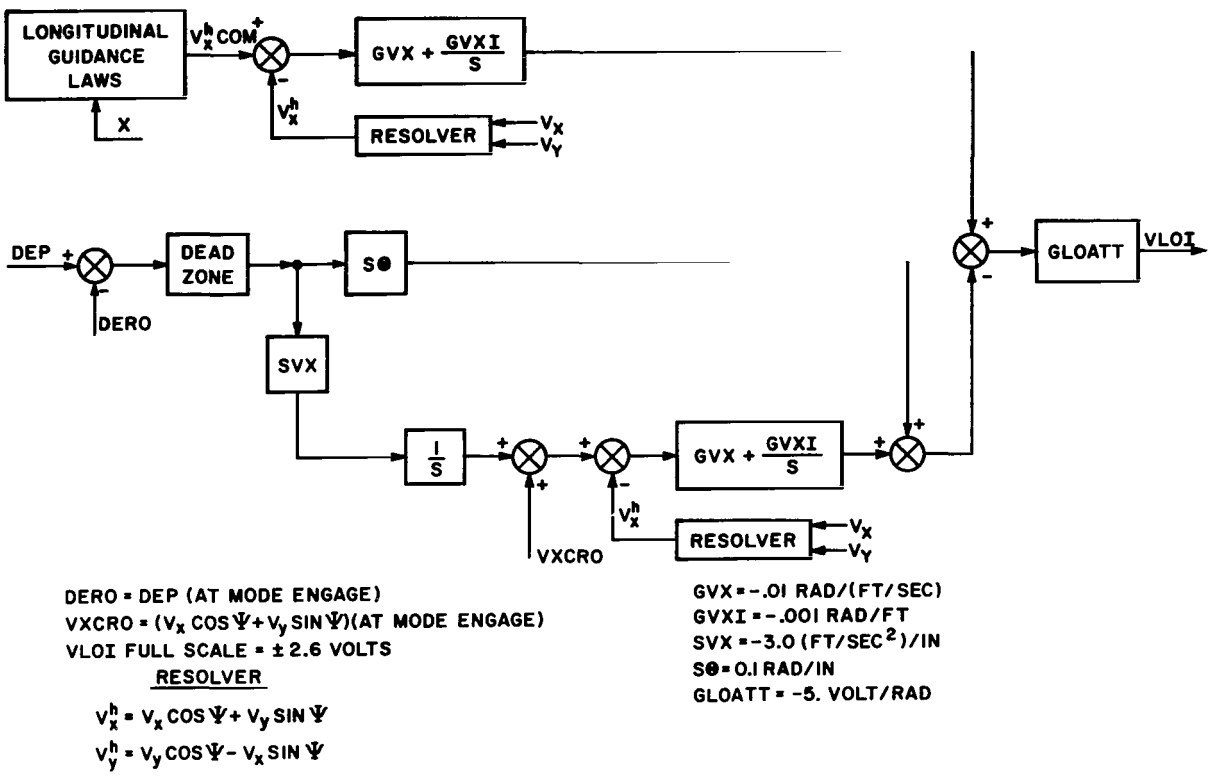

Figure 16.- VLOI/FDI axis of Velocity Command Mode

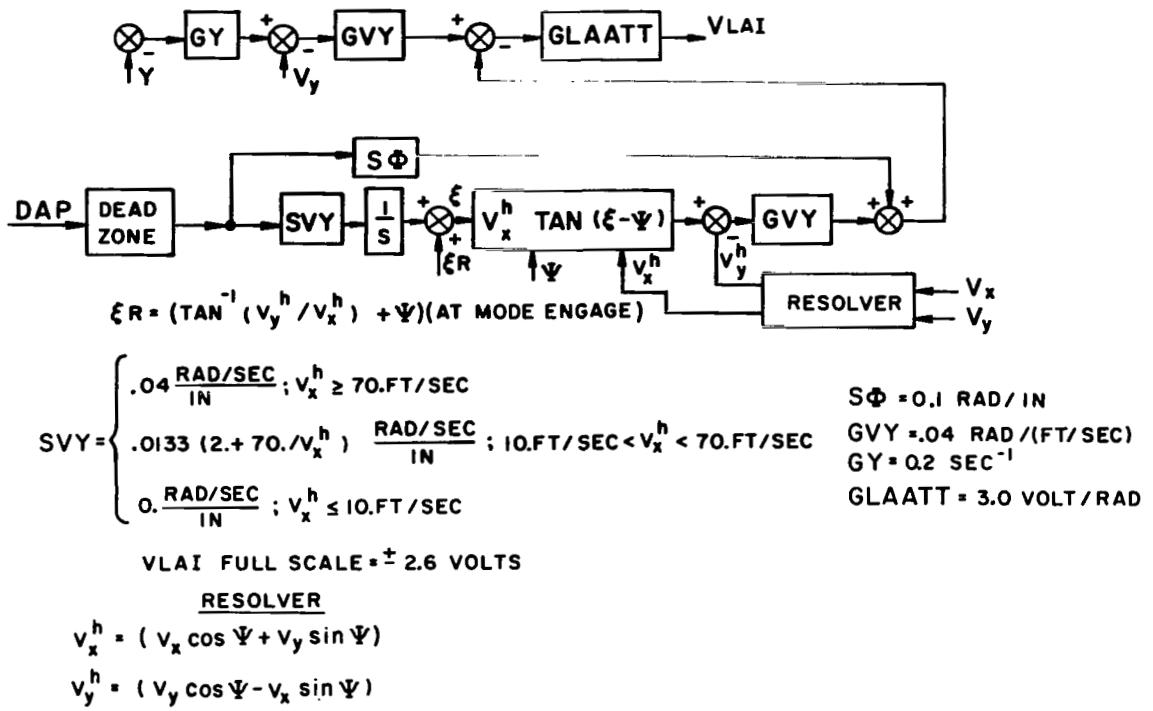

Figure 17.- VLAI/FDI axis of Velocity Command Mode

A precise definition of the control and FDI inputs for this mode follows.

DEP — input is interpreted as a rate of change command on the longitudinal translational velocity of the aircraft along the X-axis of the vertical heading axis system. The helicopter responds to the input by adopting and holding a rate of change of this velocity proportional to the DEP input. Zero input is a velocity hold.

DAP — input is interpreted as an angular rate of change command on the course of the aircraft. The helicopter responds to the input by adopting and holding a rate of change of course proportional to the DAP input. Zero input is a course hold.

VLOI — output represents the error between the pitch attitude desired by the landing system outer loops and the pitch attitude currently being commanded by the longitudinal velocity rate command system.

VLAI output represents the error between the roll attitude desired by the landing system outer loops and the roll attitude currently being commanded by the course rate command system.

Automatic Mode.- The automatic mode does not accept pilot command signals. The FDI is inoperative with the pilot monitoring the mission with raw data displayed via conventional instruments. The instrument panel layout is shown in Figure 18. The block diagrams are presented in Figures 19 to 22. The longitudinal and vertical guidance laws required by this mode and the FDI modes are presented in Figures 23 and 24.

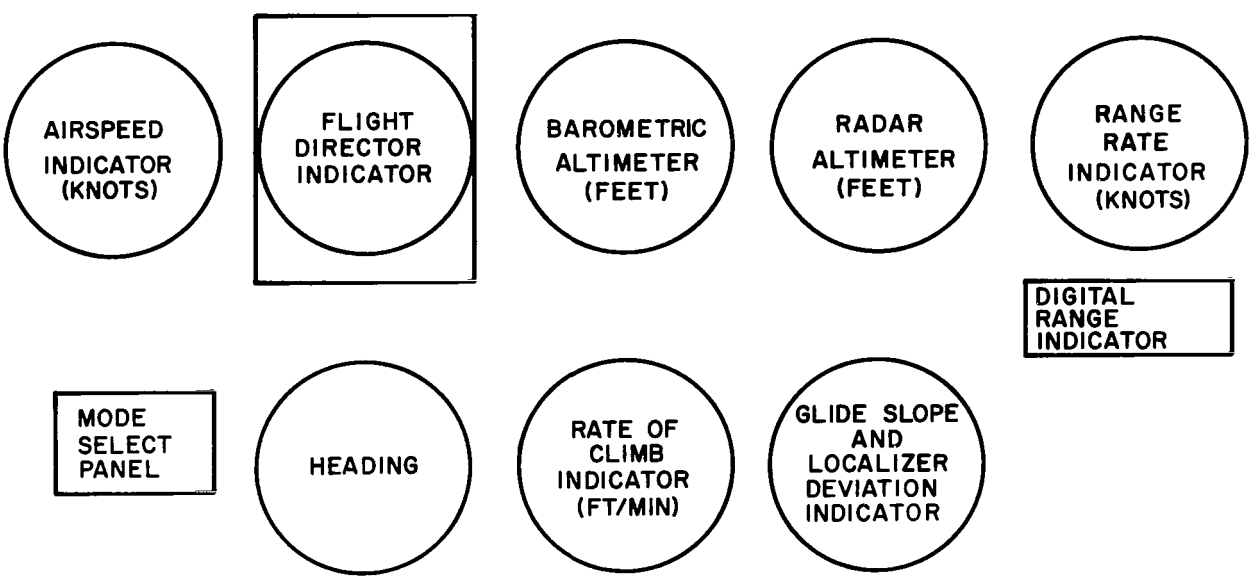

Figure 18.- Instrument panel layout

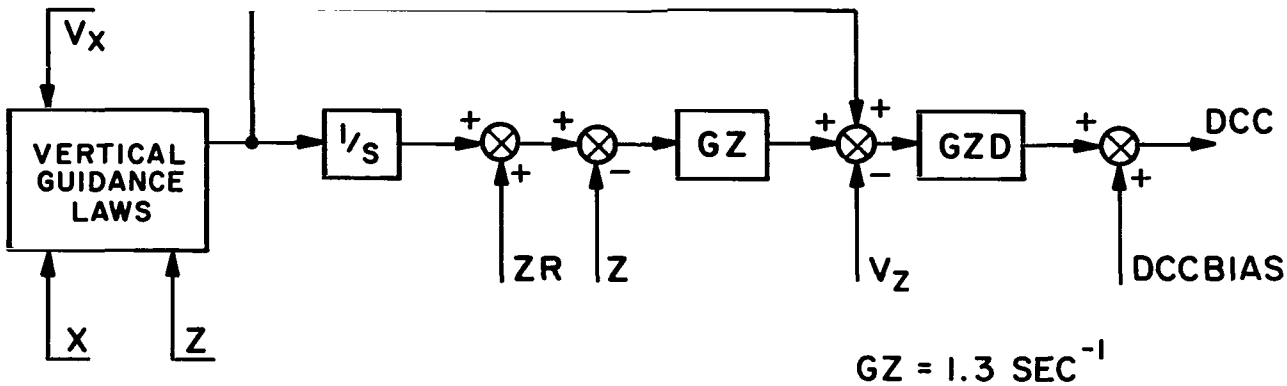

$GZ = 1.3\ SEC^{-1}$

$GZD = -.2\ IN/(FT/SEC)$

$ZR = Z$ (AT MODE ENGAGE)

$DCCBIAS = (DCC + (GZD)\,V_Z)$ (AT MODE ENGAGE)

Figure 19.- Vertical axis of Automatic Mode

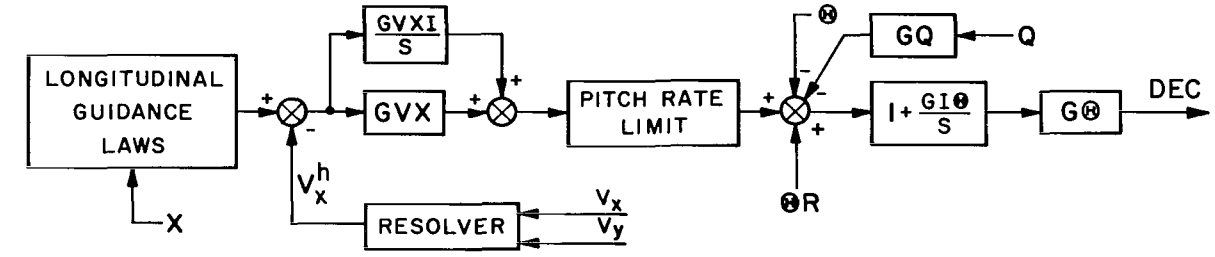

GVX = -.01 RAD/(FT/SEC)

GVXI = -.001 RAD/FT

GQ = 0.5 SEC

GΘ = 20. IN/RAD

$GI\Theta = 0.2\ SEC^{-1}$

RESOLVER:

$V_x^h = V_x \cos\Psi + V_y \sin\Psi$

PITCH RATE LIMIT = ±0.1 RAD/SEC

$\Theta R = (\Theta + DEC/G\Theta)$ (AT MODE ENGAGE)

Figure 20.- Pitch axis of Automatic Mode

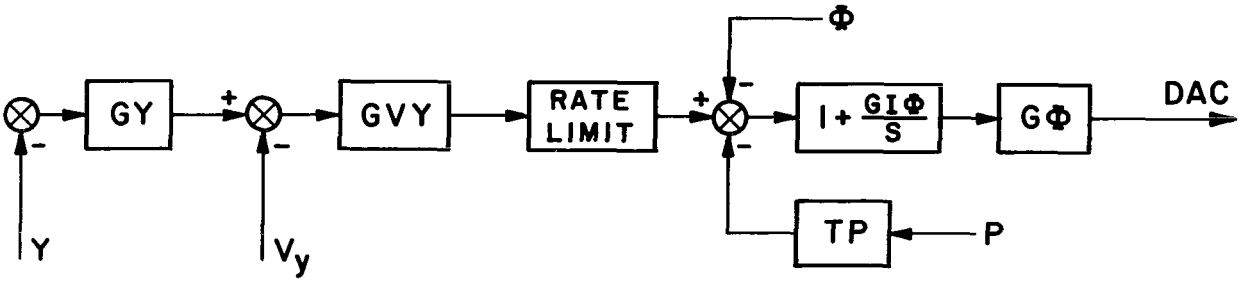

ROLL RATE LIMIT = ±0.5 RAD/SEC

GY = 0.2 SEC^{-1}
GVY = 0.04 RAD/(FT/SEC)
TP = 0.5 SEC
GIΦ = 0.35 SEC^{-1}
GΦ = 15. IN/RAD

Figure 21.- Roll axis of Automatic Mode

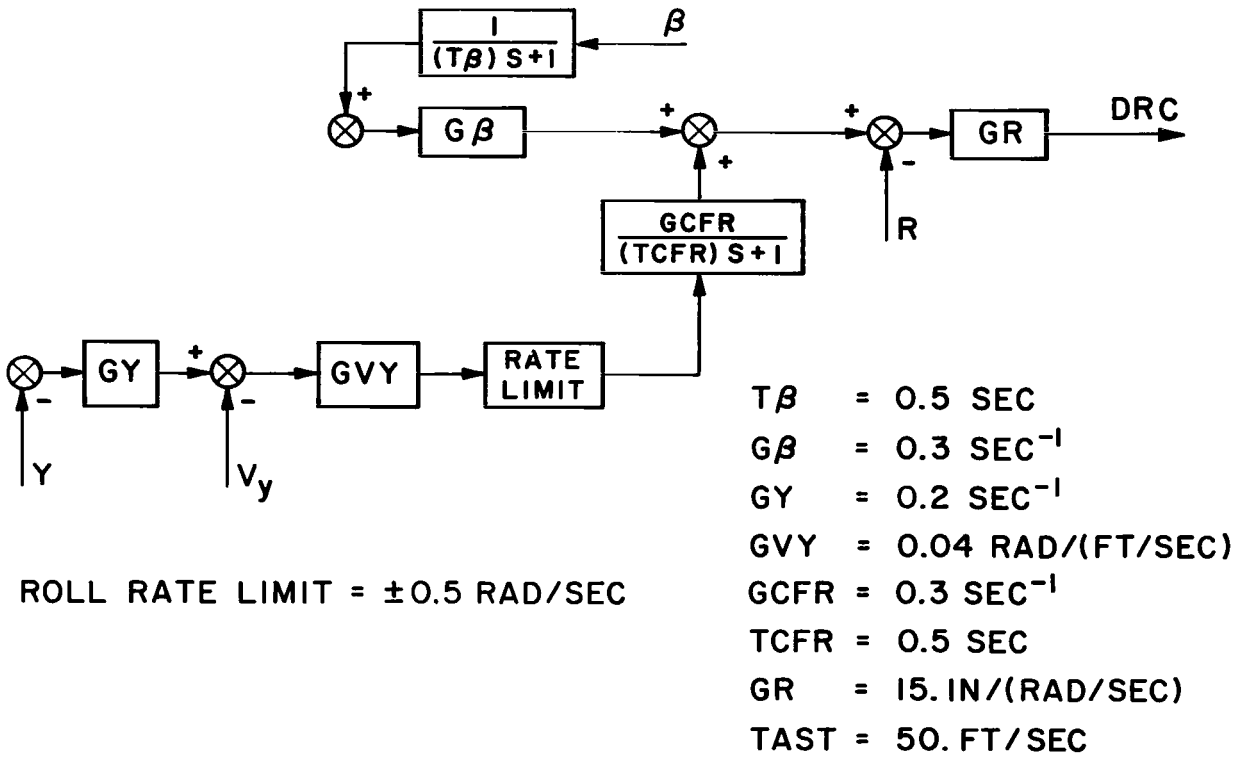

Figure 22a.- Yaw axis of Automatic Mode (TAS ≥ TAST)

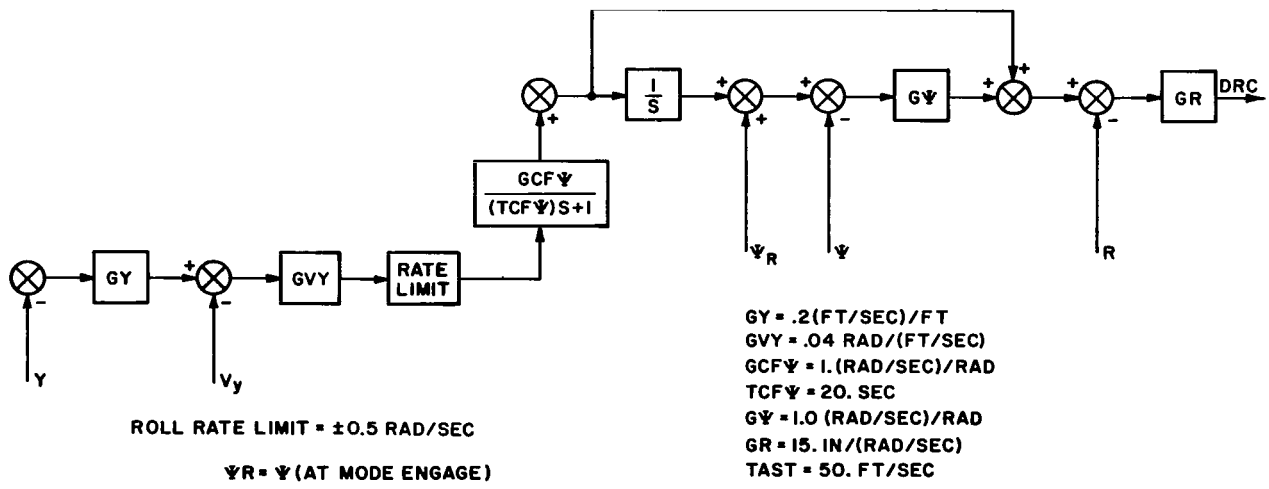

Figure 22b.- Yaw axis of Automatic Mode (TAS < TAST)

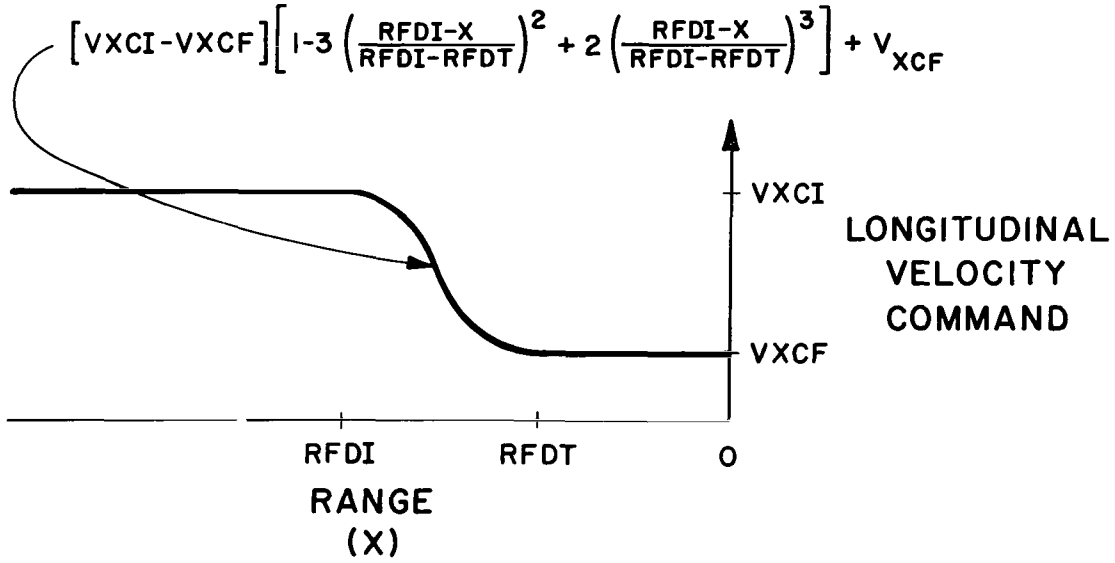

RFDI = -1550.FT. (RANGE AT INITIATION OF DECELERATION)
VXCI = 70.FT/SEC (VELOCITY COMMAND AT INITIATION OF DECELERATION)
RFDT = -275.FT. (RANGE AT TERMINATION OF DECELERATION)
VXCF = 15.FT/SEC (VELOCITY COMMAND AT TERMINATION OF DECELERATION)

Figure 23.- Longitudinal guidance laws

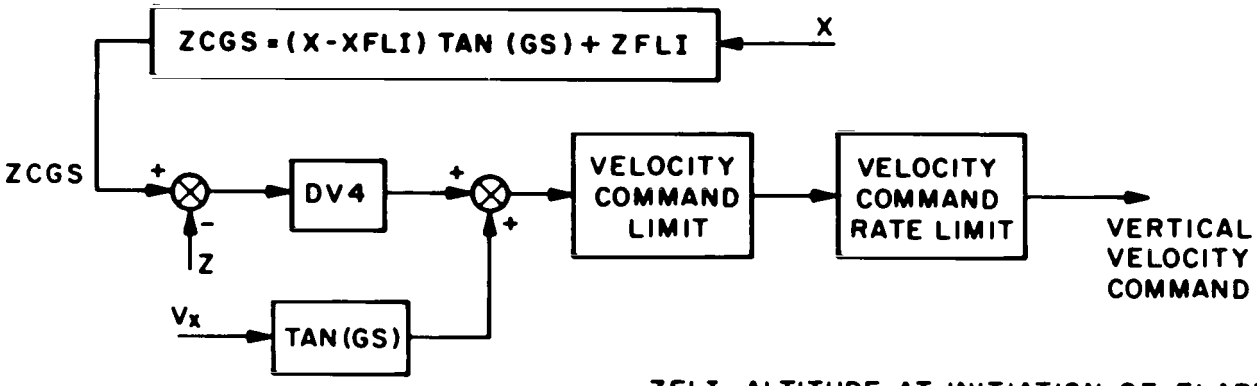

VELOCITY COMMAND LIMIT

OUTPUT
- DV2 WHEN INPUT > DV2
- INPUT WHEN 0. ≤ INPUT ≤ DV2
- 0. WHEN INPUT < 0.

VELOCITY COMMAND RATE LIMIT = ±DV5

NOTE: VELOCITY COMMAND LIMIT PROVIDES FOR A GLIDE SLOPE INTERCEPT

ZFLI - ALTITUDE AT INITIATION OF FLARE

XFLI - RANGE AT INITIATION OF FLARE

GS - GLIDE SLOPE ANGLE

ZCGS - GLIDE SLOPE ALTITUDE AT CURRENT RANGE

ZFLI = -150.FT

XFLI = -1550.FT

GS = .1 RAD

DV4 = .2 SEC^{-1}

DV2 = 15.FT/SEC

DV5 = 5.FT/SEC^2

Figure 24a.- Vertical guidance laws ($|Z| \geq |ZFLI|$)

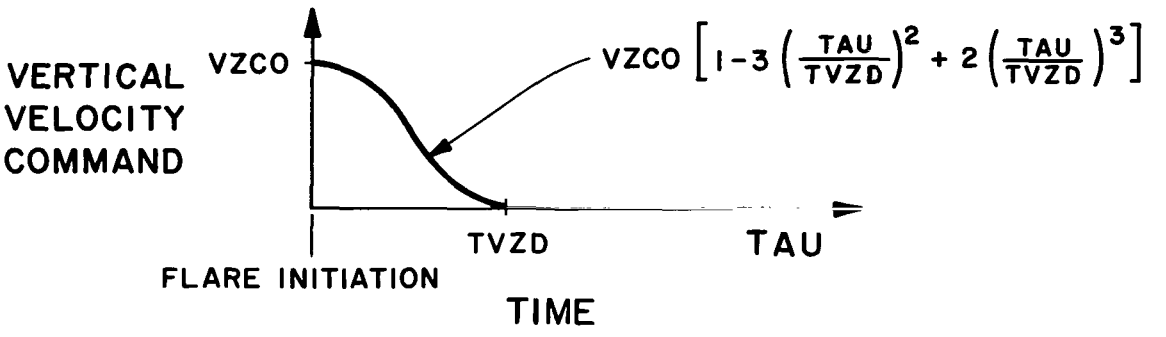

VZCO = 7.0 FT/SEC (INITIAL VELOCITY COMMAND FOR FLARE)

TVZD = 23.0 SEC (TOTAL TIME OF OPEN LOOP FLARE)

TAU IS ELAPSED TIME FROM FLARE INITIATION. WHEN TAU = TVZD THE SYSTEM REVERTS TO AN ALTITUDE HOLD SHOWN BELOW.

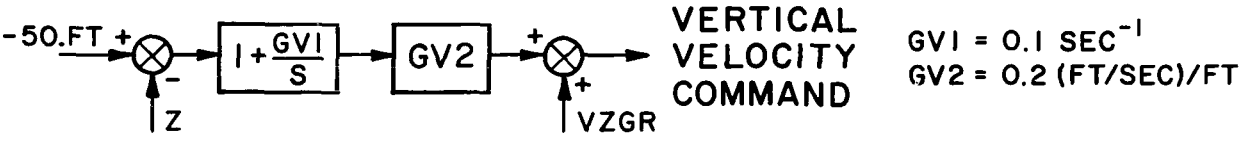

VZGR = (50.+ Z) GV2 (WHEN TAU = TVZD)

Figure 24b.- Vertical guidance laws (|Z| < |ZFLI|)

SYSTEM SYNTHESIS

The flight control modes were synthesized using classical linear analysis, fixed point hybrid simulation and mission simulation. First, gain estimates were made with linear analysis. Then, the analysis was verified on the simulation. Based upon both the analysis and the simulation, final gain selection was made. This section presents the results of that synthesis procedure.

Analysis

This section presents the design development and system performance of each flight control mode, based on linear analysis. Since the control system was to be implemented digitally, the effect of a sampled system as opposed to a continuous one had to

be considered. Based upon the recommendations of reference 9, a sample period of .032 sec. was initially chosen. This sample rate was considered high enough to warrant using continuous analysis in preliminary system synthesis and discrete system analysis for performance verification. This approach was taken with the digital system being modeled by a sample and hold network plus a computational lag in the forword loop.

The design objective of each flight control mode was to fully develop its dynamic capability in realizing a desirable system transient response and to minimize the error of the output in following a step input. The step response specification was a fast response with as little overshoot as possible. Translated in terms of conventional performance criteria, the dominant system roots were desired to be slightly overdamped while making the system's bandwidth reasonably large with a minimum of compensation. Integral plus proportional compensation was inserted in the forward loops of several modes to assure zero steady state error.

The CH-46C helicopter was modeled by two sets (longitudinal and lateral) of uncoupled differential equations with appropriate stability and control derivatives depending on the flight condition of the helicopter. The stability and control derivatives were obtained from the airframe manufacturer. The various flight conditions investigated are listed in Table I. The stability and control derivatives for Flight Condition 1 are listed in Appendix B. The perturbation equations of motion of the helicopter were written in terms of Euler angles and inertial velocities with respect to an Approach Navigation Frame (ANF). These equations allowed the helicopter to be controlled with respect to a preselected landing site. In addition, each input to the airframe equations was passed through a second order actuator model with damping ratio 0.6 and frequency 15.0 rad/sec. The design approach for each flight control system was based on the normal flight condition (flight condition 1) at hover where the pitch axis is decoupled from the vertical axis and the roll axis is decoupled from the rudder axis. Compensation was first selected for this condition and then analyzed for each cruise flight condition where these aircraft axes became coupled. Adjustments were made in the few cases where the design was unacceptable at other flight conditions.

The flight control modes are separated into the longitudinal axis and the lateral axis for convenience of presentation.

Longitudinal Axis (General)

The linearized longitudinal equations of motion of the helicopter in the ANF coordinate system are shown in Figure 25. The bare helicopter roots for flight condition 1 are shown in Figure 26 as a function of forward velocity. It is apparent

TABLE I.- CH46C AVAILABLE FLIGHT CONDITIONS

Flight Condition #	Gross Weight (LBS)	Altitude (FT)	C.G. Position	Climb Rate (FPM)	Forward Speed (KTS)
1	13,400.	Sea Level	Normal	0.	0,40,60,80,100,120,140
2			Most Fwd		
3			Most Aft		
4		10,000.	Normal		40,60,80,100
5			Most Aft		
6	15,500.	Sea Level	Normal	0.	0,40,60,80,100,120,140
7			Most Aft		
8	13,400.	Sea Level	Normal	-1500.	0,40,60,80
9			Normal	+1500.	

that the helicopter exhibits an inherent instability throughout the flight velocity regime. The migration of the roots indicates a change from a pendulum type instability to a speed type instability (i.e., real root in right-half plane) as the helicopter passes from the hover phase through transition.

$$\begin{bmatrix} \left[(\cos\theta_{TR})S-\left(\frac{X_u}{m}\cos\theta_{TR}+\frac{X_w}{m}\sin\theta_{TR}\right)\right] & \left[(-\sin\theta_{TR})S+\left(\frac{X_u}{m}\sin\theta_{TR}-\frac{X_w}{m}\cos\theta_{TR}\right)\right] & \left[-\frac{X_q}{m}S+\frac{X_u}{m}W_{TR}-\frac{X_w}{m}U_{TR}+g\cos\theta_{TR}\right] \\ \left[(\sin\theta_{TR})S-\left(\frac{Z_u}{m}\cos\theta_{TR}+\frac{Z_w}{m}\sin\theta_{TR}\right)\right] & \left[(\cos\theta_{TR})S+\left(\frac{Z_u}{m}\sin\theta_{TR}-\frac{Z_w}{m}\cos\theta_{TR}\right)\right] & \left[-\frac{Z_q}{m}S+\frac{Z_u}{m}W_{TR}-\frac{Z_w}{m}U_{TR}+g\sin\theta_{TR}\right] \\ \left[-\frac{M_u}{I_{yy}}\cos\theta_{TR}-\frac{M_w}{I_{yy}}\sin\theta_{TR}\right] & \left[\frac{M_u}{I_{yy}}\sin\theta_{TR}-\frac{M_w}{I_{yy}}\cos\theta_{TR}\right] & \left[S^2-S\frac{M_q}{I_{yy}}+\frac{M_u}{I_{yy}}W_{TR}-\frac{M_w}{I_{yy}}U_{TR}\right] \end{bmatrix} \begin{bmatrix} \Delta V_x \\ \Delta V_z \\ \Delta\theta \end{bmatrix} = \begin{bmatrix} \frac{X_\delta}{m} \\ \frac{Z_\delta}{m} \\ \frac{M_\delta}{I_{yy}} \end{bmatrix} \delta$$

WHERE $V_{XTR} \triangleq U_{TR}\cos\theta_{TR}+W_{TR}\sin\theta_{TR}$, $B \triangleq I_{zz}\cos\theta_{TR}-J_{xz}\sin\theta_{TR}$ AND $S \triangleq \frac{d}{dt}$ THE LAPLACE DIFFERENTIAL OPERATOR.

Figure 25.- Longitudinal perturbation equations

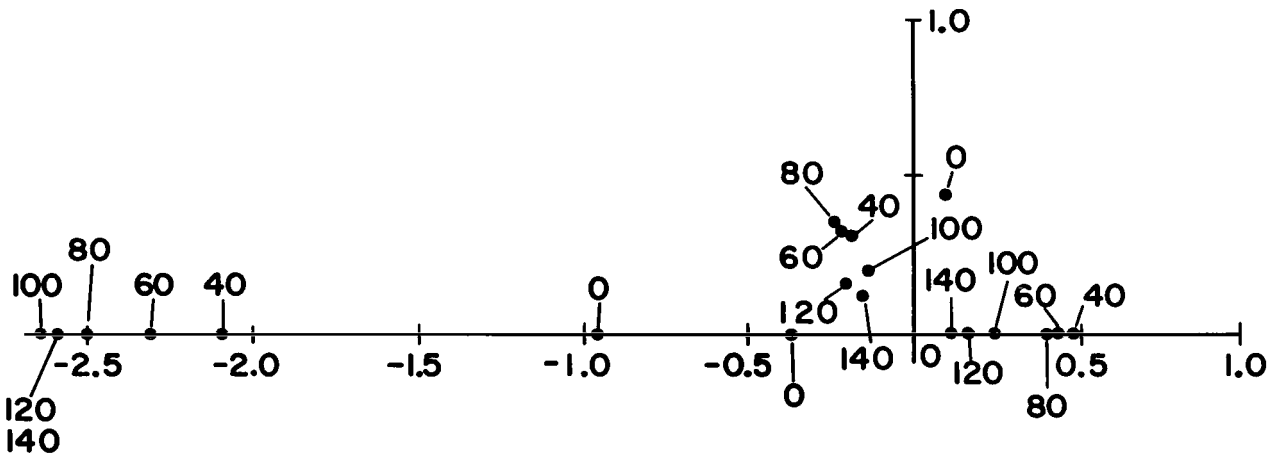

Figure 26.- Longitudinal perturbation equation root migration as a function of airspeed (Flight Condition 1)

Attitude Command Mode I (Longitudinal Axis)

The open-loop frequency response of the pitch to DEC channel of the helicopter at hover including actuator dynamics is shown in Figure 27. The poor low-frequency response prompted the insertion of an integral plus proportional compensation in the forward loop of the pitch axis. The integrator gain, GIΘ, is essentially the zero location of a lead term as shown by the block diagram of the integral plus proportional compensation in Figure 28. The optimum value of GIΘ was determined from the open-loop frequency response which is repeated in Figure 29. The results of making the break frequency, GIΘ of the lead term equal to the natural frequency of the open-loop system, .45 radians/sec, are shown. The integrator increased the gain and, therefore, performance of the low frequencies while the lead term maintained marginal stability of the system. Making the break frequency greater than the natural frequency increased the bandwidth of the system but in the process destabilized the system. Making the break frequency less than the natural frequency reduced the destabilizing effect but the low frequency performance deteriorated. Selecting GIΘ = .2 radians/sec appeared to be a reasonable compromise. Note that the system is also gain insensitive as indicated by the fairly flat phase curve over the region of stability. With a lower break frequency on the lead term the system became somewhat more gain sensitive.

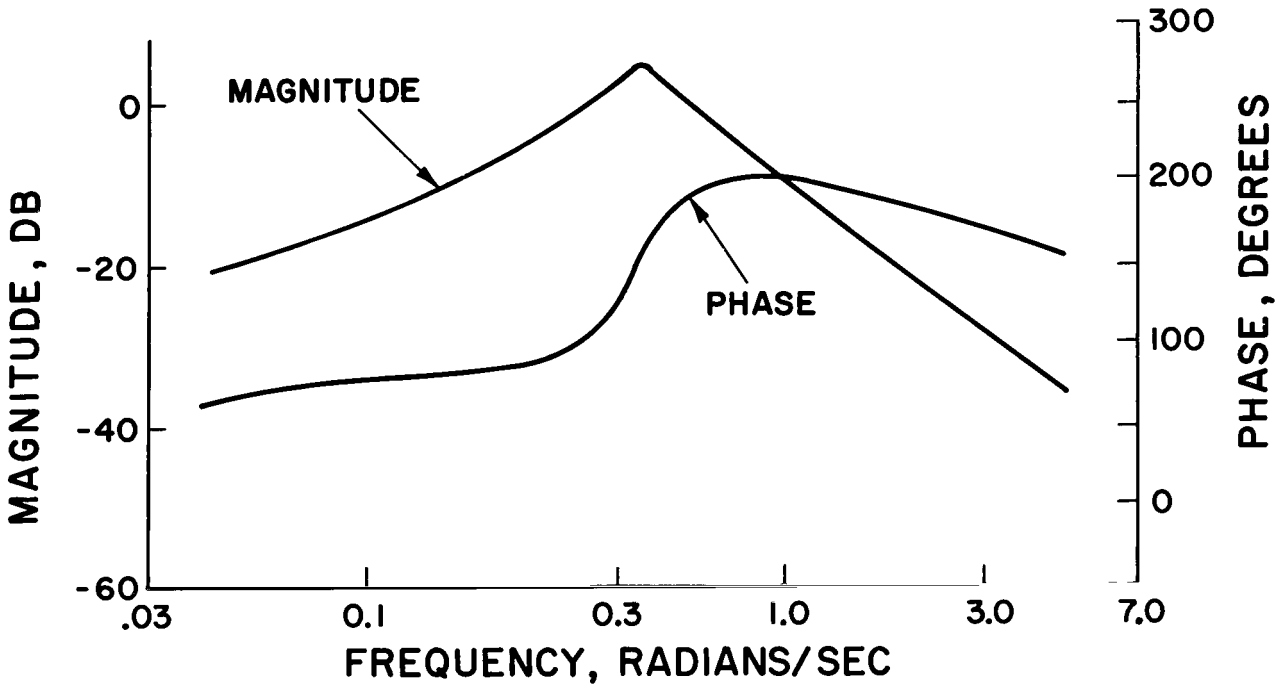

Figure 27.- Θ/DEC open-loop frequency response at hover

Figure 28.- Integral plus proportional compensation

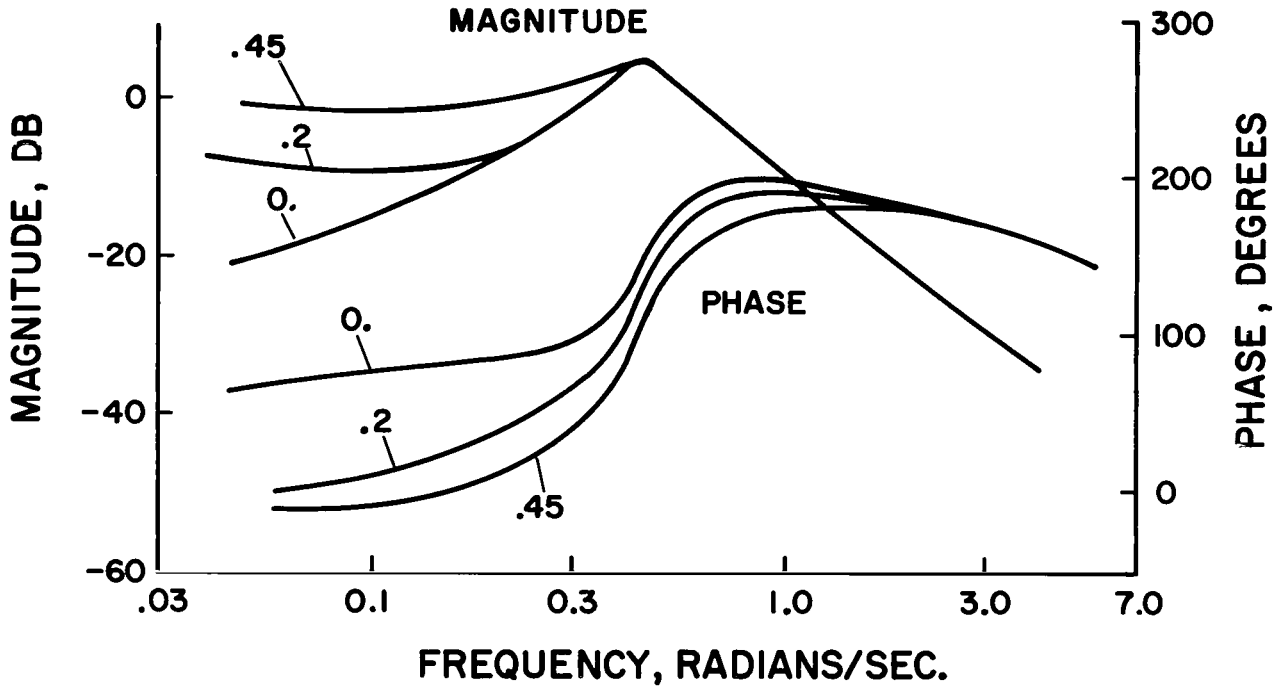

Figure 29.- θ/DEC open-loop frequency response at hover with integral plus proportional compensation in the forward loop as a function of GIθ

In order to achieve an adequately damped pitch attitude command system, some rate feedback was anticipated. A root-locus analysis was used to determine the rate feedback gain and attitude forward loop gain. The system configuration is shown in Figure 30. Figures 31, 32, and 33 show the attitude loop

root locus with gain parameter GΘ and with GQ = .25, .5, and 2. respectively. When GQ = .25 the locus emanating from the actuator poles was drawn into the real axis, but the locus emanating from the helicopter complex poles did not become sufficiently damped. Increasing GQ to .5 (this corresponds to moving the real open loop zero from -4 to -2) drew the complex locus to the real axis in the left half plane. This case was considered near optimum since the break-away angle from the complex poles is approximately 45° suggesting a maximum excursion of the locus into the left half plane. Increasing the rate gain from .5 to 2. drew the complex locus into the real axis abruptly resulting in a sluggish system. The attitude gain selected from Figure 32 was 20. inches/radian.

Since the helicopter is not augmented in the vertical axis in Attitude Command Mode I, this completed the continuous analysis for this mode in the Longitudinal Axis. The system dynamics for Attitude Command Mode I were not verified analytically for the remaining flight conditions. This was left to the simulation.

The root locus of the pitch attitude loop at hover with GΘ as the gain parameter and with sampler and hold plus a computational lag in the forward loop is shown in the S plane in Figure 34. The system damping is reduced somewhat when the system is digitalized.

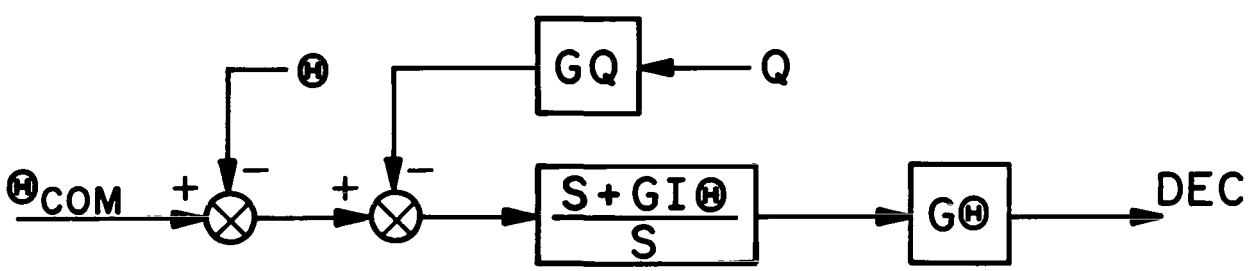

Figure 30.- Pitch Attitude Command system

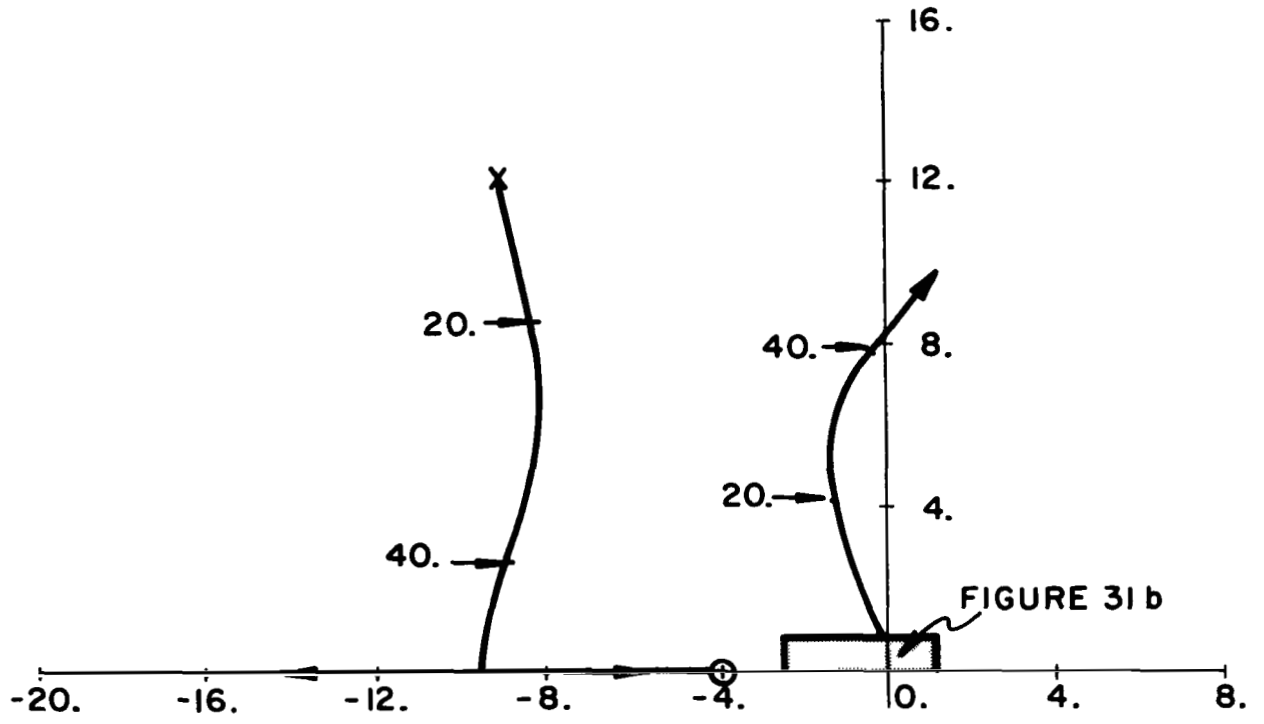

Figure 31a.- Root locus of the pitch loop at hover (GIθ = .2, GQ = .25)

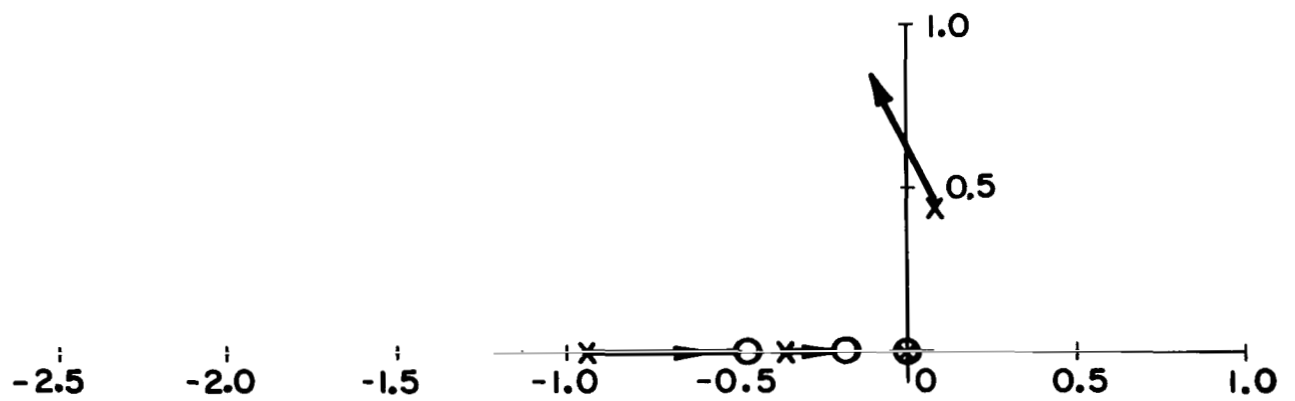

Figure 31b.- Root locus at origin of pitch loop at hover (GIθ = .2, GQ = .25)

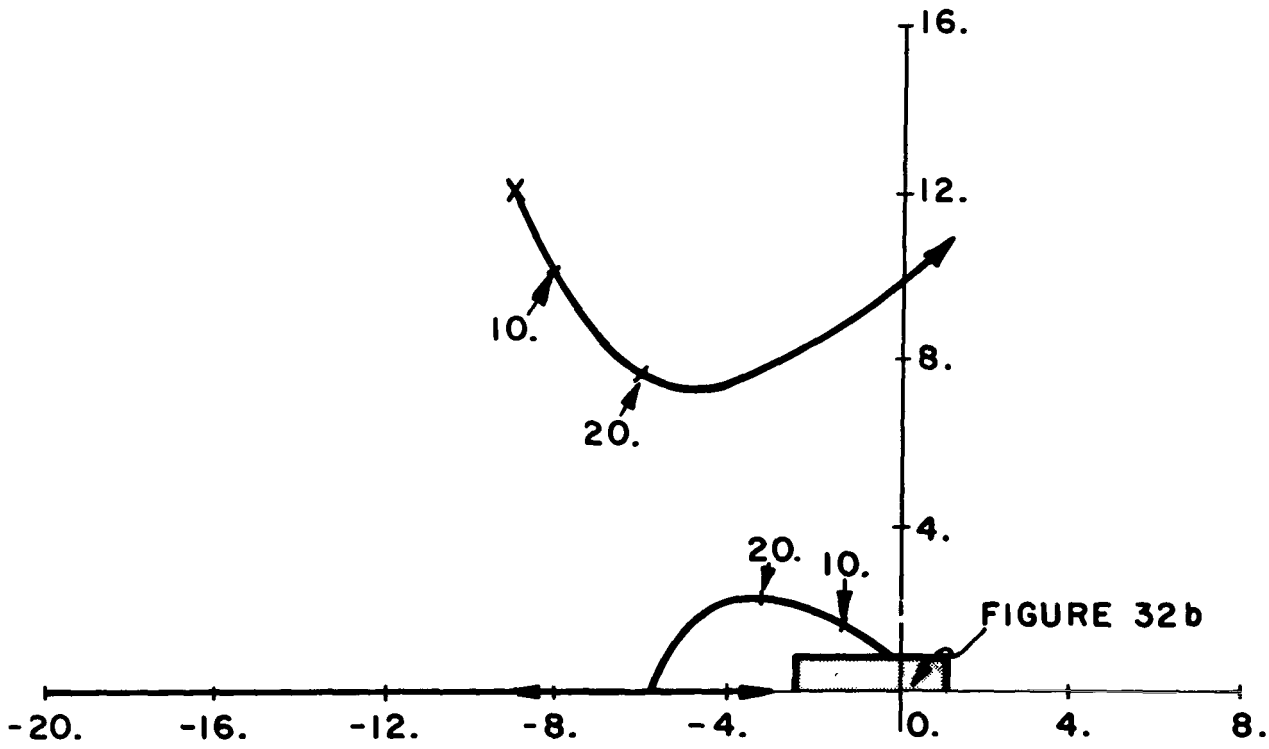

Figure 32a.- Root locus of pitch loop at hover (GIθ = .2, GQ = .5)

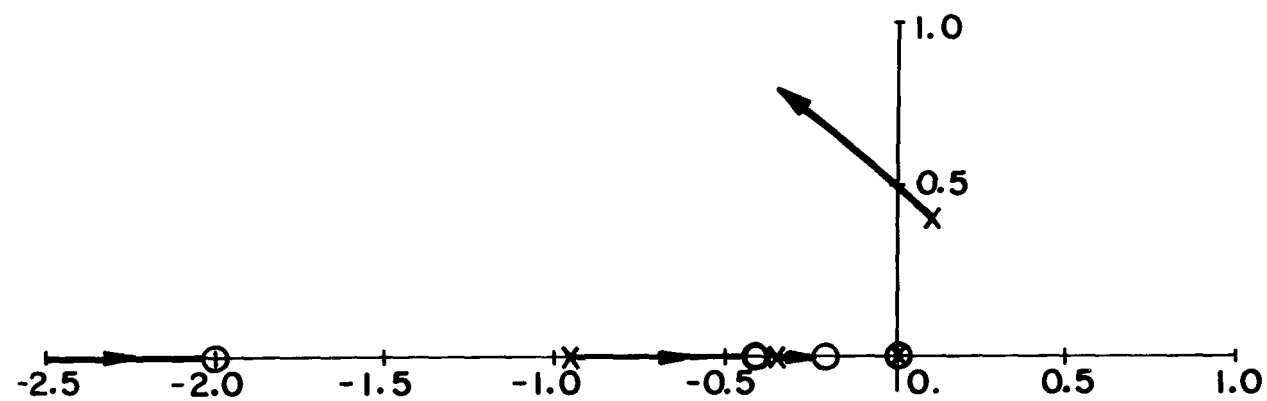

Figure 32b.- Root locus at origin of pitch loop at hover (GIθ = .2, GQ = .5)

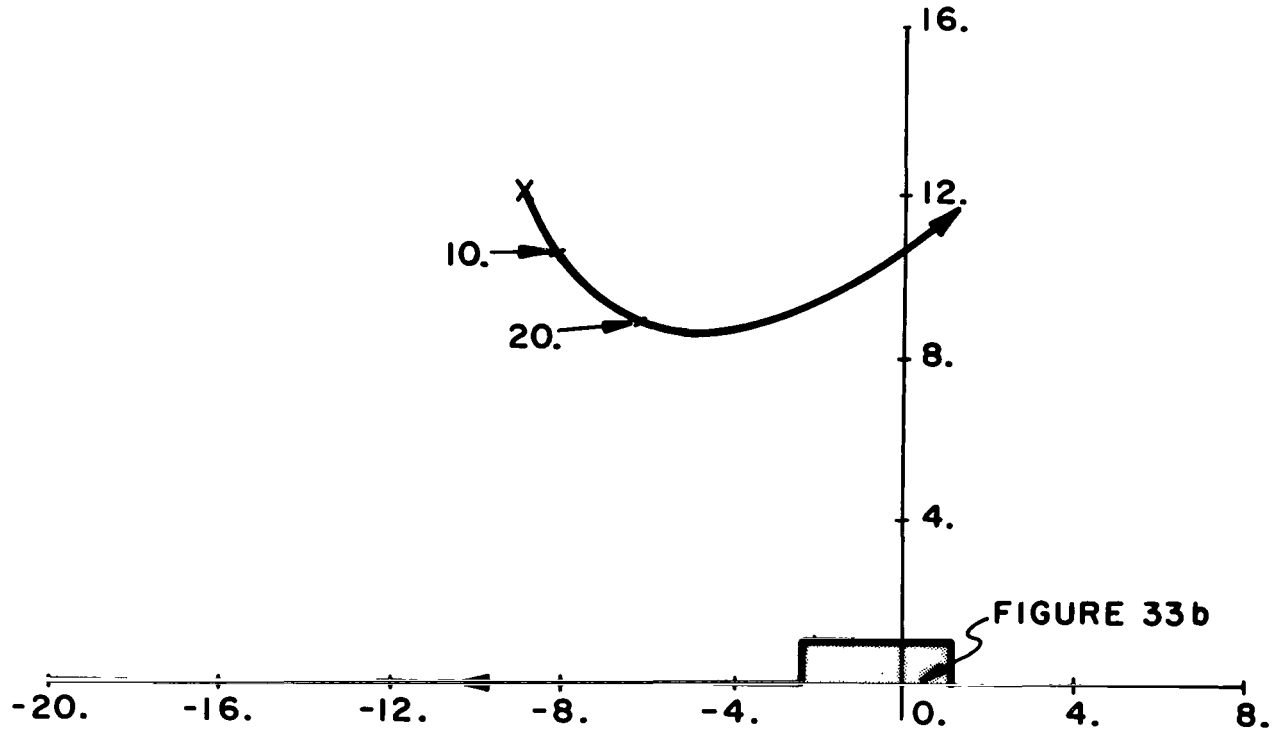

Figure 33a.- Root locus of pitch loop at hover (GIΘ = .2, GQ = 2.)

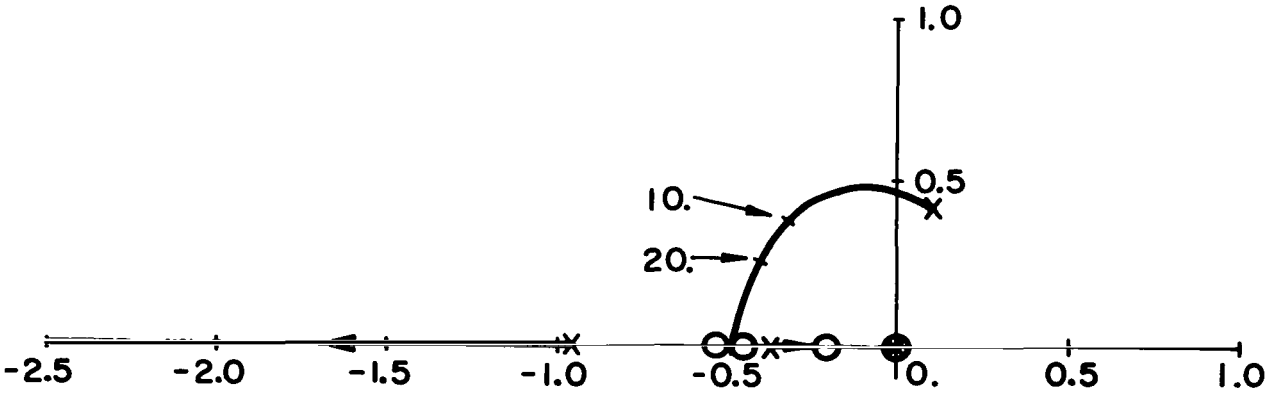

Figure 33b.- Root locus at origin of pitch loop at hover (GIΘ = .2, GQ = 2.)

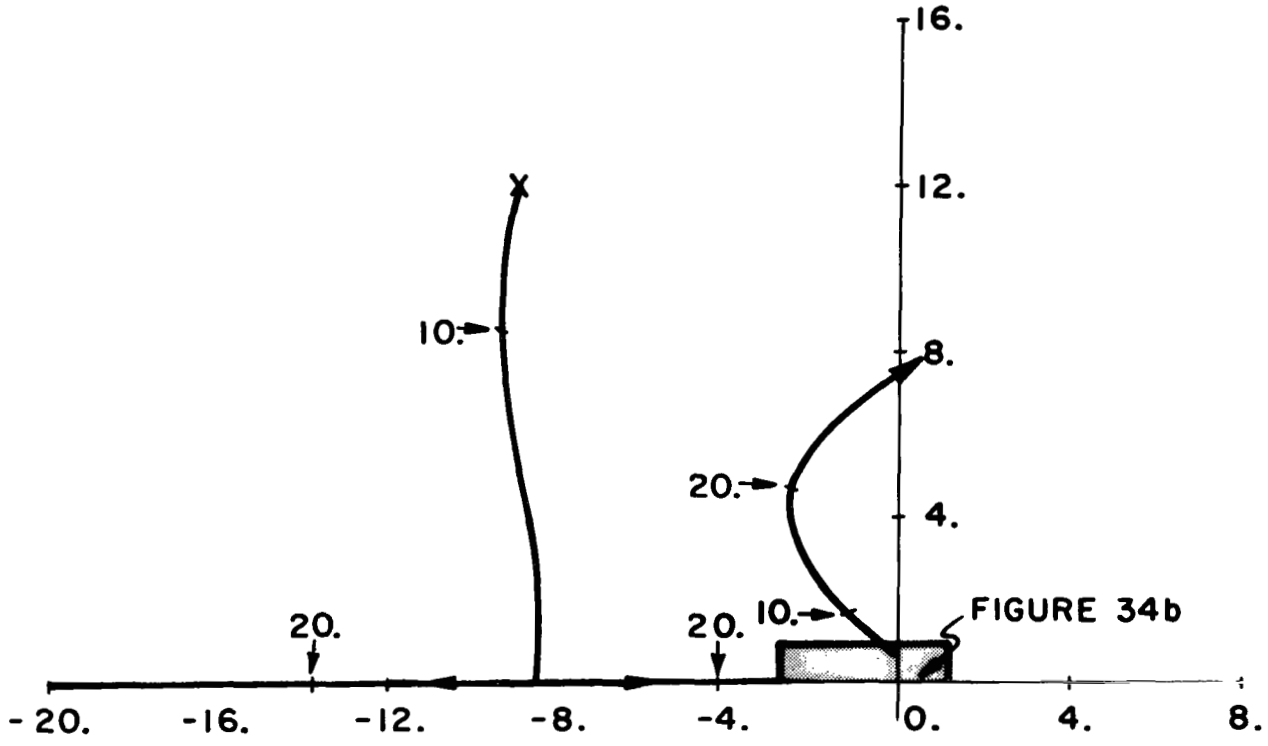

Figure 34a.- Root locus of pitch loop at hover with sampler and hold plus computational lag in the forward loop (GIθ = .2, GQ = .5). Sample period = .032 second.

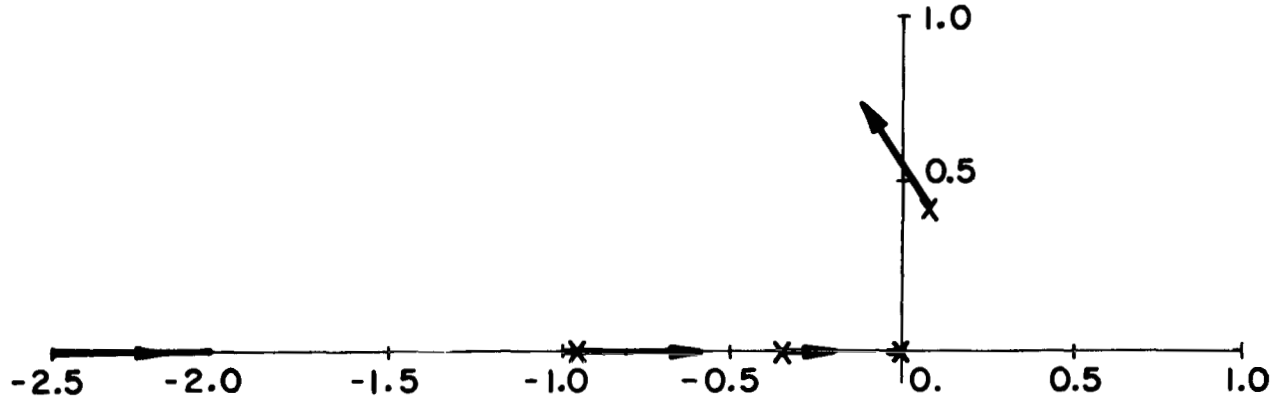

Figure 34b.- Root locus at origin of pitch loop at hover with sampler and hold plus computational lag in the forward loop (GIθ = .2, GQ = .5). Sample period = .032 second.

Attitude Command Mode II (Longitudinal Axis)

The pitch axis for this mode is the same as in Attitude Command Mode I. A simple Rate of Descent Command system can be implemented in the vertical axis by feeding back the vertical velocity with forward loop gain as shown in Figure 35. The rate of descent V_Z is defined positive downwards and collective rotor pitch (DCC) is defined positive for upward force or lift. Therefore, to achieve the correct sense in the simple rate of descent command system, the velocity gain GZD must necessarily be negative.

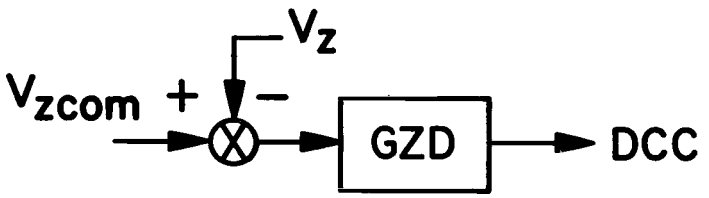

Figure 35.- Simple rate of Descent Command system

The root locus of the simple rate of descent loop with gain parameter GZD is shown in Figure 36. The output response speed can be increased as the velocity gain is increased. The closed loop frequency response corresponding to a velocity gain of -.2 in/(ft/sec) is shown in Figure 37. The resulting bandwidth of the vertical axis is 3 radians/sec, while the steady state error was 20 percent. Increasing the velocity gain widened the bandwidth slightly and decreased the steady state error at the cost of decreasing the damping of the system. This simple system was thus precluded as an effective rate of descent command system.

To improve the system, an altitude feedback loop was added in such a way as to be equivalent to inserting an integral plus proportional compensation. The system is shown in Figure 38. The root locus for this system with GZ as the gain parameter and with GZD = -.4 in/(ft/sec) is shown in Figure 39. A reasonable choice for GZ, anticipating a decrease in damping with forward velocity, was 1.6 (ft/sec)/ft. The closed loop frequency response is shown in Figure 40. The steady rate of descent error was zero while the bandwidth was increased to 5. radians/sec. This represented a major improvement over the previous rate of descent command system. Also, this system has altitude hold capability.

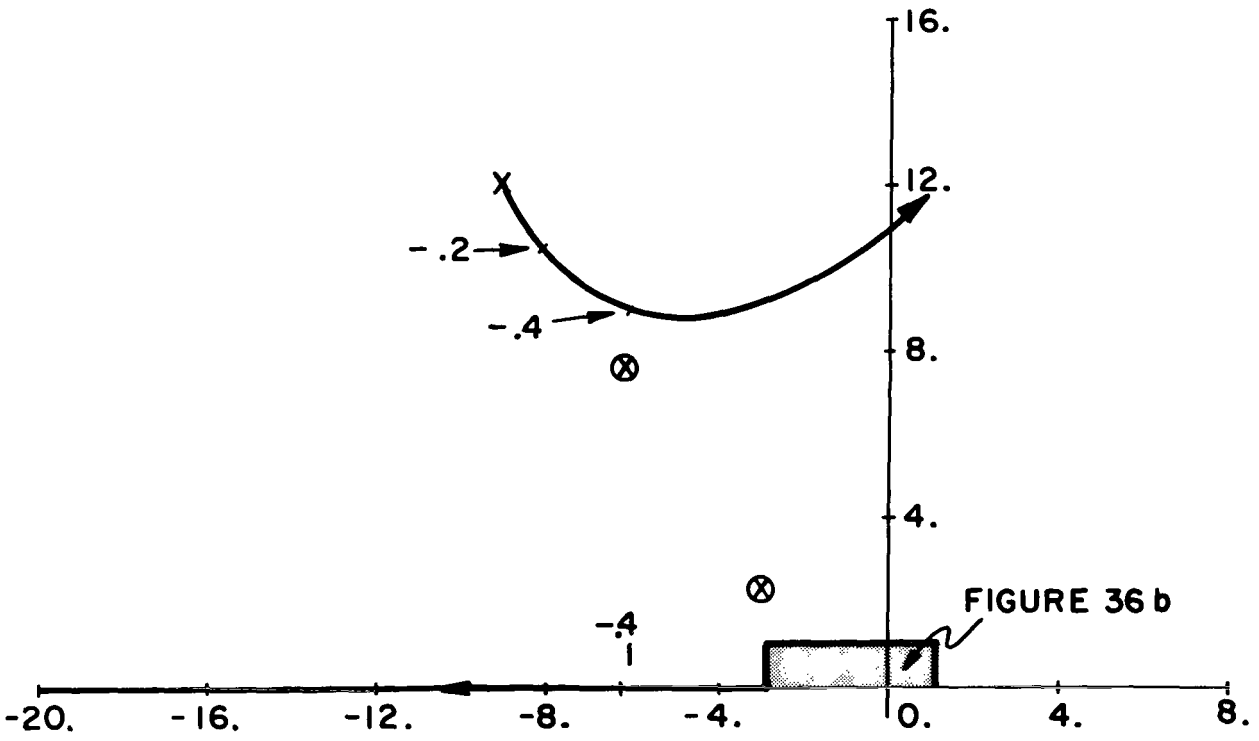

Figure 36a.- Root locus of the simple rate-of-descent loop at hover with pitch loop closed (GQ = .5, GΘ = 20.)

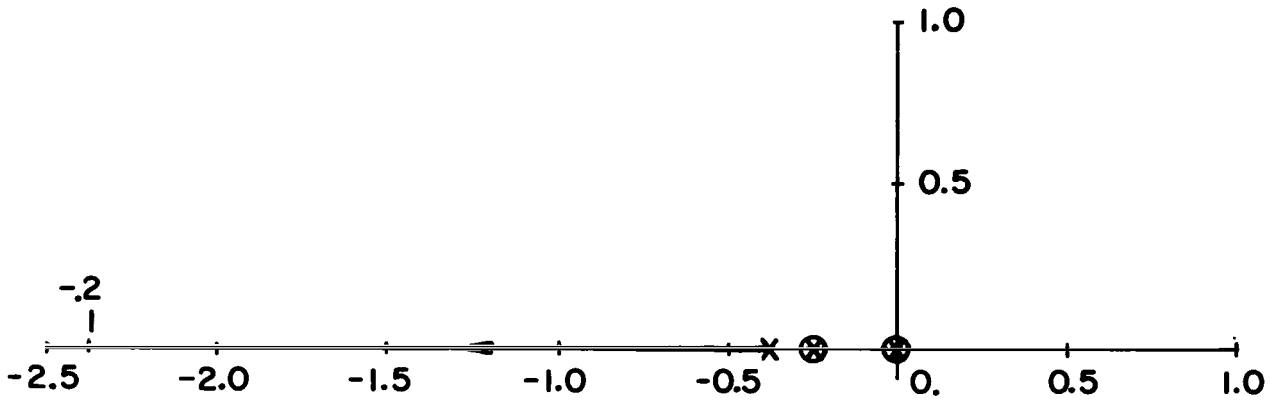

Figure 36b.- Root locus at origin of the simple rate-of-descent loop at hover with pitch loop closed (GIΘ = .2, GQ = .5, GΘ = 20.)

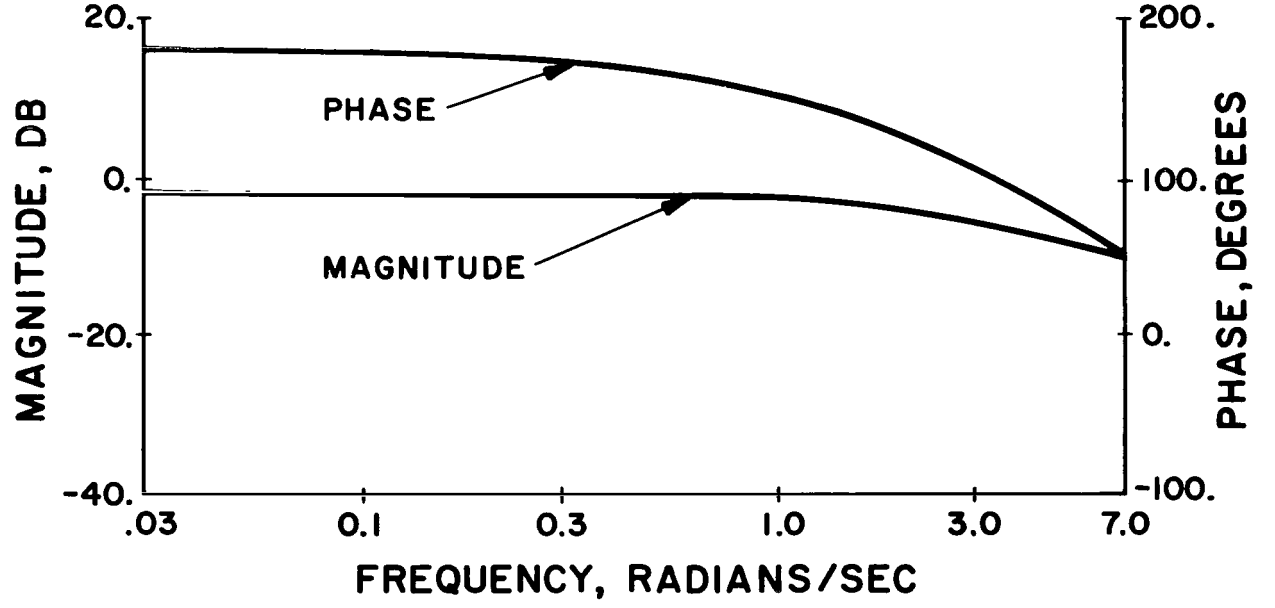

Figure 37.- V_Z/V_{ZCOM} closed-loop frequency response for simple rate-of-descent command system at hover with pitch loop closed (GIΘ = .2, GQ = .5, GΘ = 20., GZD = -.2)

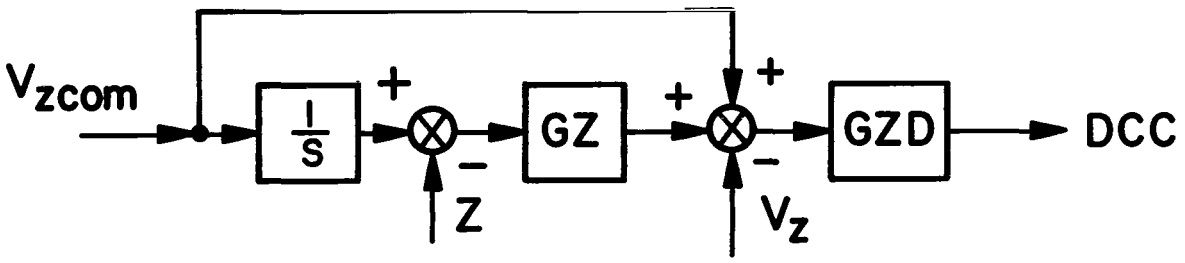

Figure 38.- Rate of Descent Command system

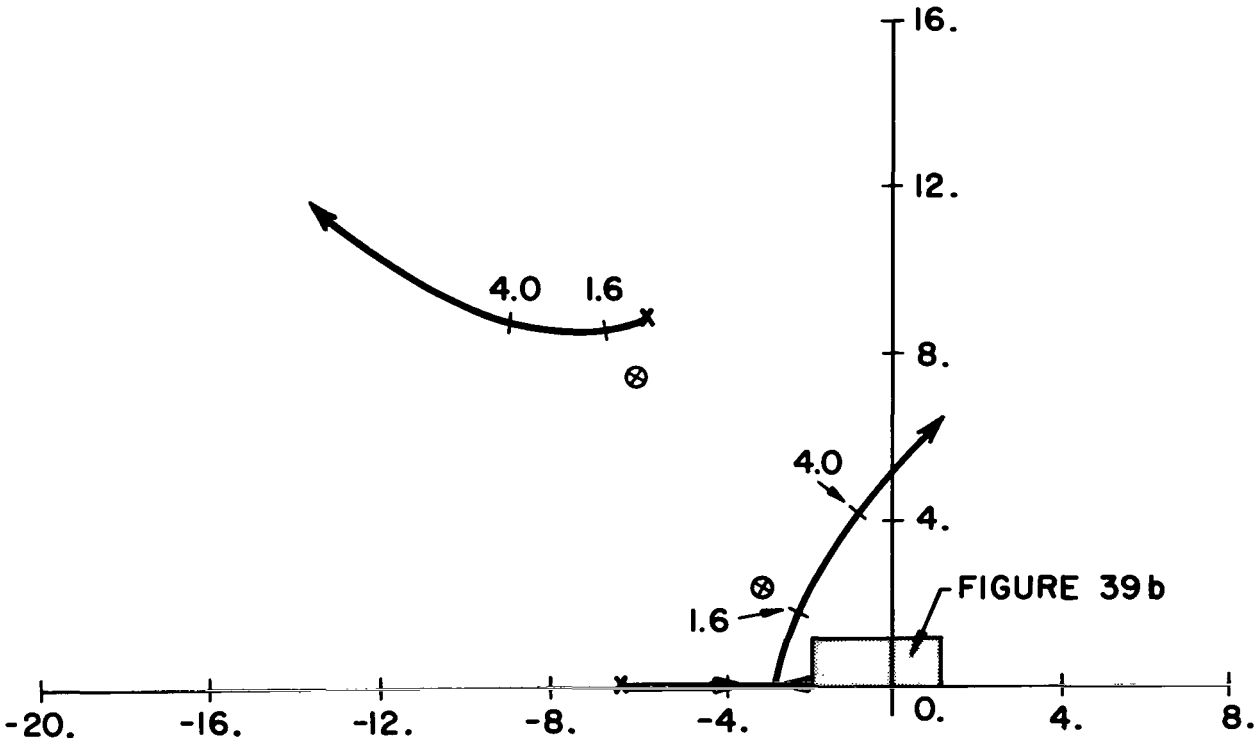

Figure 39a.- Root locus of the altitude loop at hover with pitch loop closed (GIΘ = .2, GQ = .5, GΘ = 20., GZD = -.4)

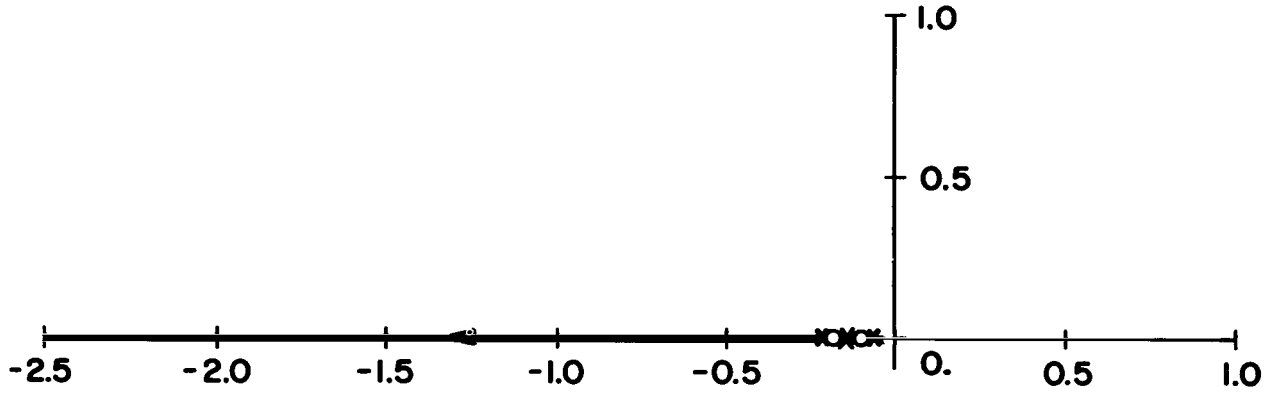

Figure 39b.- Root locus at origin of the altitude loop at hover with pitch loop closed (GIθ = .2, GQ = .5, Gθ = 20., GZD = -.4)

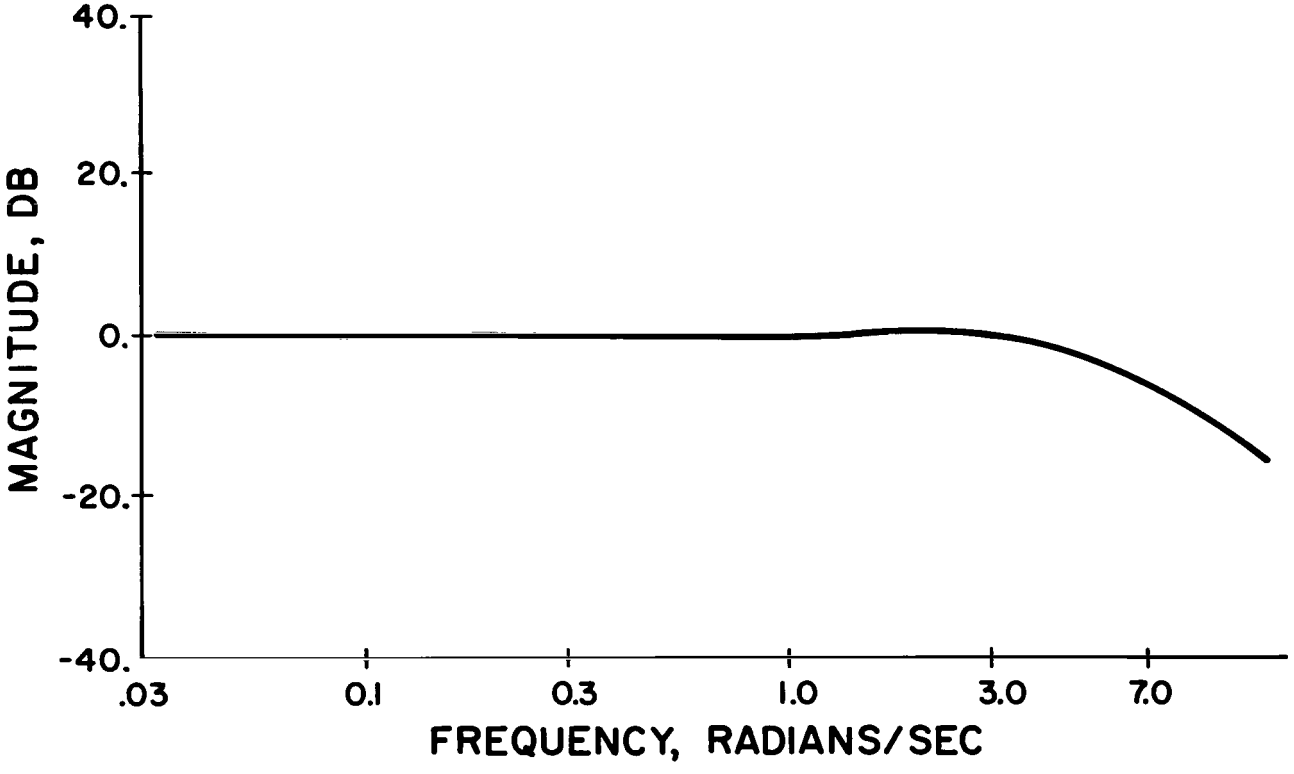

Figure 40.- V_Z/V_{ZCOM} closed-loop frequency response at hover with altitude feedback and pitch loop closed (GIθ = .2, GQ = .5, Gθ = 20., GZD = -.4, GZ = 1.6)

The root variations of the final Rate of Descent Command Mode system as a function of forward velocity are shown in Figure 41. The bandwidth and damping were both considered satisfactory for the flight velocities of interest.

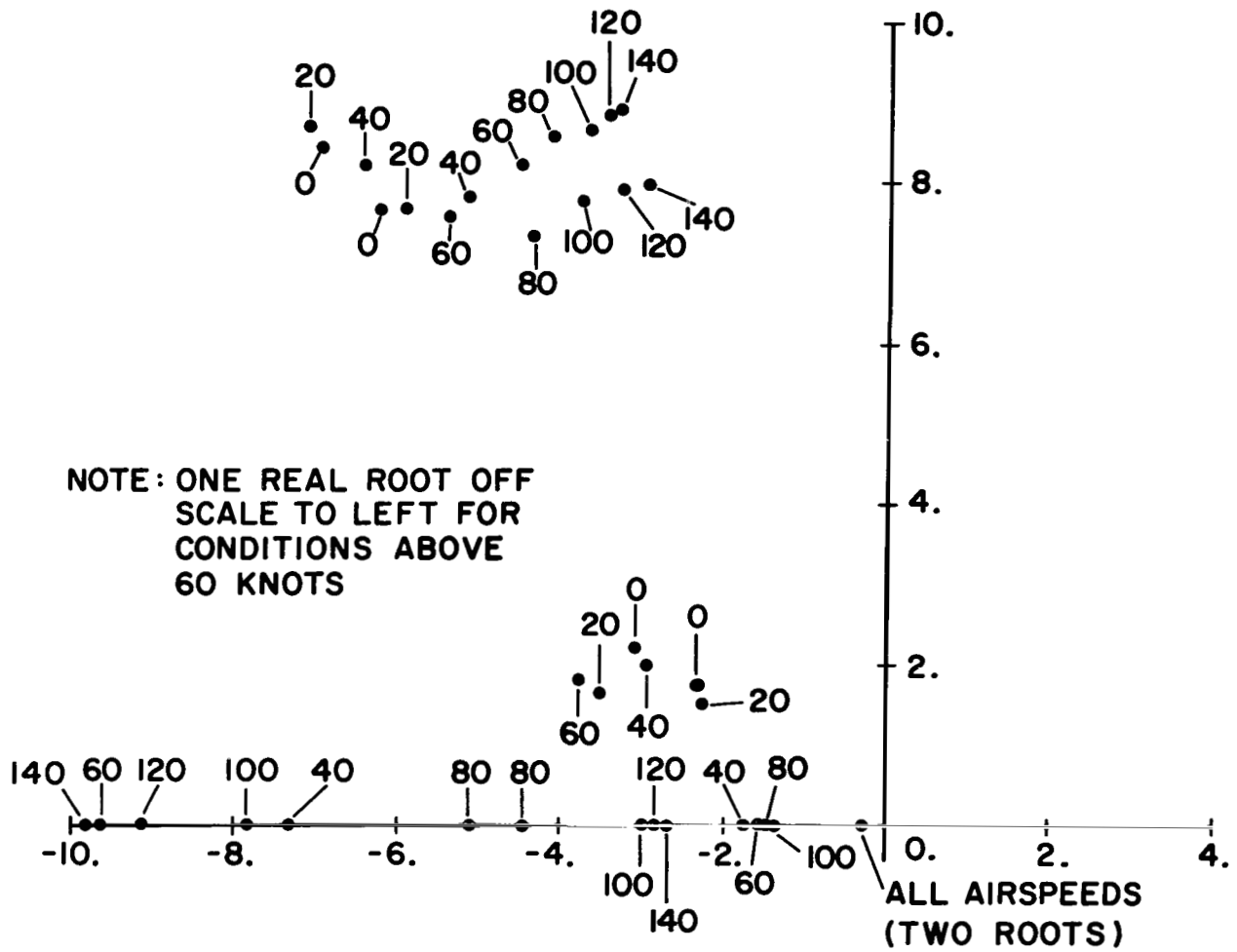

Figure 41.- Root variations of the rate of descent Command System as a function of airspeed with pitch loop closed (GIθ = .2, GQ = .5, Gθ = 20., GZD = -.4, GZ = 1.6)

The root locus of the Rate of Descent Command loop at hover with GZ as the gain parameter and with sampler and hold plus a computational lag in each axis of the Attitude Command Mode II

system is shown in the S plane in Figure 42. Only the damping of the system was changed (reduced slightly with GZ = 1.6 (ft/sec)/ft) as the system was digitalized.

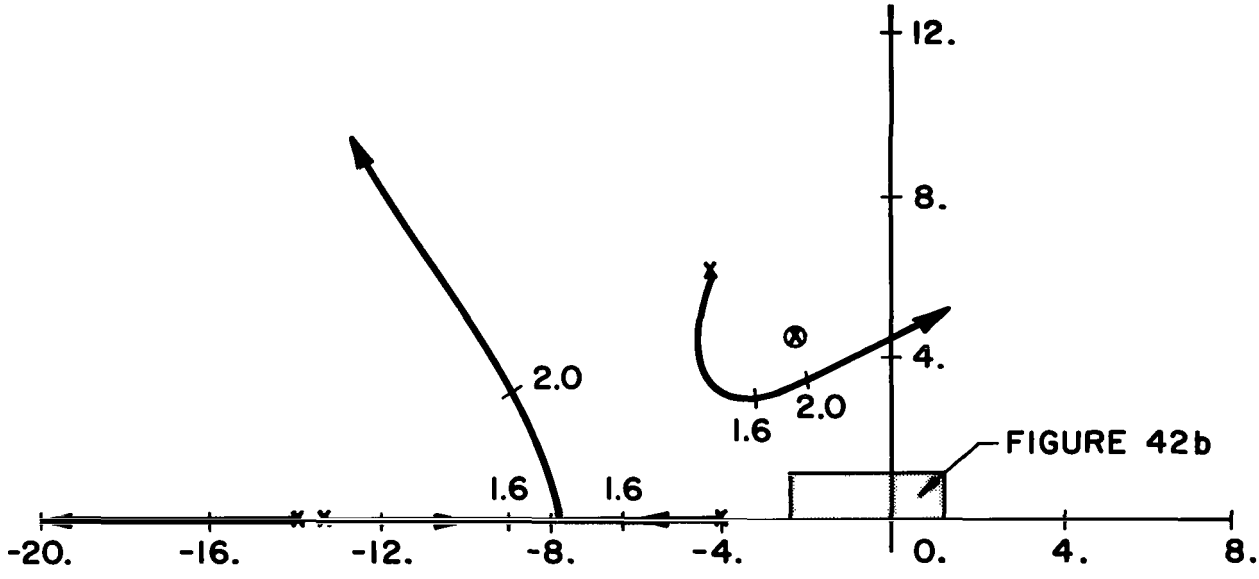

Figure 42a.- Root locus of rate-of-descent command loop at hover with sampler and hold plus computational lag (GIΘ = .2, GQ = .5, GΘ = 20., GZD = -.4) Sample period = .032 sec

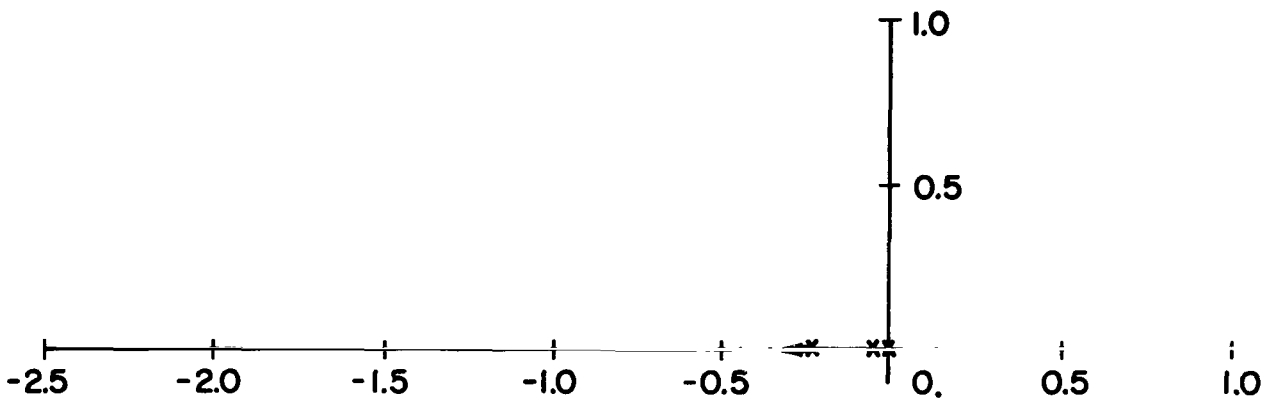

Figure 42b.- Root locus of origin of rate-of-descent command loop at hover with sampler and hold plus computational lag (GIΘ = .2, GQ = .5, GΘ = 20., GZD = -.4) Sample period = .032 sec

Velocity Command Mode (Longitudinal Axis)

The vertical axis of this mode is the same as in Attitude Command Mode II. A forward velocity command system was implemented by feeding back the forward velocity in the pitch axis as shown in Figure 43. Since positive pitch command generates negative V_X the forward velocity gain must be negative. The root locus of the velocity command system at hover with velocity gain GVX as the gain parameter is shown in Figure 44. The velocity gain GVX = -.016 radians/(ft/sec) was selected. The closed-loop frequency response is shown in Figure 45. It indicates a bandwidth of about 1 radian/sec. The velocity loop closure in the pitch axis had little effect on the vertical axis velocity response. The root variation of the Velocity Command Mode as a function of forward velocity is shown in Figure 46. The system was considered acceptable for all the flight conditions of interest.

The root locus of the forward velocity loop at hover with GVX as the gain parameter and with sampler and hold plus a computational lag in the forward loops of each axis of the Velocity Command Mode system is shown in the S plane in Figure 47. Again, the main effect of digitalizing the system is a slight change in the system's damping (GVX = -.016).

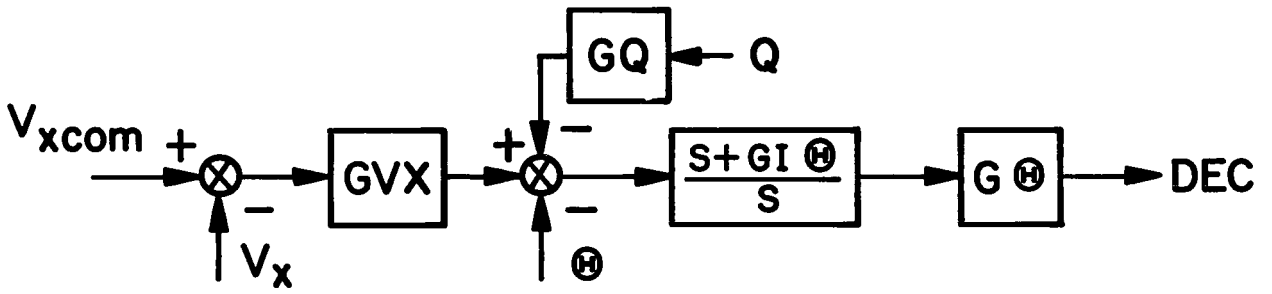

Figure 43.- Forward velocity command system

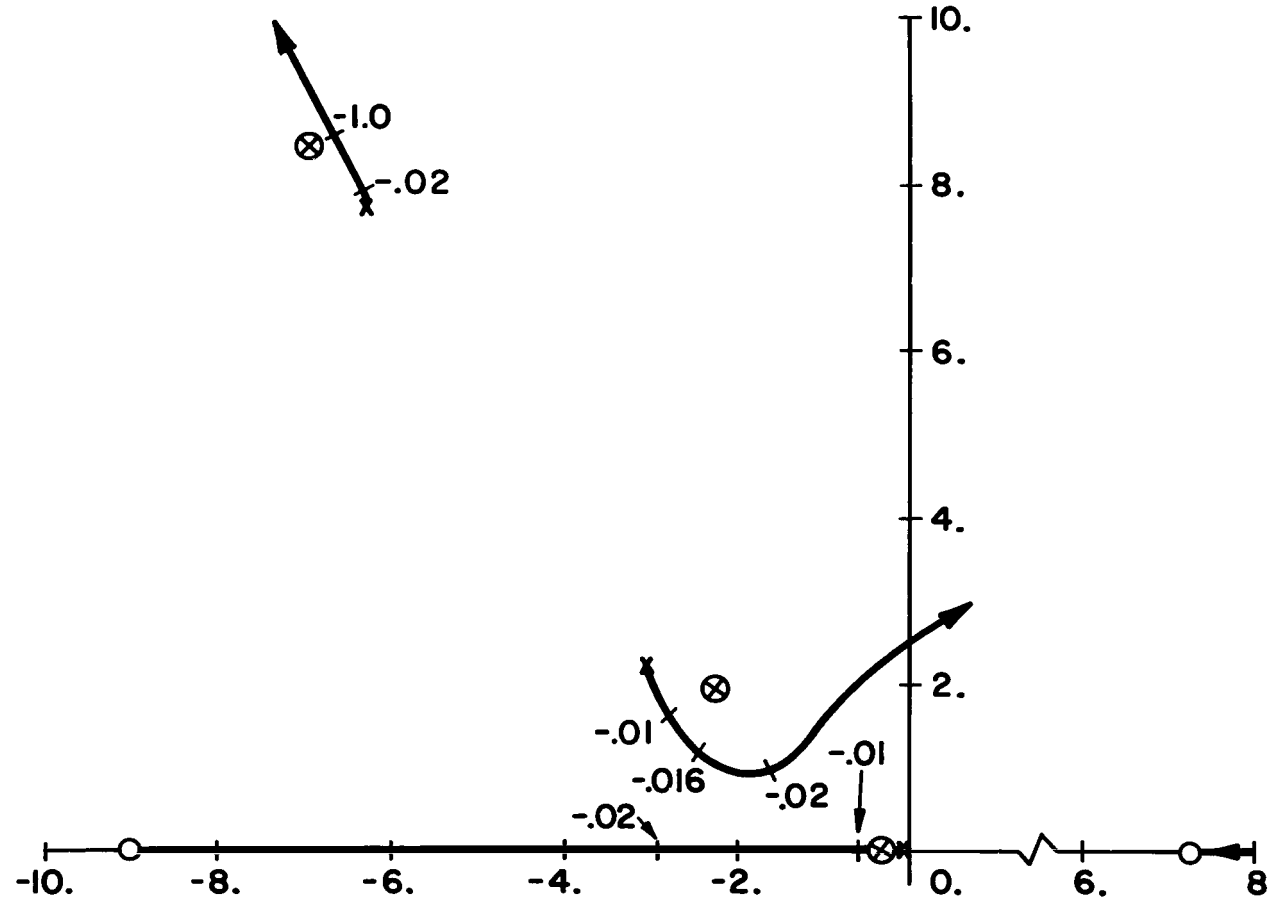

Figure 44.- Root locus of forward velocity loop of Velocity Command System at hover (GIΘ = .2, GQ = .5, GΘ = 20., GZD = -.4, GZ = 1.6)

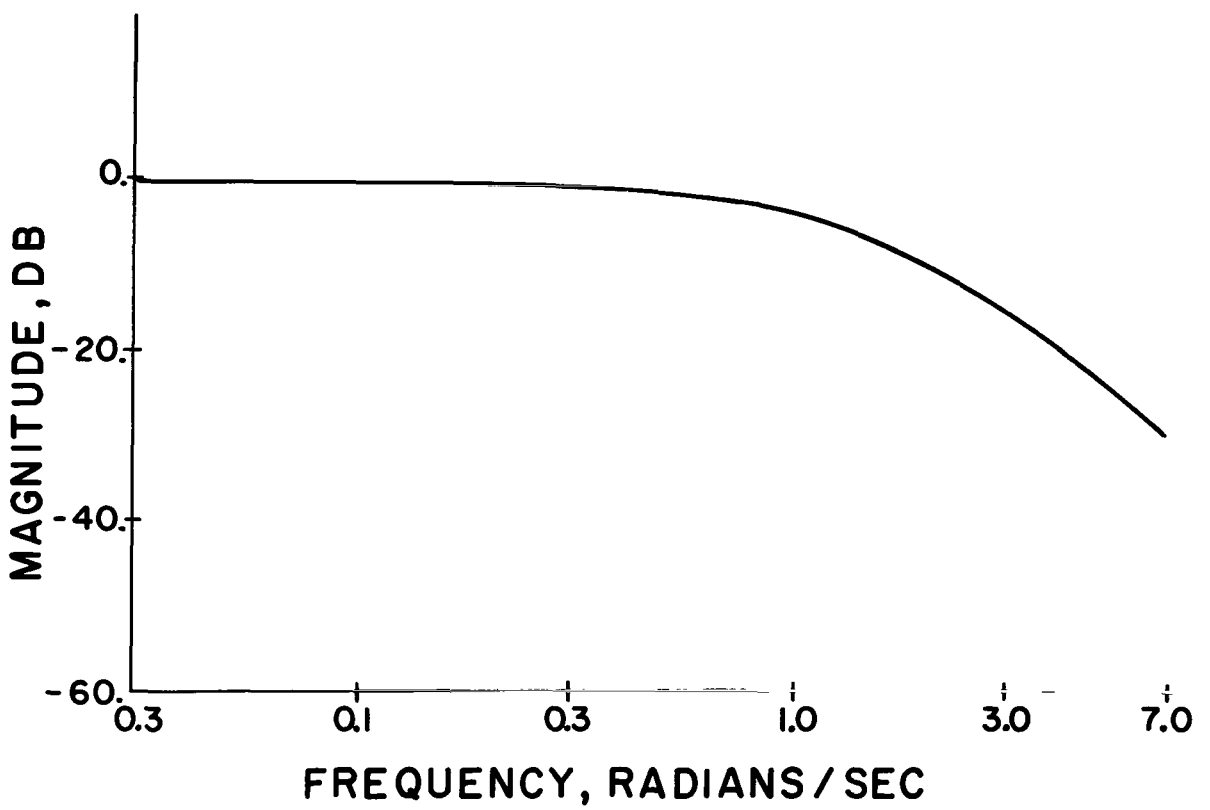

Figure 45.- V_X/V_{XCOM} closed loop frequency response of Velocity Command System at hover (GIθ = .2, GQ = .5, Gθ = 20., GZD = -.4, GZ = 1.6, GVX = -.016)

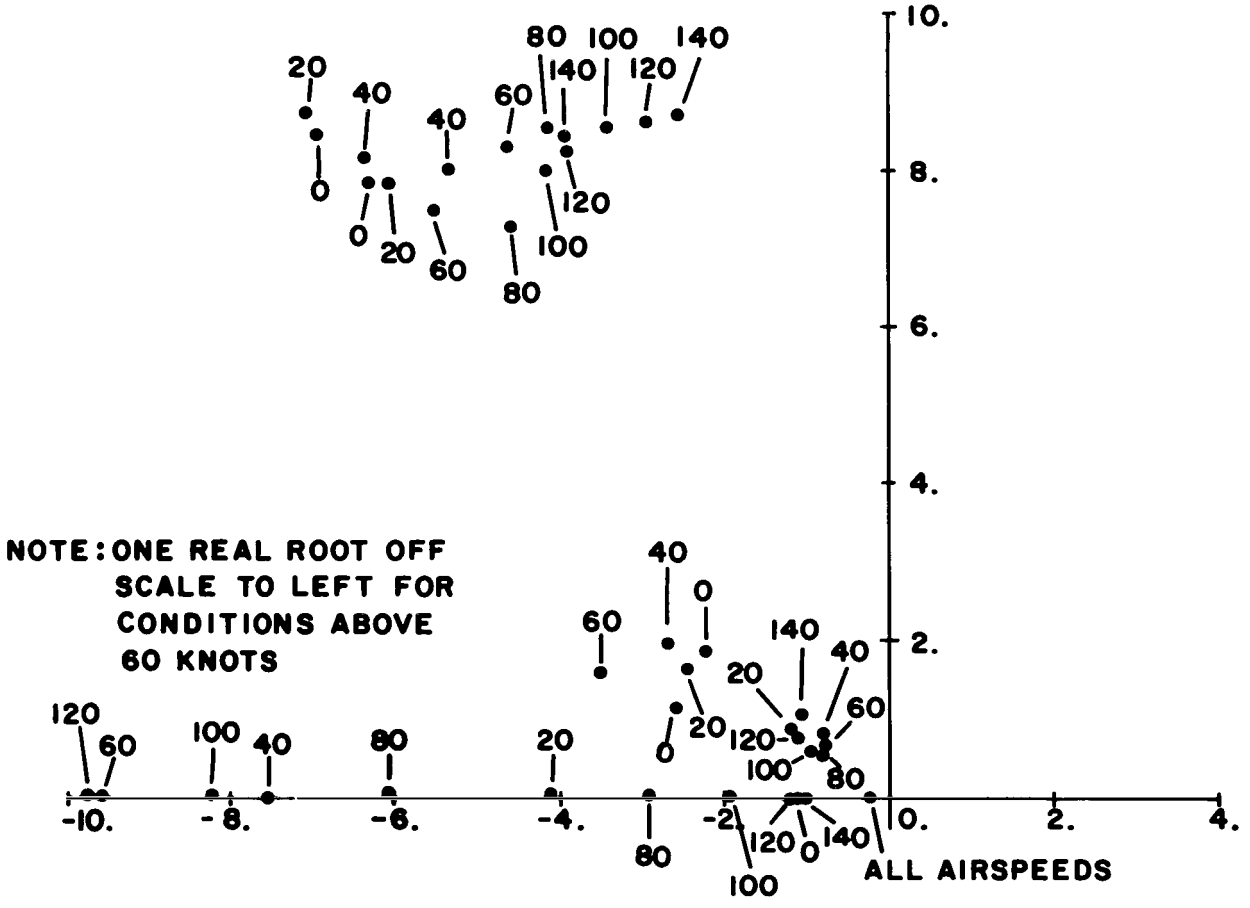

Figure 46.- Root variation of Velocity Command System as a function of airspeed (GIΘ = .2, GQ = .5, GΘ = 20., GZD = -.4, GZ = 1.6, GVX = -.016)

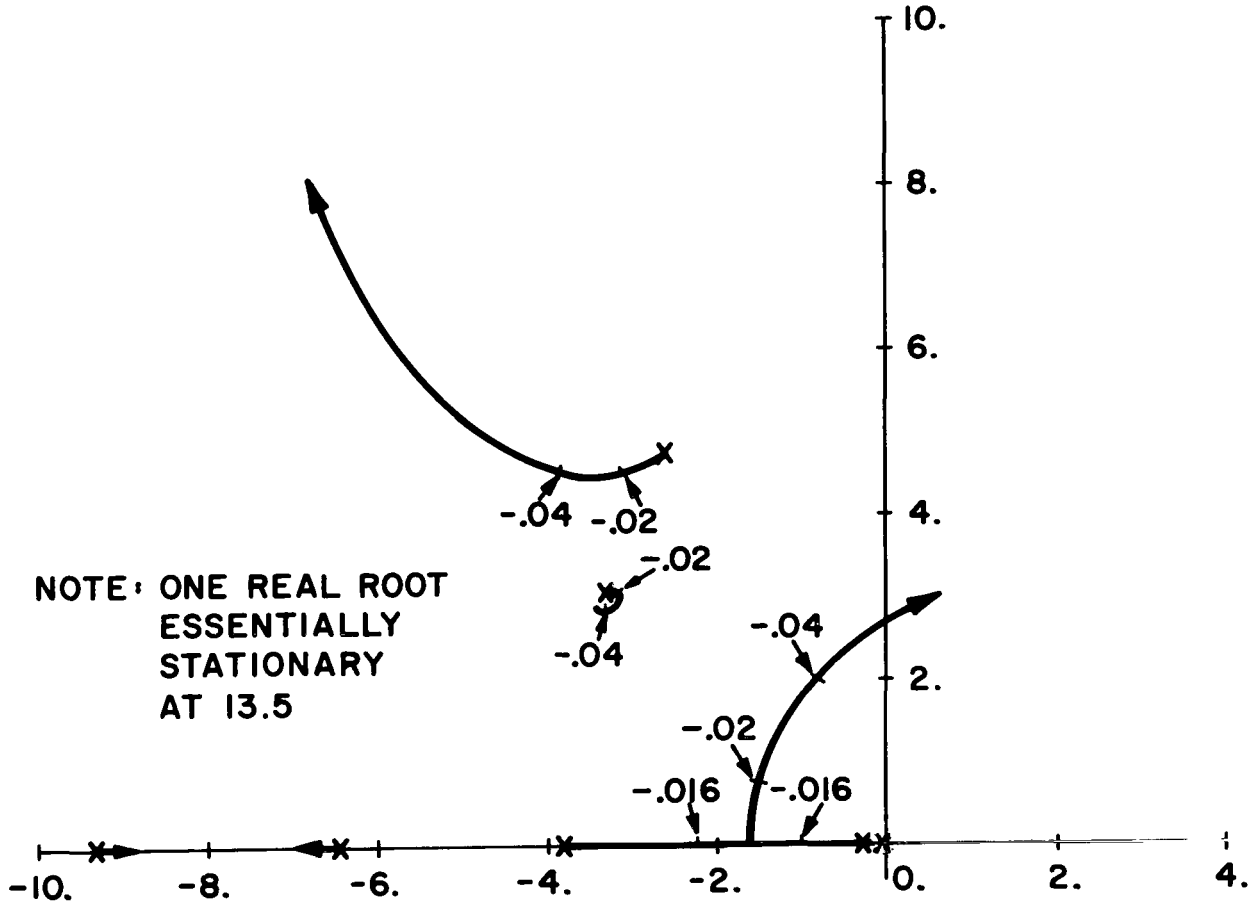

Figure 47.- Root locus of forward velocity loop of Velocity Command System at hover with sampler and hold plus computational lag ($GI\Theta$ = .2, GQ = .5, $G\Theta$ = 20., GZD = -.4, GZ = 1.6) Sample period = .032 sec

Lateral Axis (General)

The linearized lateral equations of motion of the helicopter in the ANF coordinate system are shown in Figure 48. The bare helicopter roots for Flight Condition 1 are shown in Figure 49 as a function of forward velocity. The first task of the lateral system was to simply stabilize the vehicle.

$$\begin{bmatrix} \left[S-\frac{Y_v}{m}\right] & \left[-\frac{Y_p}{m}S-\left(g\cos\theta_{TR}+\frac{Y_v}{m}W_{TR}\right)\right] & \left[\left(\frac{Y_p}{m}\sin\theta_{TR}-\frac{Y_r}{m}\cos\theta_{TR}\right)S+\frac{Y_v}{m}V_{XTR}\right] \\ \left[-\frac{L_v}{I_{xx}}\right] & \left[S^2-\frac{L_p}{I_{xx}}S-\frac{L_v}{I_{xx}}W_{TR}\right] & \left[\left(\frac{J_{xz}}{I_{xx}}\cos\theta_{TR}-\sin\theta_{TR}\right)S^2+\left(\frac{L_p}{I_{xx}}\sin\theta_{TR}-\frac{L_r}{I_{xx}}\cos\theta_{TR}\right)S+\frac{L_v}{I_{xx}}V_{XTR}\right] \\ \left[-\frac{N_v}{B}\right] & \left[\frac{J_{xz}}{B}S^2-\frac{N_p}{B}S-\frac{N_v}{B}W_{TR}\right] & \left[S^2+\left(\frac{N_p}{B}\sin\theta_{TR}-\frac{N_r}{B}\cos\theta_{TR}\right)S+\frac{N_v}{B}V_{XTR}\right] \end{bmatrix} \begin{bmatrix} \Delta V_y \\ \Delta\Phi \\ \Delta\Psi \end{bmatrix} = \begin{bmatrix} \frac{Y_\delta}{m} \\ \frac{L_\delta}{I_{xx}} \\ \frac{N_\delta}{B} \end{bmatrix} \delta$$

WHERE $V_{XTR} \triangleq U_{TR}\cos\theta_{TR} + W_{TR}\sin\theta_{TR}$, $B \triangleq I_{zz}\cos\theta_{TR} - J_{xz}\sin\theta_{TR}$ AND $S \triangleq \frac{d}{dt}$ THE LAPLACE DIFFERENTIAL OPERATOR.

Figure 48.- Lateral-directional perturbation equations

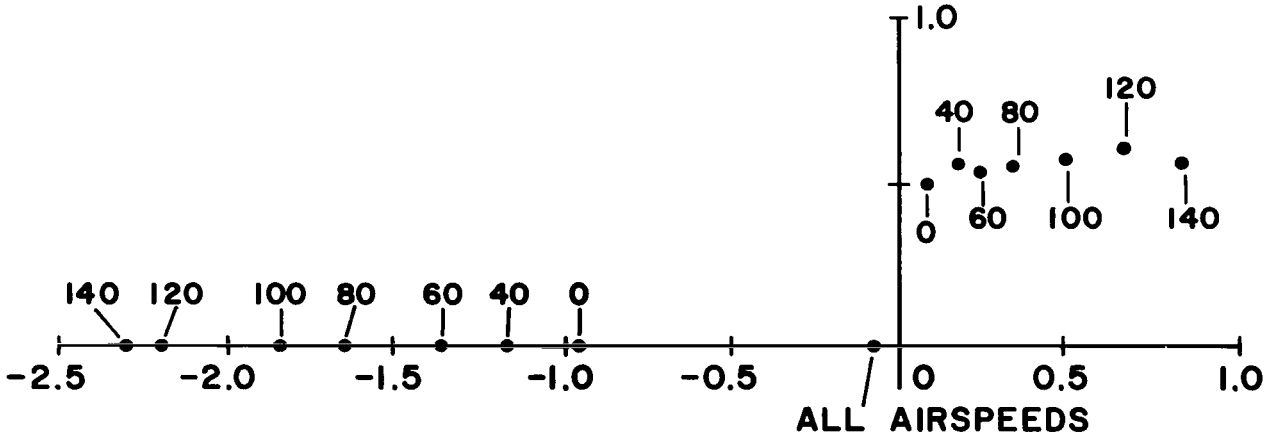

Figure 49.- Lateral-directional perturbation equation root migration as a function of airspeed (Flight Condition I)

Due to the near coincidence of the complex zeros with the complex divergent poles, as shown in Figure 50, it was apparent that the "Dutch Roll" mode could not be stabilized with simple yaw rate feedback through the rudder channel. However, the roll axis zeros shown in Figure 51 indicated that the divergent oscillatory "Dutch Roll" mode could be stabilized and satisfactorily damped by applying roll attitude plus roll rate feedback through the DAC channel. The roll axis, therefore, was considered first.

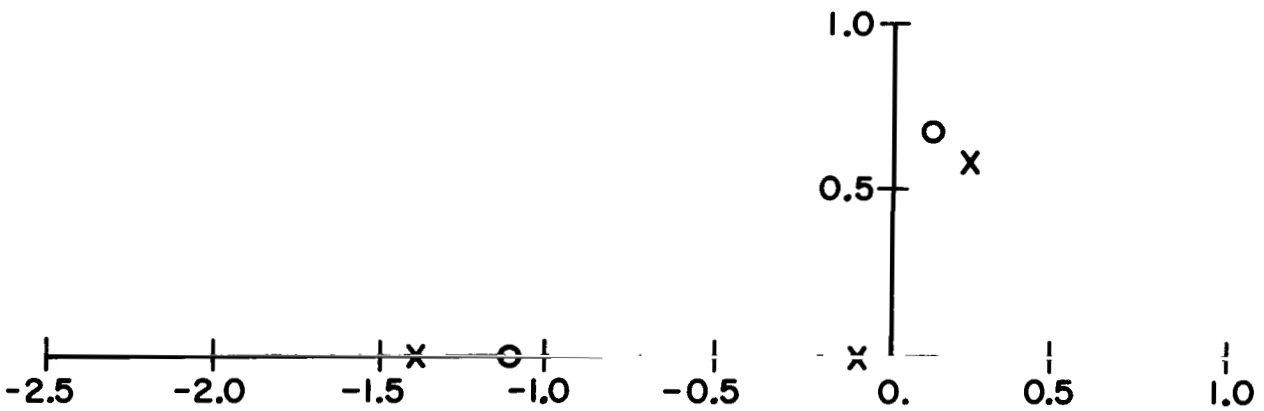

Figure 50.- $\dot{\Psi}/\delta_r$ transfer function poles and zeros at 60 knots

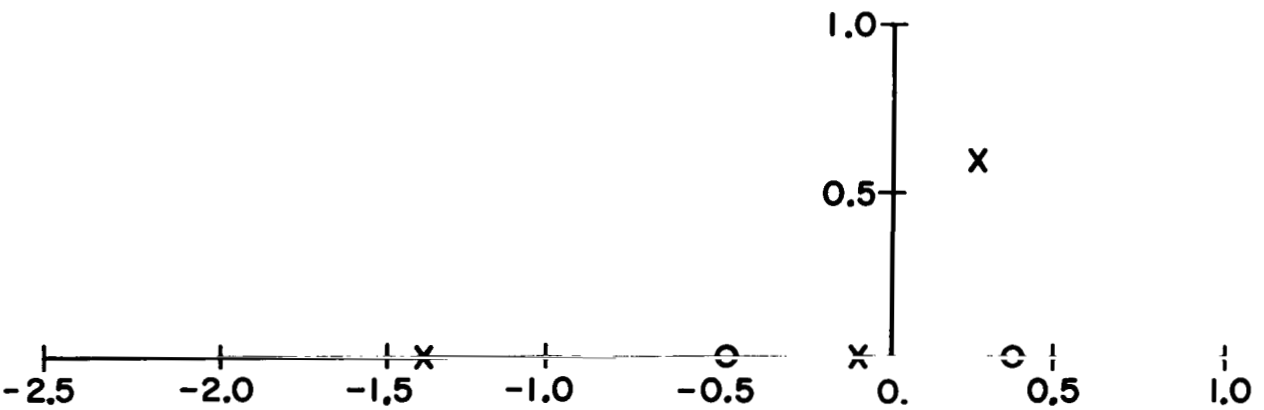

Figure 51.- Φ/δ_a transfer function poles and zeros at 60 knots

The open-loop frequency response of the roll to DAC channel at hover including actuator dynamics is shown in Figure 52. The poor low-frequency performance indication prompted the insertion of an integral plus proportional compensation in the forward loop. This assured an ideal steady-state follower system. The open-loop frequency response as a function of integrator gain, $GI\Phi$, is shown in Figure 53. $GI\Phi$ was chosen to be .35 sec^{-1}. The rationale for this selection is similar to that given in the longitudinal axis.

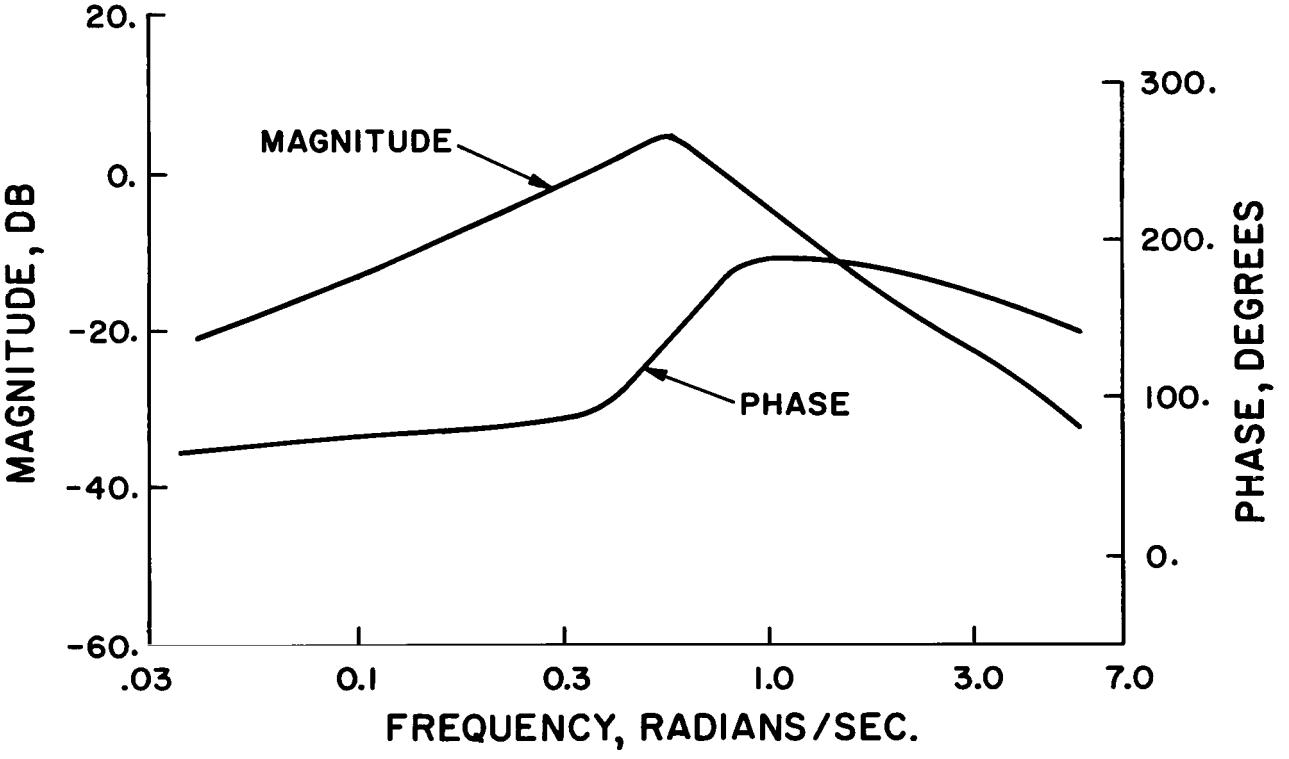

Figure 52.- Φ/DAC open-loop frequency response at hover

The roll attitude command system was then configured as shown in Figure 54. The roll rate gain TP was determined from the open-loop frequency response of the DAC to roll channel at hover with integral plus proportional compensation in the forward loop. This is shown in Figure 55. A value TP = .5 sec provided the potential for sufficient phase margin (system damping) without

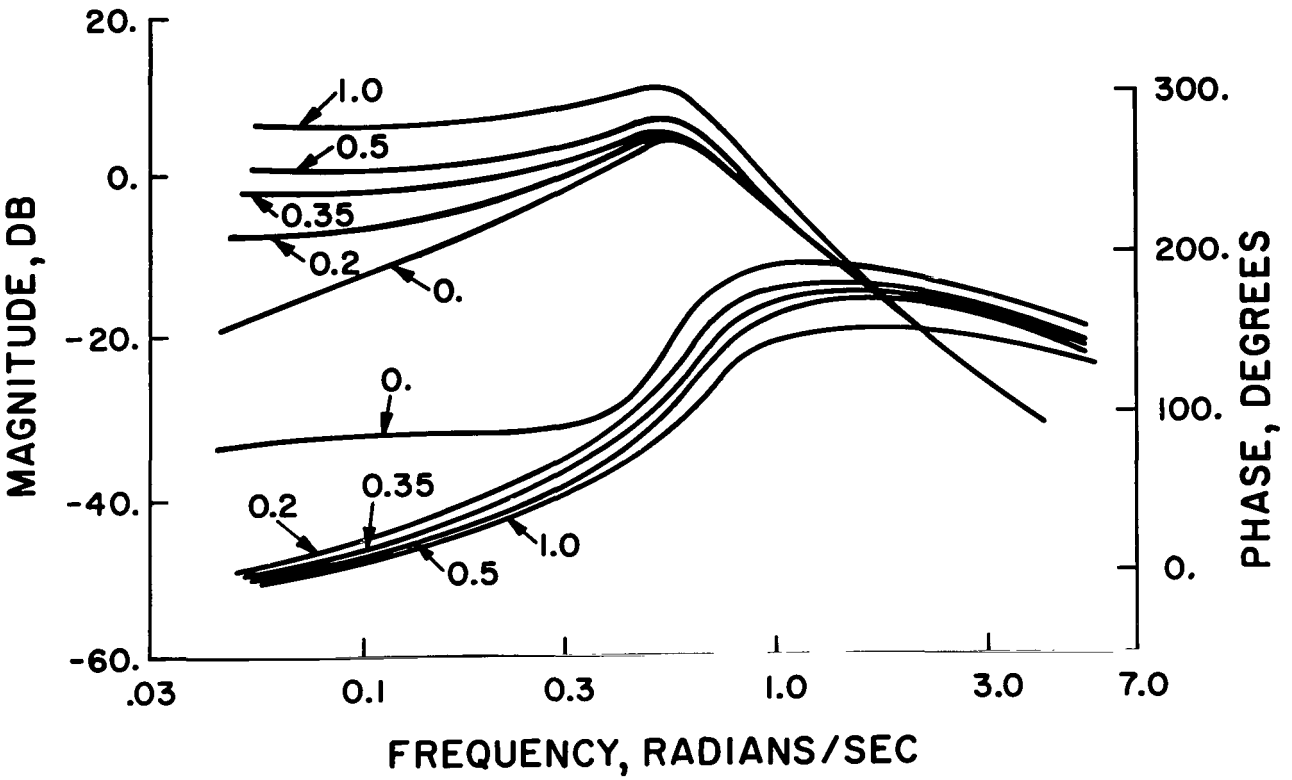

Figure 53.- Φ/DAC open-loop frequency response at hover with integral plus proportional compensation in the forward loop

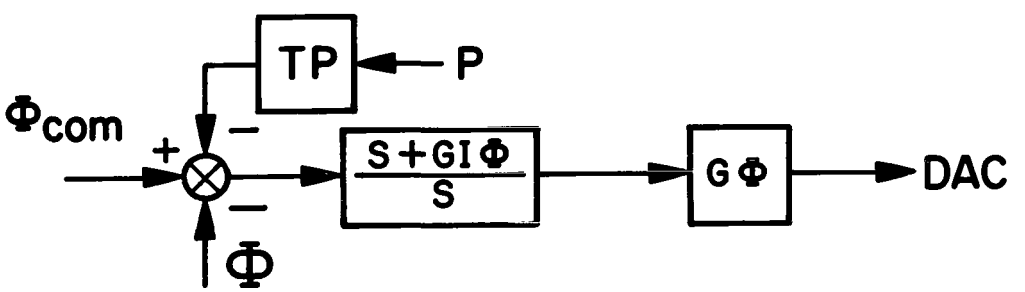

Figure 54.- Roll Altitude Command System

degrading the system bandwidth. The roll angle gain, GΦ, was determined from a root-locus plot of DAC to roll channel with GIΦ = .35 sec^{-1} and TP = .5 sec and with GΦ as the gain parameter. This is shown in Figure 56. GΦ = 15 in/rad was selected as the roll angle gain.

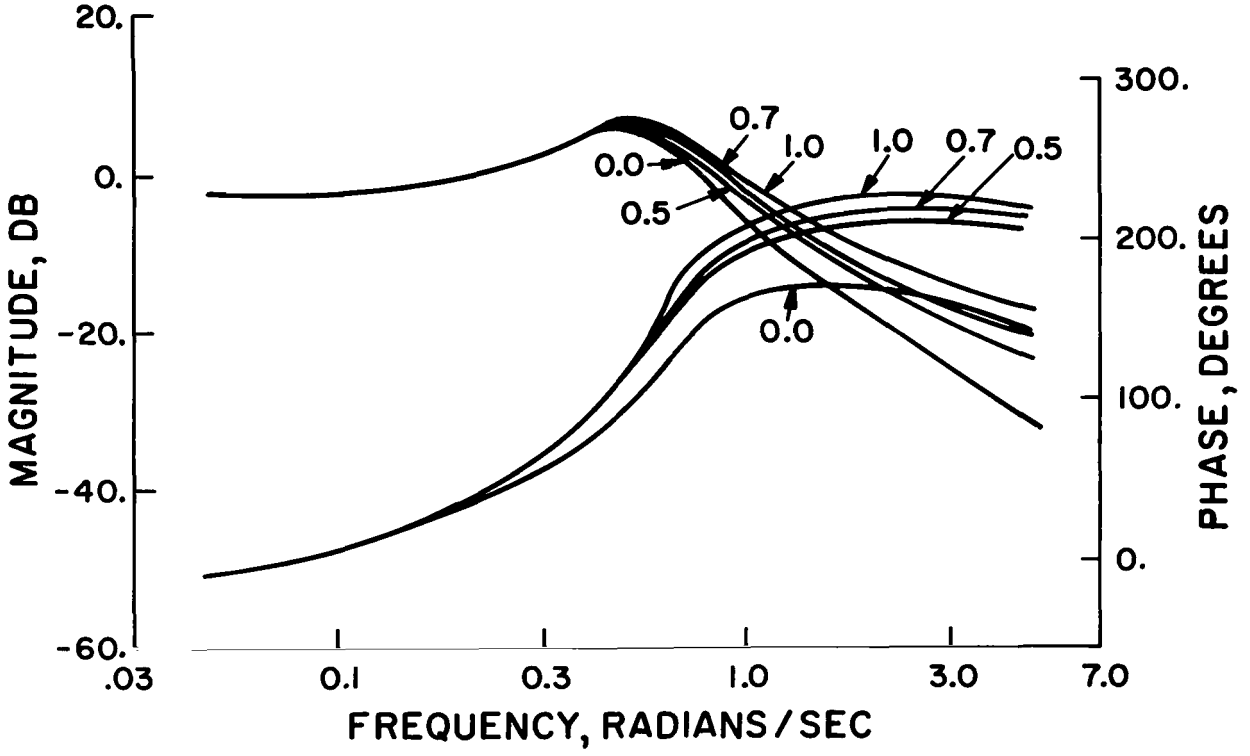

Figure 55.- Φ/DAC open-loop frequency response at hover with 0.35 integral plus proportional compensation with varying rate feedback

Note that with this gain value a slowly divergent heading mode exists and augmentation in the yaw channel was required. Stability was achieved with a yaw damper control loop as shown in Figure 57. The root locus of the rudder to yaw rate channel with GR as the gain parameter is shown in Figure 58. With GR = 30 in/(rad/sec) the heading was stable and the "Dutch Roll" damping was not affected. However, examination of the mode during cruise revealed a root in the right-half plane. This

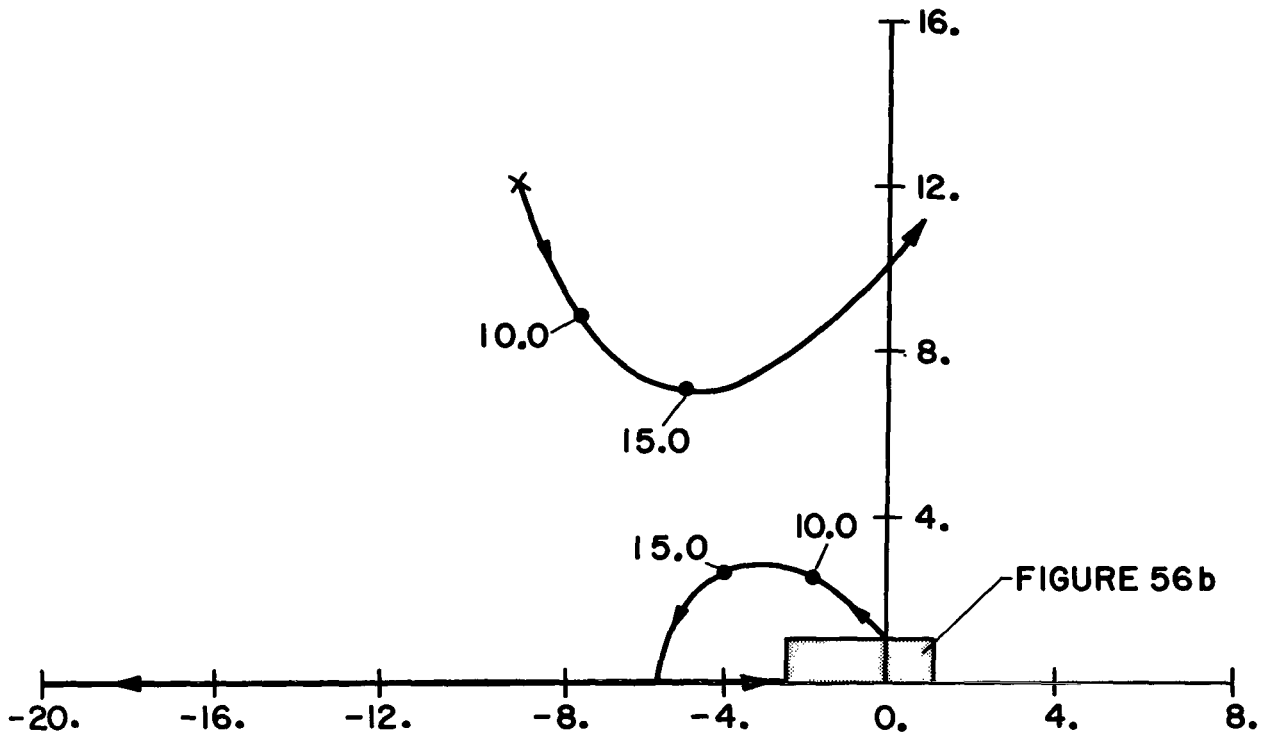

Figure 56a.- Root locus of roll attitude loop at hover (GIΦ = 0.35, TP = 0.5)

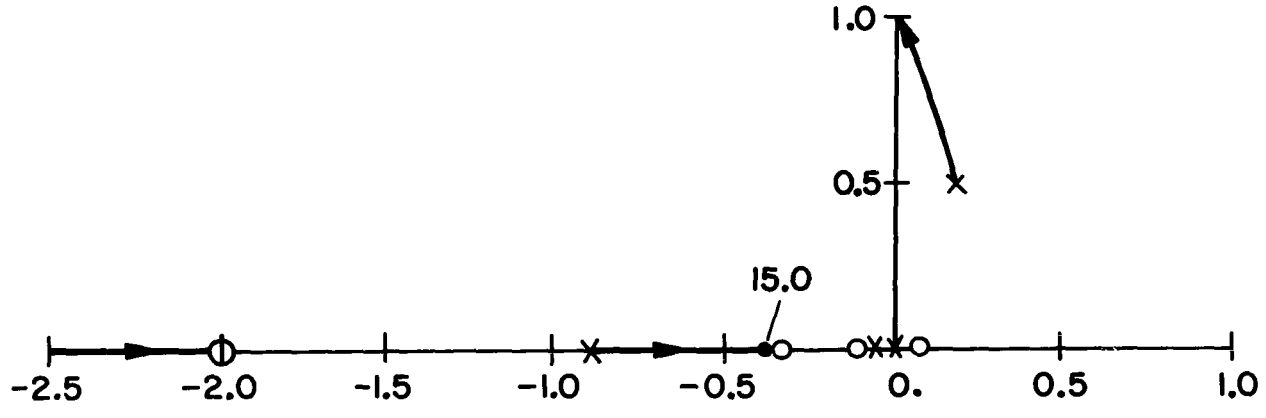

Figure 56b.- Root locus at origin of roll attitude loop at hover (GIΦ = 0.35, TP = 0.5)

instability was removed at high airspeeds with a sideslip feedback loop in the yaw channel. The Sideslip Stabilization System during cruise is shown in Figure 59. The root locus of DRC to sideslip angle channel with Gβ as the gain parameter is shown in Figure 60 for the 100-knot flight condition. Gβ = 1. (rad/sec)/rad was selected as the sideslip angle gain. Note that positive feedback was required.

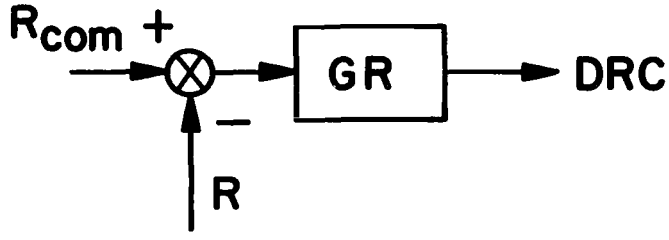

Figure 57.- Yaw Damper System

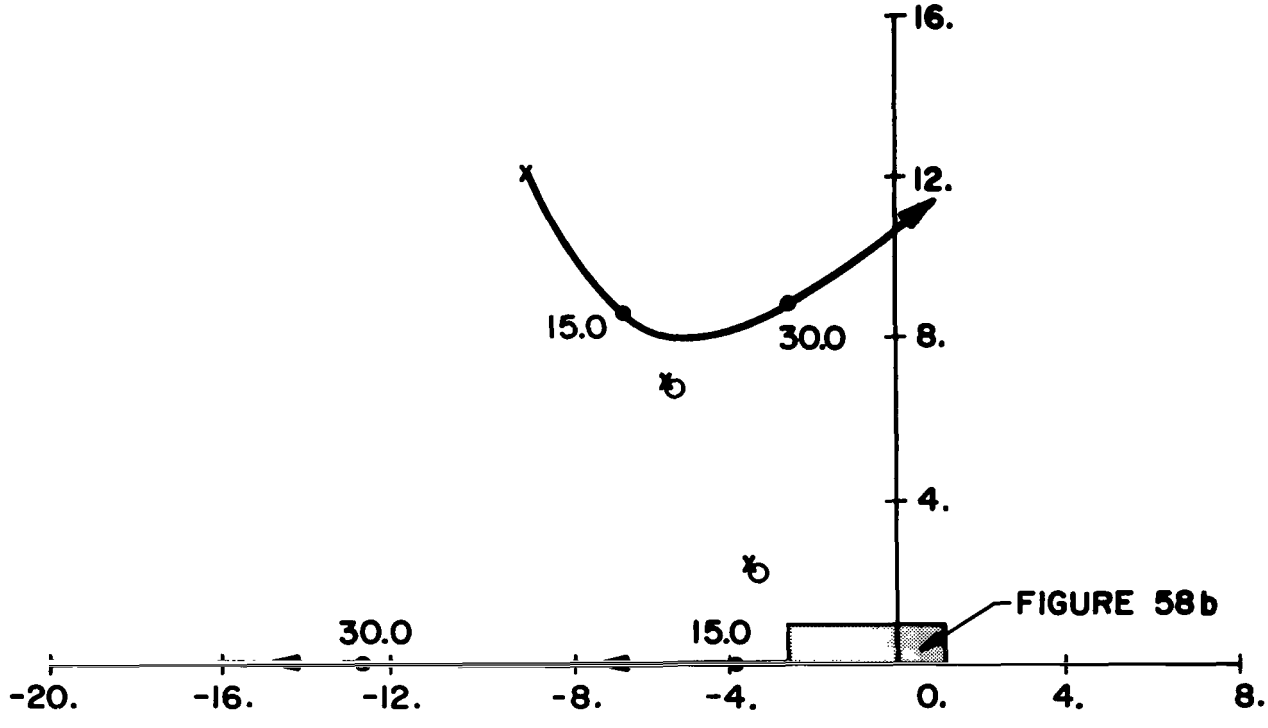

Figure 58a.- Root locus of yaw rate loop with roll loop closed at hover (GIΦ = 0.35, TP = 0.5, GΦ = 15.0)

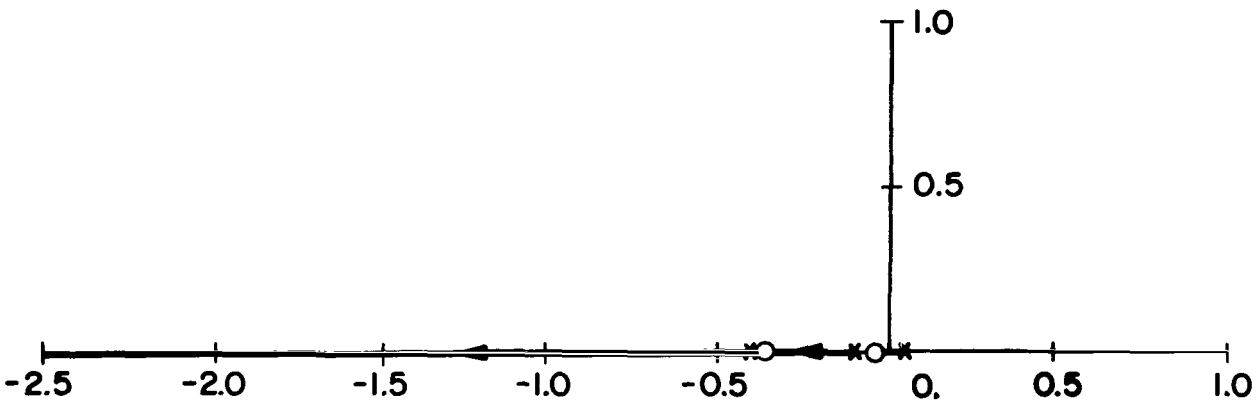

Figure 58b.- Root locus at origin of yaw rate loop with roll loop closed at hover (GIΦ = 0.35, TP = 0.5, GΦ = 15.0)

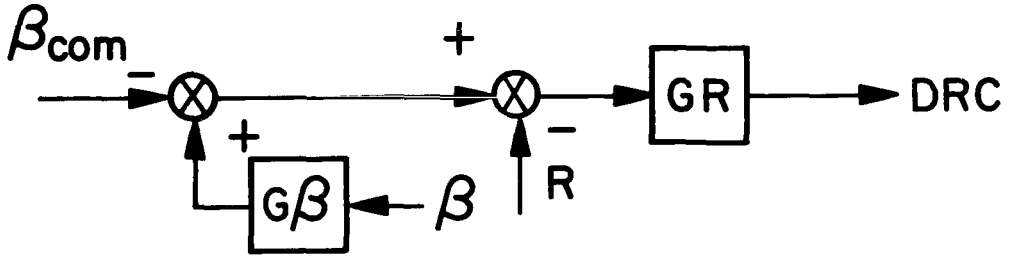

Figure 59.- Sideslip stabilization system during cruise

Attitude Command Modes I and II (Lateral Axis)

The mission requirement for the roll axis was roll attitude command. This was provided for in the basic stabilized system. The mission requirement for the yaw axis was for heading hold at low airspeeds and turn coordination at high airspeeds. To improve the turn coordination a cross-feed drive between the yaw rate and roll channels was developed assuming small angles and a simple roll angle response. The resulting cross feed-drive function became

$$R_C = \frac{g/U}{(TCFR)S + 1}\,\Phi_C \triangleq \frac{GCFR}{(TCFR)S + 1}\,\Phi_C$$

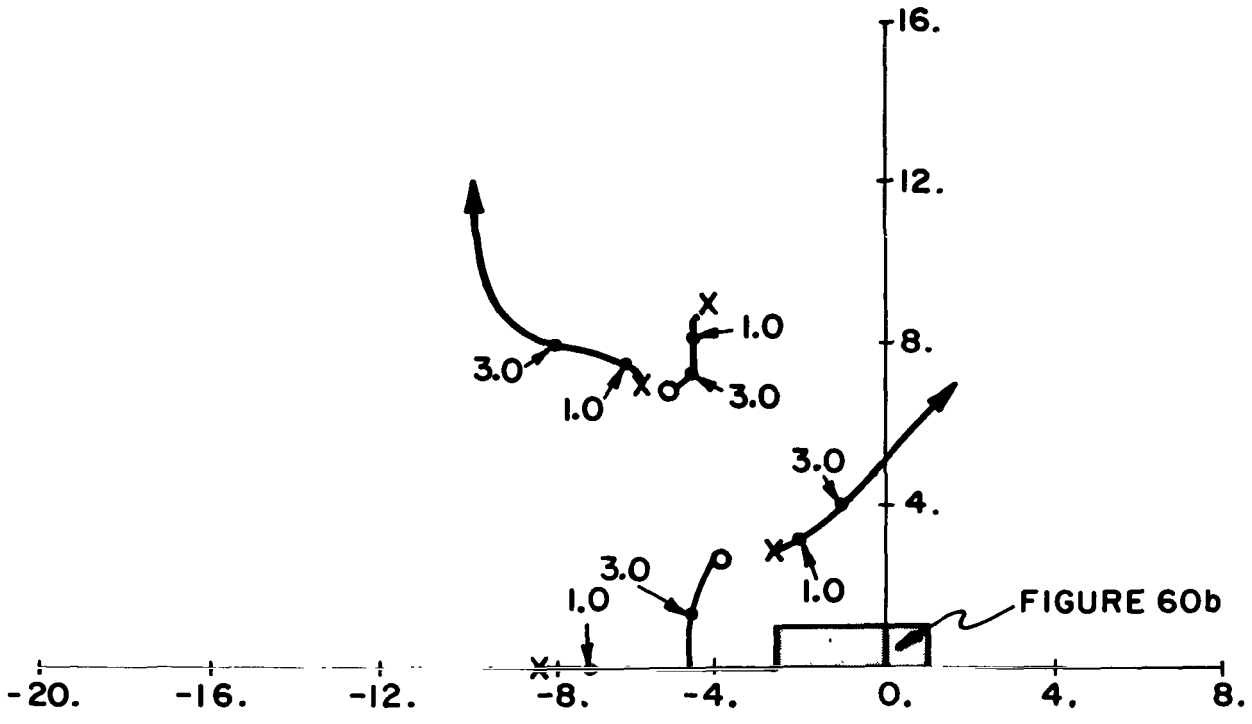

Figure 60a.- Root locus of sideslip feedback loop with roll and yaw rate loops closed at 100 knots (GIΦ = 0.35, TP = 0.5, GΦ = 15.0, GR = 30.)

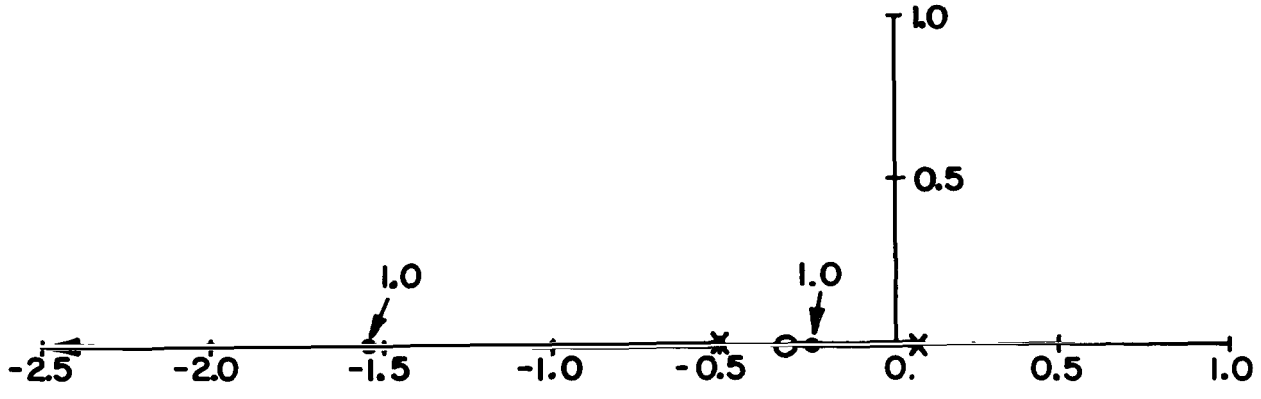

Figure 60b.- Root locus at origin of sideslip feedback loop with roll and yaw rate loops closed at 100 knots (GIΦ = 0.35, TP = 0.5, GΦ = 15.0, GR = 30.)

GCFR and TCFR were evaluated at a nominal forward velocity of 60 KTS giving GCFR = .3 and TCFR = .5 sec. The roll channel now controlled roll attitude while the crossfeed drive assisted the sideslip feedback in turning flight. The roll angle command system is shown in Figure 61.

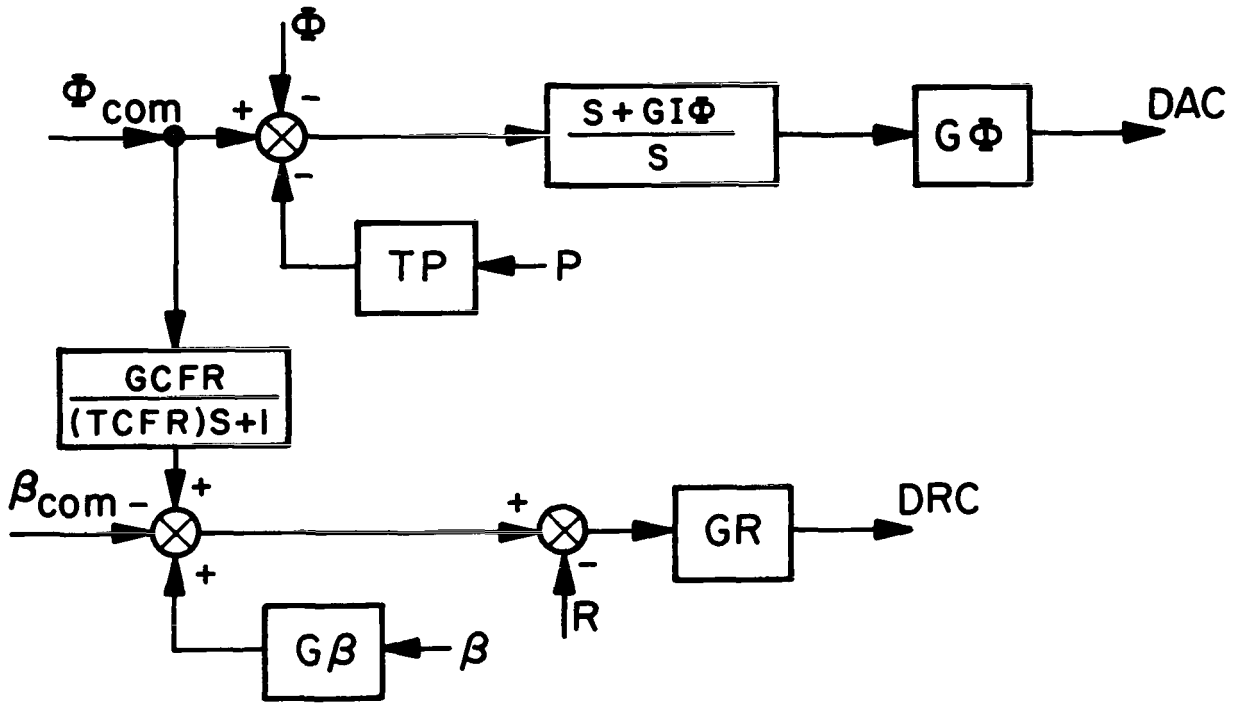

Figure 61.- Roll Attitude Command System for coordinated flight during cruise

At low airspeeds, a heading hold command system was accomplished with the system depicted in Figure 62. The heading gain, $G\psi$, was determined from a root locus of the heading channel at hover. The value $G\psi$ = 1.0 (rad/sec)/rad provided a reasonable trade off between the speed of the heading loop and the actuator damping.

Velocity Command Mode (Lateral Axis)

The velocity mode required a lateral velocity command system in the vertical heading axis system. This lateral velocity command mode was implemented with a velocity loop closure around

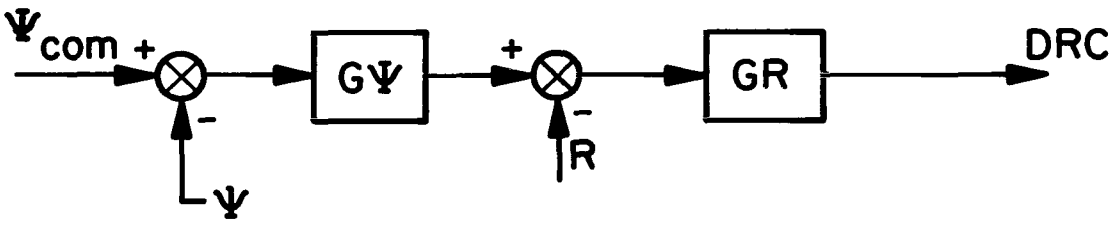

Figure 62.- Heading Command System at low speeds

the roll axis with the yaw axis remaining as in the Attitude Command Modes. This is shown in Figure 63. The root locus of the lateral velocity command loop with GVY as the gain parameter is shown in Figure 64. GVY = .02 rad/(ft/sec) was selected as the velocity gain. The root variations with airspeed of the Lateral Velocity Command System for Coordinated Flight, with GVY = .02 rad/(ft/sec), is shown in Figure 65. The roots of the system are adequately damped for all the flight velocities of interest.

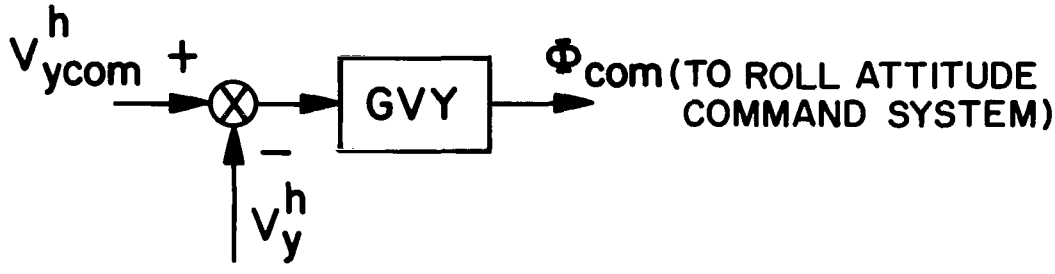

Figure 63.- Lateral Velocity Command Mode

Automatic Mode (Lateral Axis)

The lateral axis of the Automatic Mode was implemented by closing lateral position and velocity about the roll command system. This is shown in Figure 66. The root locus of this system with GY as the gain parameter is shown in the Figure 67. A gain value of GY = 0.2 (ft/sec)/ft was selected.

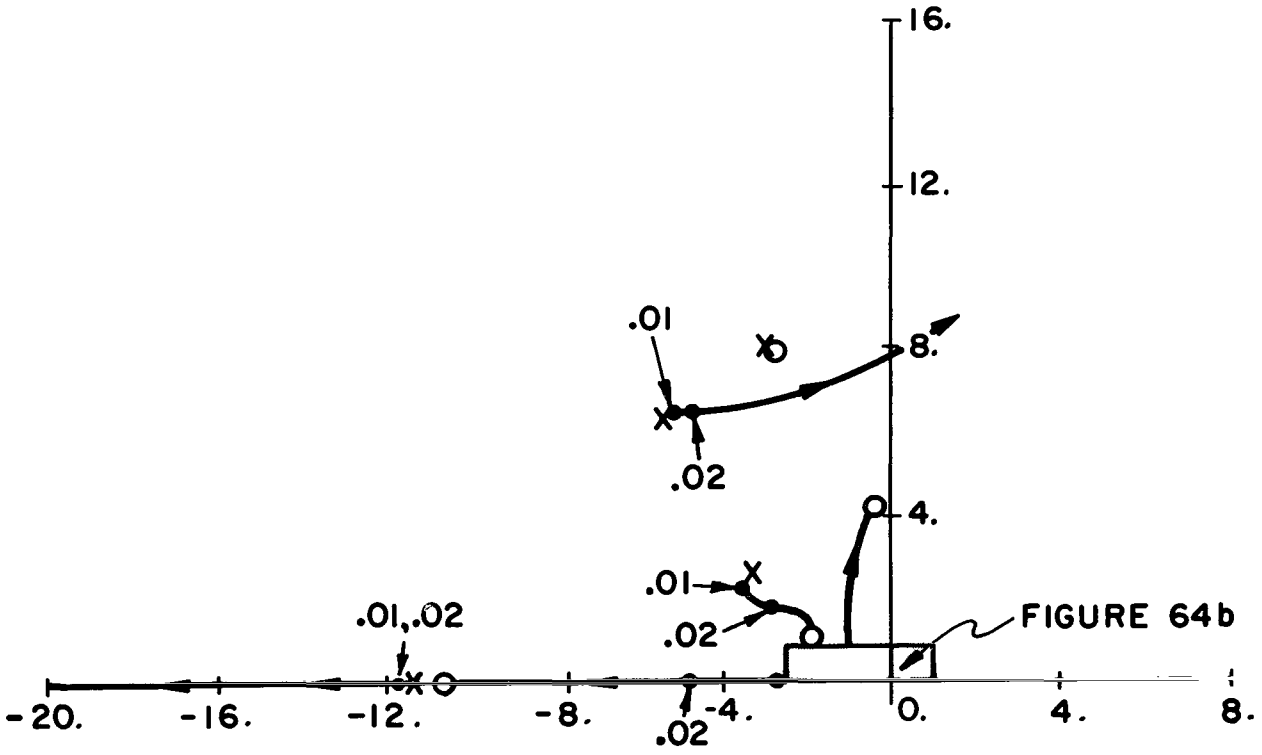

Figure 64a.- Root locus of lateral velocity loop with roll, yaw rate, and sideslip loops closed (GIΦ = 0.35, TP = 0.5, GΦ = 15.0, GR = 30., Gβ = 1.0) at 100 knots

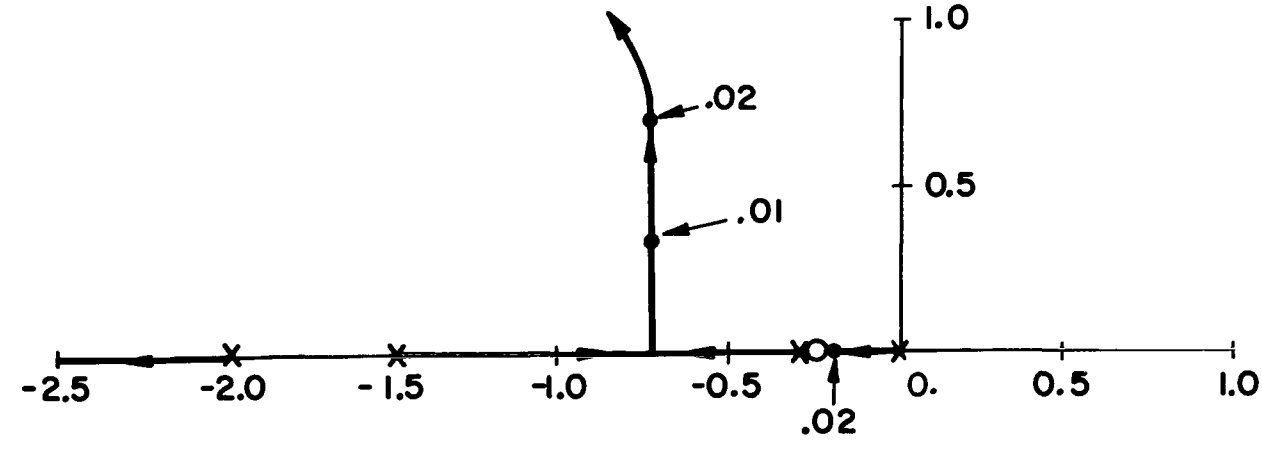

Figure 64b.- Root locus at origin of lateral velocity loop with roll, yaw rate, and sideslip loops closed (GIΦ = 0.35, TP = 0.5, GΦ = 15.0, GR = 30., Gβ = 1.0) at 100 knots

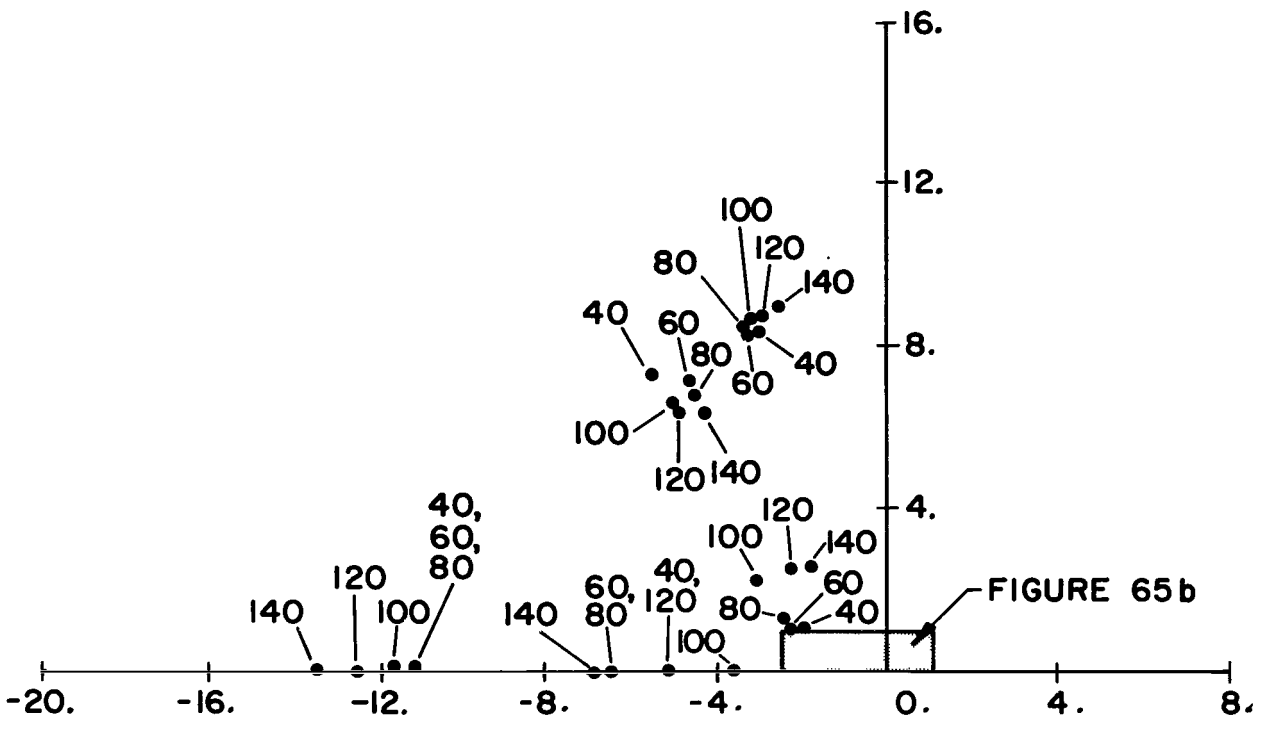

Figure 65a.- Root variations at Lateral Velocity Command System (GIΦ = 0.35, TP = 0.5, GΦ = 15., GR = 30., Gβ = 1., GVY = .02)

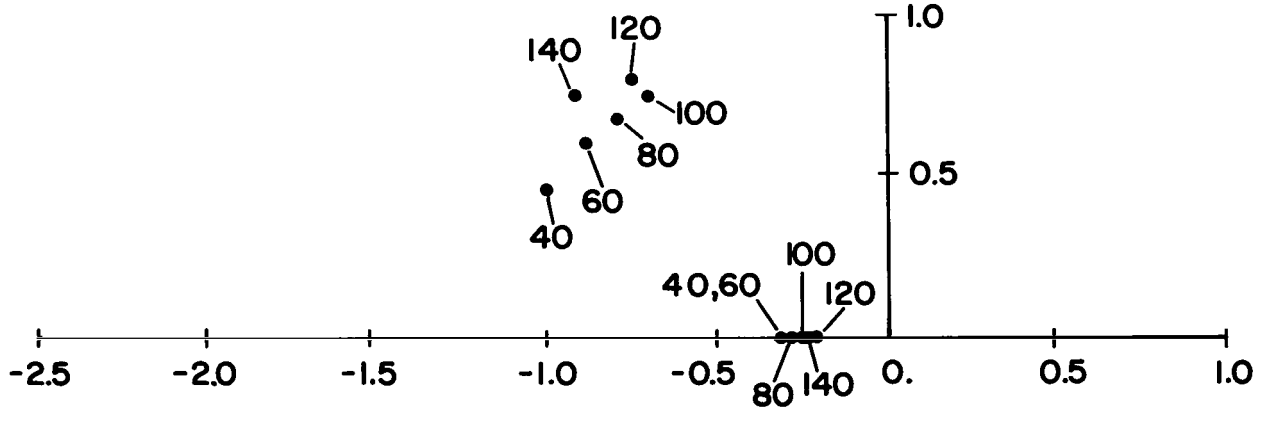

Figure 65b.- Root variations at origin of Lateral Velocity Command System (GIΦ = 0.35, TP = 0.5, GΦ = 15., GR = 30., Gβ = 1., GVY = .02)

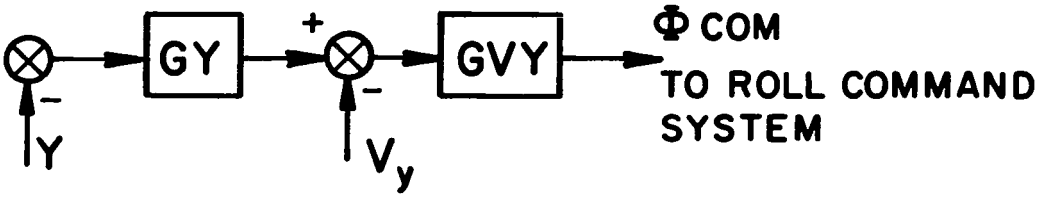

Figure 66.- Lateral position loop of the automatic modes

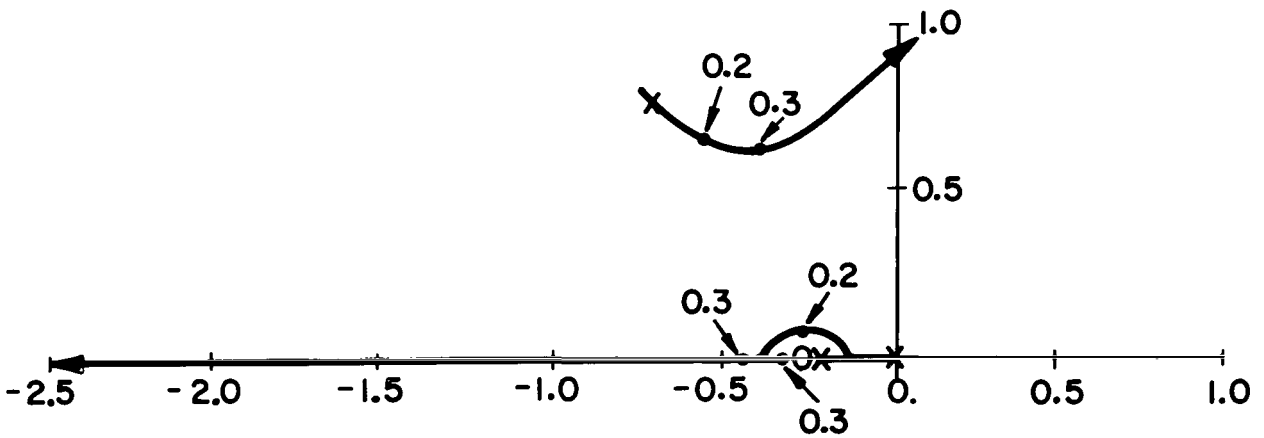

Figure 67.- Root locus at origin of lateral position feedback loop with roll, yaw, sideslip, and lateral velocity loops closed at 100 knots

Final System Definition

With the linear analysis completed, the final system was configured and the final gain selections were determined from the simulation of the flight control modes. First, the agreement of the linear analysis and the simulation was confirmed via the correspondence of crossover gains and frequencies. Then, the performance of each mode was evaluated for the gains determined from the linear analysis. This evaluation was performed with both fixed-point and mission-simulation. Most of the gains were found acceptable with the exceptions noted below.

In the longitudinal axis, the velocity system response was too fast for pilot acceptance (e.g., the helicopter pitched over

too far for small velocity commands). The effective bandwidth of this system was therefore reduced by decreasing GZD, GZ, and GVX to -0.2 in/(ft/sec), 1.3 (ft/sec)/ft, and -.01 radians/(ft/sec), respectively. In addition, an integral plus proportional compensation was found necessary in the forward velocity command system. This served as a trim adjustment on pitch attitude which is a nonlinear function of forward velocity. The integrator gain GVXI, was adjusted to -.001 radians/(ft/sec).

In the lateral axis, the bandwidth of the yaw channel was too wide, allowing high-frequency wind noise to excite this axis excessively. To avoid this, GR and Gβ were reduced to 15. in/(radian/sec) and .3 (radian/sec)/radian respectively, and at high airspeeds a first-order lag (time constant Tβ = .5 sec) was added in the sideslip feedback loop. On the other hand, the velocity command system was too slow, hence, GVY was increased to .04 radian/(ft/sec).

The lateral axis of the automatic system was adjusted during simulation to provide maximum performance in the presence of gusts. Accordingly, at low airspeeds a crossfeed drive with large time constant was inserted to absorb steady state winds through a heading change while maintaining the localizer track. This system, together with the gain values, is presented in the block diagrams.

Finally, all the stick sensitivities were determined experimentally and are listed in the block diagrams.

SIMULATION DESCRIPTION

The source of performance data for the various low-visibility landing systems was a fixed-base simulation. The simulation was comprised of a single-seat cockpit and a hybrid computer. The analog portion of the hybrid computer simulated the helicopter, while the digital portion simulated the digital multi-mode landing system. In this section, the physical characteristics of the simulator are presented; the simulated helicopter equations of motion are developed; the simulation set-up procedure is discussed; the gust model, which was implemented on the digital computer, is presented, and the technique used to determine the performance level of each approach is shown.

Cockpit Description

The simulation cockpit represented one-seat of a helicopter with the standard controls (i.e., pedals, center stick, and the collective stick to the left of the pilot). The pedals and

center stick were force centered about their respective null positions. The force gradients were:

	Measured	Acceptable Range (Ref. 10)
Longitudinal Center Stick	2.0 lb/in	0.5 to 2.0 lb/in
Lateral Center Stick	1.0 lb/in	0.5 to 2.0 lb/in
Pedals	23.0 lb	15.0 lb (max. deflection)

Although the pedal forces were slightly high, they proved acceptable to the pilots. The center stick did not have a trim capability and the collective stick had an adjustable friction setting.

The instrument panel layout (Figure 18) was based on the arrangement preferred by B.L.E.U., reference 11, with the addition of both a range and a range rate indicator. The Flight Director Indicator (Figure 3) was used to display attitude information and as a three-axis "fly to" command display. An upward displacement of the vertical tab was interpreted as a command to fly up by means of the collective stick. A displacement to the left by the vertical bar meant that the cross-range rate was to be increased to the left by means of the lateral center stick. An upward displacement of the horizontal bar was interpreted as a command to pitch up by means of the longitudinal center stick. The radar altimeter was scaled from zero to 200 ft. The Mode Selection Panel consisted of two buttons which permitted the pilot to begin his approach after the completion of the simulation setup and to return the simulator back to the setup mode at the end of the mission. The digital range indicator had a resolution of .01 nautical miles, and its full scale was 9.99 nautical miles. Figure 68 shows the overall cockpit. Although the instrument panel in the photograph is an earlier version of the one described, the two are similar.

Analog Computer Hardware

The cockpit interfaced with the Beckman 2200 analog computer which simulated the helicopter's dynamics, powered the cockpit instrumentation, and served as a transfer point for signals to and from the cockpit and the digital computer. The following list has been included to show the capability of the analog computer and the extent to which it was utilized.

Figure 68.- Simulator cockpit

Component	Number Available	Allocation
Operational Amplifiers	120	100
Integrators	72	36 & 29 as summers
Multipliers	48	28 & 10 as summers
Function Generators	12	10
Bistable Multivibrators	40	10
Monstable Multivibrators	18	5
Or Gates	114	95
Resolvers	3	3

Approximately 80 percent of the analog computer's capacity, therefore, was utilized for this simulation. Of this percentage, 60 percent was required to model the vehicle's dynamics and the remaining 40 percent was required to operate the cockpit. Associated hardware consisted of two eight-channel recorders, which were used to monitor pertinent state variables during each approach.

Digital Computer Hardware

The SDS 9300 digital computer interfaced with the analog computer and simulated the multimode digital flight control system, generated gusts, and reduced data pertinent to the performance of the helicopter during each approach. The computer cycle time was 1.75 μ seconds, add time was 2 cycles for single precision and from 6 to 11 cycles for floating point precision, multiply time was 5 cycles for single precision and 8 cycles for floating point precision. The allocation of its memory was:

Flight Control/Flight Director Laws	16K
Guidance Laws	7K
Performance Data	2K
Gust Generation	1K
Miscellaneous	2K

This was a total of 28K or 90 percent of the computer's 32K storage capacity. This storage requirement could have been significantly reduced if the program, which was written in a Fortran-like language, had been rewritten in assembly language. Associated hardware consisted of the typewriter, through which the operation of the simulator was controlled, and the line printer, for digital performance data output at the end of each approach.

Interface

The interface between the two computers consisted of analog to digital lines (ADL), digital to analog lines (DAL), interrupt lines, signal lines, and test lines. Interrupt lines permitted the analog computer to affect the digital computer by means of pulses, while the signal lines allowed the converse to take place, and the test lines permitted the digital computer to ascertain the state of certain components in the analog computer. The capacity of the interface and its utilization in this simulation are shown in the following list.

Trunk Line	Number Available	Allocation
ADL's	40	20
DAL's	40	33
Interrupt Lines	10	1
Signal Lines	16	4
Test Lines	16	11

ANALOG COMPUTER PROGRAM

Actuator System Equations

The actuator model lumped the dynamics of the electro-hydraulic actuator, the lower hydraulic power boost, the upper hydraulic power boost and all the interconnecting linkage into a second order lag. The model was the same in each of the four input channels and the equations were:

$$\ddot{A}_c + 2\zeta_a\omega_a\dot{A}_c + \omega_a^2 A_c = \omega_a^2 \text{ DCC}$$

$$\ddot{A}_e + 2\zeta_a\omega_a\dot{A}_e + \omega_a^2 A_e = \omega_a^2 \text{ DEC}$$

$$\ddot{A}_a + 2\zeta_a\omega_a\dot{A}_a + \omega_a^2 A_a = \omega_a^2 \text{ DAC} \qquad (1)$$

$$\ddot{A}_r + 2\zeta_a\omega_a\dot{A}_r + \omega_a^2 A_r = \omega_a^2 \text{ DRC}$$

where $\zeta_a = 0.6$ and $\omega_a = 15$ radians/sec. Since each actuator travel is limited, the following limits were imposed on the outputs from the actuator models.

A_c travel limited to 0. to 10.0 inches

A_e travel limited to ± 3.0 inches

A_a travel limited to ± 3.0 inches

A_r travel limited to ± 4.0 inches

Rotor System Equations

Forces and moments on the helicopter are produced by the rotors. Either the collective angle of attack of the rotor blades or the cyclic angle of attack is changed by the control input. In either case, the rotor system exhibits some dynamics before settling out at the new operating point. In this simulation, the dynamics were modelled by a second order system. This model appeared in all four channels of input.

The equations were:

$$\ddot{\delta}_c + \frac{\gamma\Omega}{8}\dot{\delta}_c + \Omega^2\delta_c = \Omega^2 A_c$$

$$\ddot{\delta}_e + \frac{\gamma\Omega}{8}\dot{\delta}_e + \Omega^2\delta_e = \Omega^2 A_e$$

$$\ddot{\delta}_a + \frac{\gamma\Omega}{8}\dot{\delta}_a + \Omega^2\delta_a = \Omega^2 A_a \qquad (2)$$

$$\ddot{\delta}_r + \frac{\gamma\Omega}{8}\dot{\delta}_r + \Omega^2\delta_r = \Omega^2 A_r$$

where the Locke Number, γ = 10. and the angular rate of the rotor Ω = 27. radians/sec.

Helicopter Equations

The simulation equation for the forward velocity of the helicopter is developed in this section. The other five equations of motion were determined in a similar fashion.

The nonlinear forward velocity equation is written:

$$\dot{U} = RV - QW + \frac{X_A}{m} - g \sin \Theta \tag{3}$$

The terms in Eq. (3) were easily implemented with the exception of X_A, which contains the aerodynamic characteristics of the helicopter. The aerodynamic force, X_A, is a function of the helicopter state variables. It was assumed that the longitudinal and lateral-directional modes were aerodynamically decoupled and, therefore, that:

$$X_A = X_A(U, Q, W, \delta_e, \delta_c). \tag{4}$$

Although not always a valid assumption for helicopters, it was believed to be valid for the CH-46C. This assumption had been made with success by other investigators for this helicopter.

The force was then expanded about a steady flight condition of level flight. For such a flight condition, the specification of forward velocity specified $Q_{TR} = 0$, $W_{TR}(U_{TR})$, $\delta_{eTR}(U_{TR})$, $\delta_{cTR}(U_{TR})$, and $\Theta_{TR}(U_{TR})$. The expanded force was then:

$$\begin{aligned} X_A = {} & X_A(U_{TR}, 0, W_{TR}(U_{TR}), \delta_{eTR}(U_{TR}), \delta_{cTR}(U_{TR})) \\ & + \frac{\partial X_A}{\partial U}(U_{TR}, 0, W_{TR}(U_{TR}), \delta_{eTR}(U_{TR}), \delta_{cTR}(U_{TR}))\ (U-U_{TR}) + \cdots \\ & + \frac{\partial X_A}{\partial \delta_c}(U_{TR}, 0, W_{TR}(U_{TR}), \delta_{eTR}(U_{TR}), \delta_{cTR}(U_{TR}))\ (\delta_c - \delta_{cTR}) \end{aligned} \tag{5}$$

In using the expanded force in the simulation, the trim point was varied as the forward speed of the aircraft varied. In this way,

the forces would always be expanded about a steady level flight condition whose velocity would be the present velocity of the helicopter. Thus, in Eq. (5) $U_{TR} = U$ dropping the second term to give:

$$X_A = X_A(U,O,W_{TR}(U),\delta_{eTR}(U),\delta_{cTR}(U))$$

$$+ \frac{\partial X_A}{\partial W}(U,O,W_{TR}(U),\delta_{eTR}(U),\delta_{cTR}(U))\ (W-W_{TR}(U)) \qquad (6)$$

$$+ \cdots + \frac{\partial X_A}{\partial \delta_c}(U,O,W_{TR}(U),\delta_{eTR}(U),\delta_{cTR}(U))\ (\delta_c-\delta_{cTR}(U))$$

The partials are the stability and control derivatives as a function of forward flight speed and were directly available. To construct the first term, the total derivative was taken with respect to U to give:

$$\frac{dX_A}{dU}(U,O,W_{TR}(U),\delta_{eTR(U)},\delta_{cTR}(U)) = \frac{\partial X_A}{\partial U}(U,O,W_{TR}(U),\delta_{eTR}(U),$$

$$\delta_{cTR}(U)) + \frac{\partial X_A}{\partial W_{TR}}(U,O,W_{TR}(U),\delta_{eTR}(U),\delta_{cTR(U)})\ \frac{\partial W_{TR}}{\partial U}(U) + \cdots \qquad (7)$$

$$+ \frac{\partial X_A}{\partial \delta_{cTR}}(U,O,W_{TR}(U),\delta_{eTR}(U),\delta_{cTR}(U))\ \frac{\partial \delta_{cTR}}{\partial U}(U)$$

The lead term is simple and was an available stability derivative, while the partials with respect to the variables $W_{TR}(U)$, $\delta_{cTR}(U)$ $\delta_{eTR}(U)$ were not available. Consequently, as a first approximation of X_A it was assumed that trim variations with forward speed were slow and that the products of partials in Eq. (7) were small when compared to the lead term. The first term of Eq. (6) was then constructed by integrating the X_u stability derivative from O to U to give:

$$X_A(U,O,W_{TR}(U),\delta_{eTR}(U),\delta_{cTR}(U)) = \int_O^U \frac{\partial X}{\partial U}(\sigma,O,W_{TR}(\sigma),$$

$$\delta_{eTR}(\sigma),\delta_{cTR}(\sigma))\ d\sigma + X_A(O,O,O,\delta_{eTR}(O),\delta_{cTR}(O)) \qquad (8)$$

The last term was found by substituting hover trim into Eq. (3) to give:

$$X_A(0,0,0,\delta_{eTR}(0),\delta_{cTR}(0)) = mg \sin \Theta_{TR}(0) \qquad (9)$$

where $\Theta_{TR}(0)$ was known. Figure 69 shows the generated trim function for the forward velocity equation, as well as those for the vertical velocity and pitching rate equations.

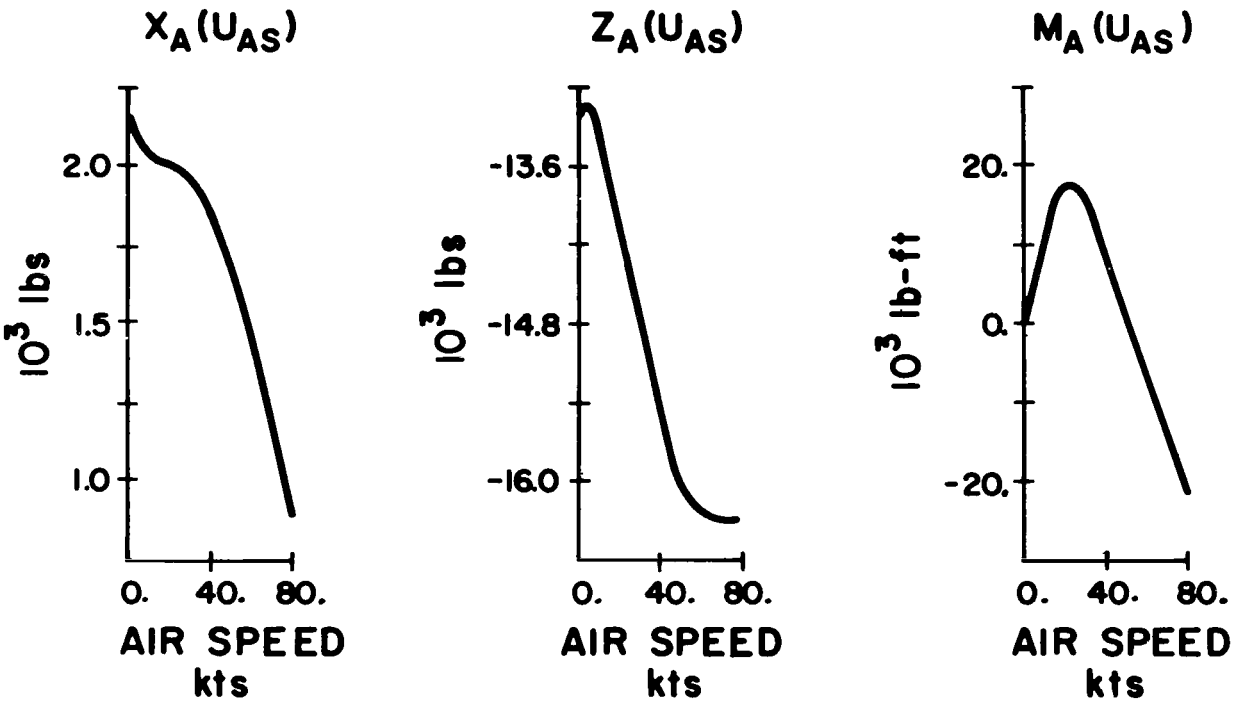

Figure 69.- Trim functions used in the simulated helicopter equations of motion

The expansion of the aerodynamic forces assumed that winds would not be present. Since this would not be the case in the simulation, U_{AS} and W_{AS} were substituted into the expansion in place of U and W where:

$$U_{AS} = U - G_{XA}$$

$$W_{AS} = W - G_{ZA}$$

The wind gusts, G_{XA} and G_{ZA} are along the body axes, X_B and Z_B.

In principal, the forward velocity equation could now be implemented on the analog computer. Hardware limitations, however, required further equation modification. In particular, the number of function generators available to simulate the velocity dependence of all the stability and control derivatives and trim variables was not sufficient. As a result, an analytic study was made to determine which derivative changes had only a minor influence on the helicopter's aerodynamic characteristics as a function of forward velocity. It was found that twenty of the thirty derivatives could be satisfactorily held at their hover values. These derivatives are listed in Table II. Figures 70(a) and (b) present the plots of the remaining velocity dependent derivatives.

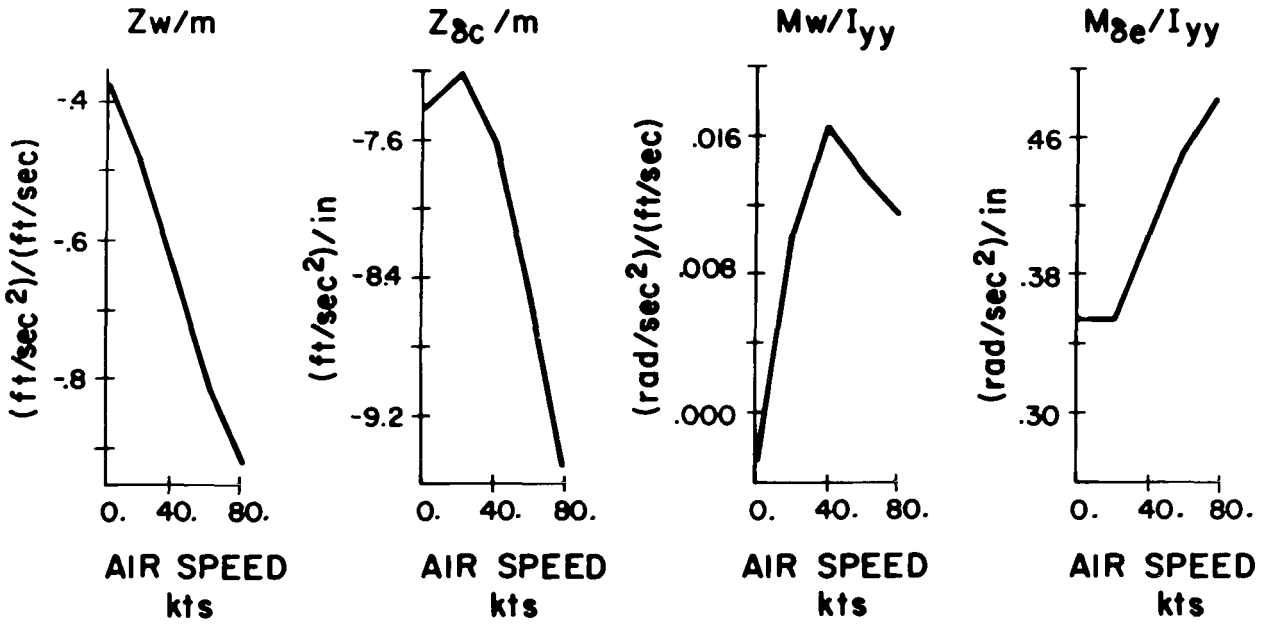

Figure 70a.- Air speed dependent coefficients used in the simulated helicopter equations of motion

TABLE II.- VALUES OF THE AIR SPEED INDEPENDENT COEFFICIENTS USED IN THE SIMULATED HELICOPTER EQUATIONS OF MOTION

X_w/m	.05449 $(ft/sec^2)/(ft/sec)$
X_q/m	.60185 $(ft/sec^2)/(rad/sec)$
$X_{\delta e}/m$	.17696 $(ft/sec^2)/in$
$X_{\delta c}/m$	1.2048 $(ft/sec^2)/in$
Z_q/m	-.71511 $(ft/sec^2)/(rad/sec)$
$Z_{\delta e}/m$	-.00407 $(ft/sec^2)/in$
M_q/I_{yy}	-.73173 $(rad/sec^2)/(rad/sec)$
$M_{\delta c}/I_{yy}$	-.04765 $(rad/sec^2)/in$
Y_v/m	-.02664 $(ft/sec^2)/(ft/sec)$
Y_p/m	-.76514 $(ft/sec^2)/(rad/sec)$
Y_r/m	-.12517 $(ft/sec^2)/(rad/sec)$
$Y_{\delta a}/m$	.99794 $(ft/sec^2)/in$
$Y_{\delta r}/m$	.14652 $(ft/sec^2)/in$
L_p/I_{xx}	-.50730 $(rad/sec^2)/(rad/sec)$
L_r/I_{xx}	-.02297 $(rad/sec^2)/(rad/sec)$
$L_{\delta a}/I_{xx}$	.46536 $(rad/sec^2)/in$
$L_{\delta r}/I_{xx}$	-.12638 $(rad/sec^2)/in$
N_p/I_{zz}	-.01831 $(rad/sec^2)/(rad/sec)$
$N_{\delta a}/I_{zz}$	.03001 $(rad/sec^2)/in$
$N_{\delta r}/I_{zz}$	.17584 $(rad/sec^2)/in$

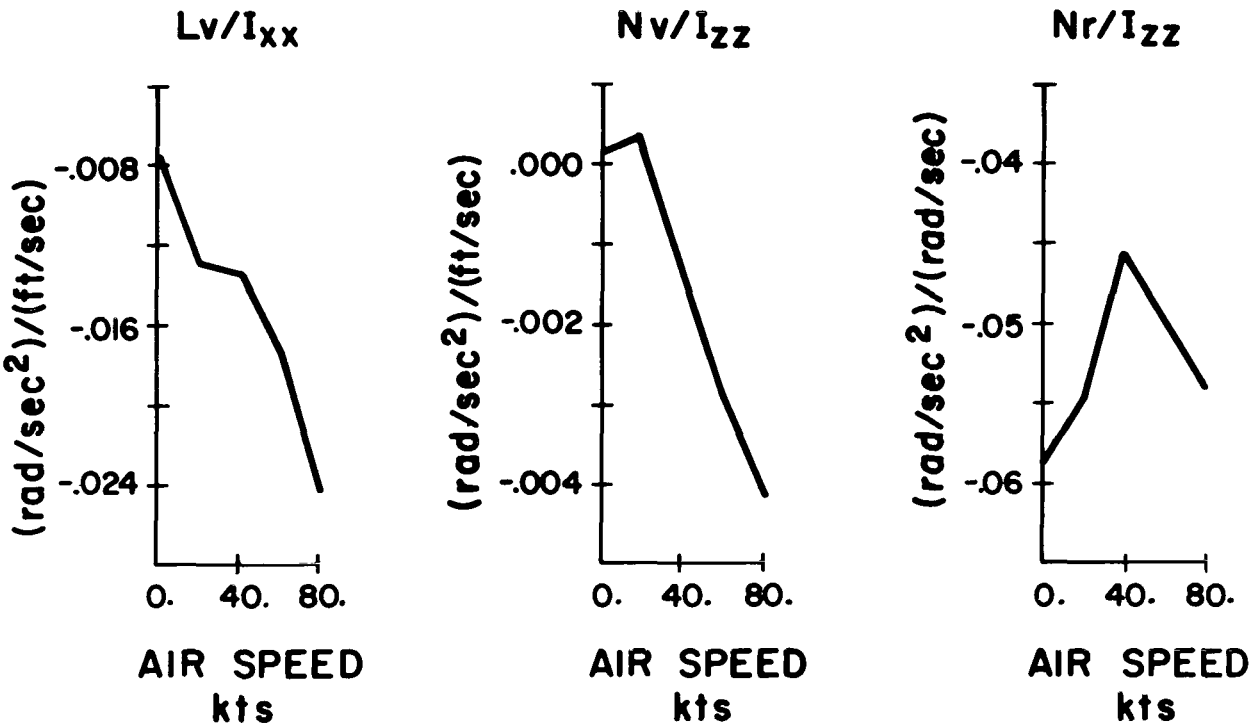

Figure 70b.- Air speed dependent coefficients used in the simulated helicopter equations of motion

As one further step in reducing the number of function generators required, the trim variables $W_{TR}(U)$, $\delta_{cTR}(U)$, $\delta_{eTR}(U)$ were also set to their hover values. The effects of neglecting these variations is discussed later in the section. The final form of the forward velocity equation used in the simulation is presented along with the other helicopter equations in Eq. 10.

$$\dot{U} = \frac{1}{m}\left[X_A(U_{AS}) + X_q(O)Q + X_w(O)(W_{AS} - W_{TR}(O)) + X_{\delta e}(O)(\delta_e - \delta_{eTR}(O)) + X_{\delta c}(O)(\delta_c - \delta_{cTR}(O))\right] + RV - QW - g \sin\Theta$$

$$\dot{W} = \frac{1}{m}\left[Z_A(U_{AS}) + Z_q(O)Q + Z_w(U_{AS})(W_{AS} - W_{TR}(O)) + Z_{\delta e}(O)(\delta_e - \delta_{eTR}(O)) + Z_{\delta c}(O)(\delta_c - \delta_{cTR}(O))\right] + QU - PV + g \cos\Phi \cos\Theta$$

$$\dot{Q} = \frac{1}{I_{YY}} [M_A(U_{AS}) + M_q(O)Q + M_w(U_{AS})(W_{AS} - W_{TR}(O))$$
$$+ M_{\delta e}(U_{AS})(\delta_e - \delta_{eTR}(O)) + M_{\delta c}(O)(\delta_c - \delta_{cTR}(O))]$$

$$\dot{V} = \frac{1}{m} [Y_v(O)V_{AS} + Y_P(O)P + Y_r(O)R + Y_{\delta a}(O)\delta_a + Y_{\delta r}(O)\delta_r]$$
$$+ PW - RU + g \sin \Phi \cos \Theta$$

$$\dot{P} = \frac{1}{I_{XX}} [I_{XZ}\dot{R} + L_P(O)P + L_r(O)R + L_v(U_{AS})V_{AS}$$
$$+ L_{\delta a}(O)\delta_a + L_{\delta r}(O)\delta_r]$$

$$\dot{R} = \frac{1}{I_{ZZ}} [I_{XZ}\dot{P} + N_P(O)P + N_r(U_{AS})R + N_v(U_{AS})V_{AS}$$
$$+ N_{\delta a}(O)\delta_a + N_{\delta r}(O)\delta_r]$$

(10)

The helicopter variables along the moving trim are defined as:

$$U_{TR} = U_{AS} \qquad \delta_{eTR}(U_{AS}) = \delta_{eTR}(O)$$

$$V_{TR}(U_{AS}) = O \qquad \delta_{cTR}(U_{AS}) = \delta_{cTR}(O)$$

$$W_{TR}(U_{AS}) = W_{TR}(O) = O \qquad \delta_{aTR}(U_{AS}) = O$$

$$P_{TR}(U_{AS}) = O \qquad \delta_{rTR}(U_{AS}) = O$$

$$Q_{TR}(U_{AS}) = O$$

$$R_{TR}(U_{AS}) = O$$

(11)

The wind gusts along the X_B, Y_B, and Z_B body axes are G_{XA}, G_{YA}, and G_{ZA}, respectively. The aircraft to air mass velocities are defined as

$$U_{AS} = U - G_{XA}$$

$$V_{AS} = V - G_{YA}$$

$$W_{AS} = W - G_{ZA}$$

(12)

The state of the helicopter at the beginning of each approach is

$$U_{IC} = U_O \qquad P_{IC} = O$$

$$W_{IC} = W_O \qquad Q_{IC} = O$$

$$V_{IC} = O \qquad R_{IC} = O$$

(13)

The approximations made during the development of the simulation version of the helicopter equations were verified. Two approximations that were made during the equation development would result in an unknown degree of simulation trim error. First, the trim terms X_A, Z_A, and M_A were constructed by integrating the X_u, Z_u, and M_u stability derivatives respectively from O to U. The second approximation came about when the velocity dependent trim variables $W_{TR}(U_{TR})$, $\delta_{eTR}(U_{TR})$, $\delta_{cTR}(U_{TR})$ were set to their hover values. To check the net effect of these two approximations on trim, simulation trim values were generated and compared against their true values. Figure 71 shows the comparison. Agreement between the simulated and the actual trim values was satisfactory.

Next, the approximation of the majority of the velocity dependent stability and control derivatives by their hover values would have an effect on the simulated aerodynamic characteristics of the helicopter. The primary aerodynamics of the uncontrolled vehicle are determined by the pole-zero locations of the open loop transfer function associated with each input channel, namely: Θ/δ_e, W/δ_c, Φ/δ_a, and R/δ_r. Figures 72 through 77 show a comparison of the aerodynamics (location of the poles and zeros) of the simplified aircraft model used in the simulation with those of the original model for each of these transfer functions. There was satisfactory agreement with respect to both the actual location of the roots and their migratory trends as a function of forward velocity. The exception to this general agreement was in the case of the numerator associated with W/δ_c (Figure 74). Although the simplified model obviously did not conform to the original in

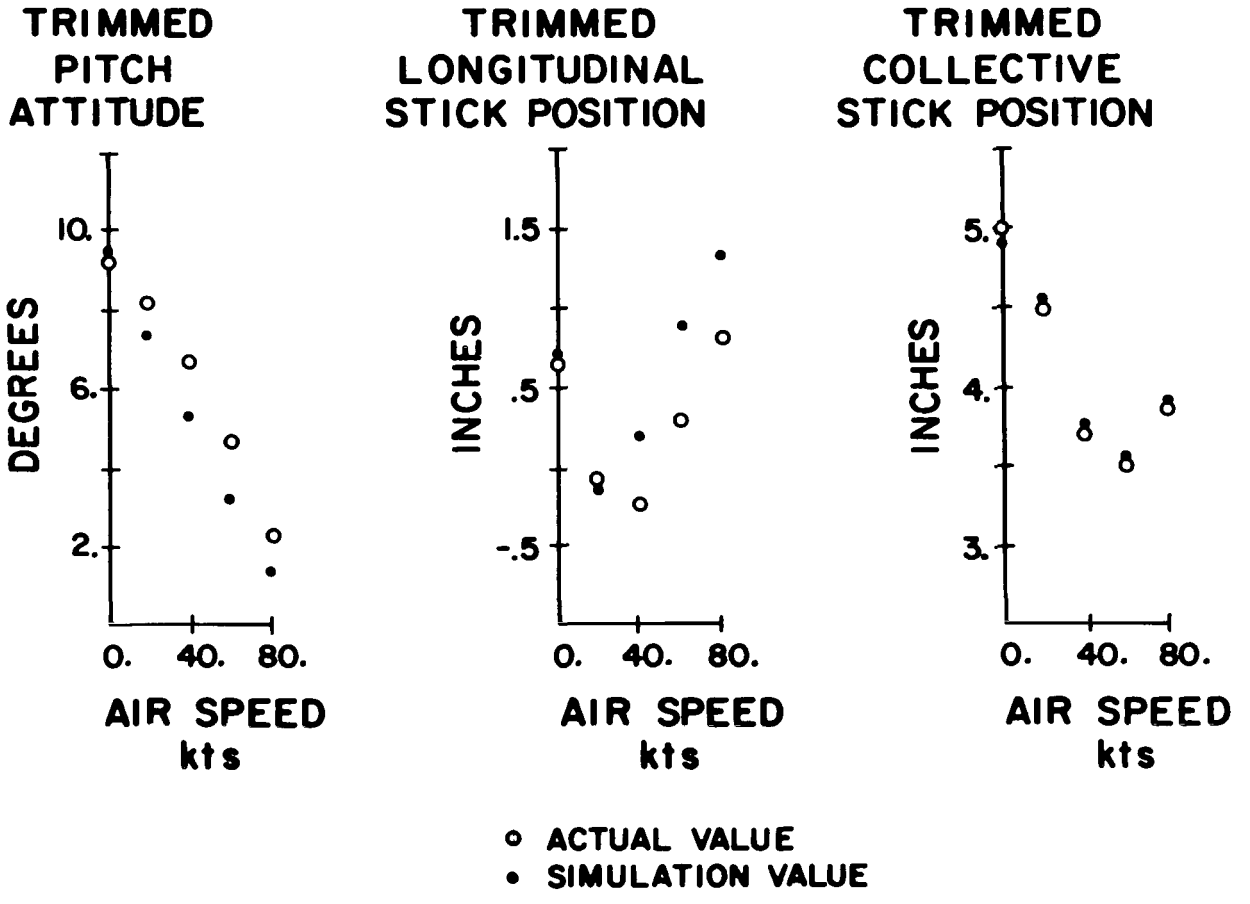

Figure 71.- Comparison of simulation trim values with the actual trim values for the CH-46C helicopter

this case, the general overall agreement of the simplified model with the original led to the acceptance of this discrepancy.

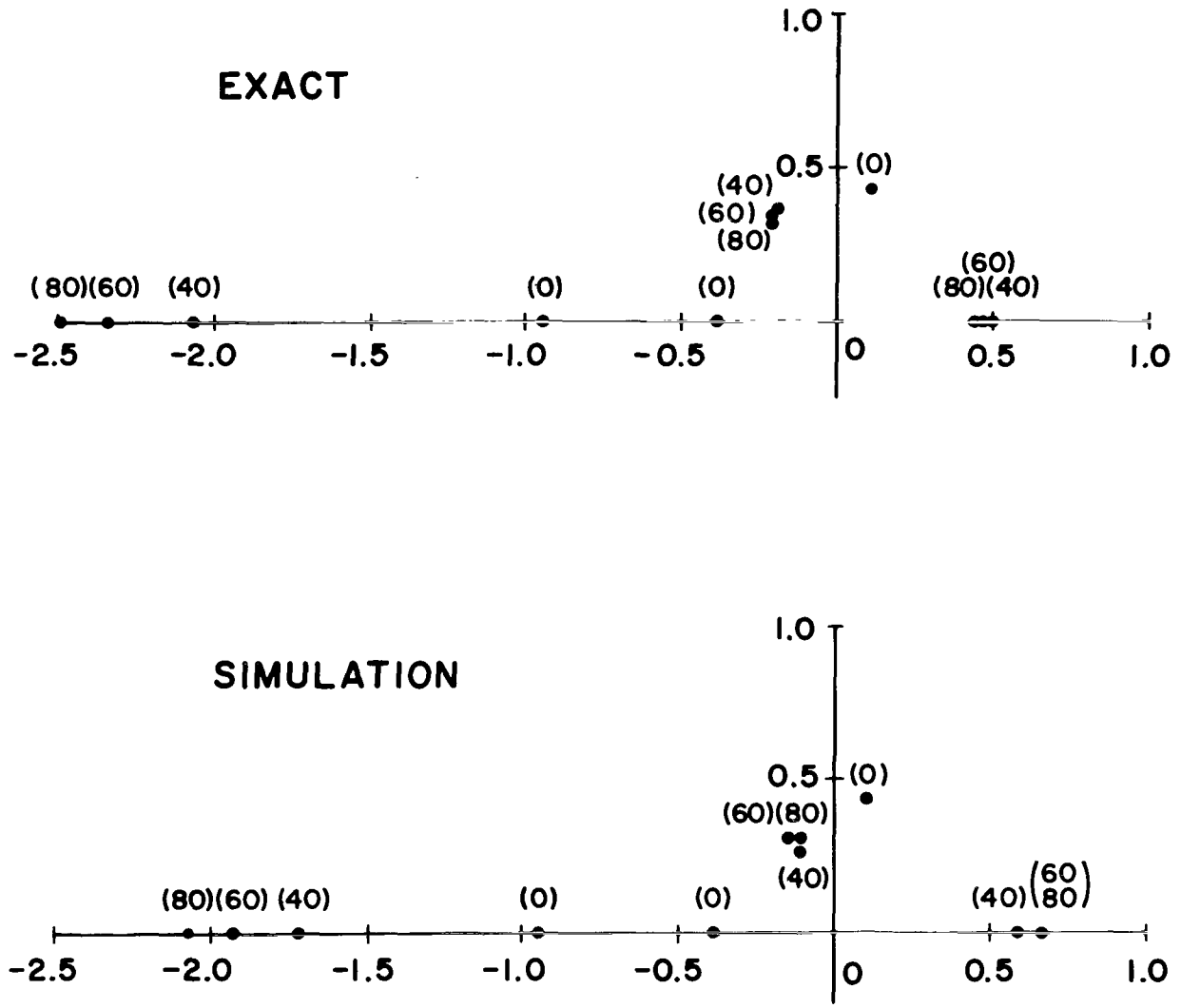

Figure 72.- The roots of the denominator associated with the longitudinal motions of the CH-46C helicopter as a function of air speed in knots

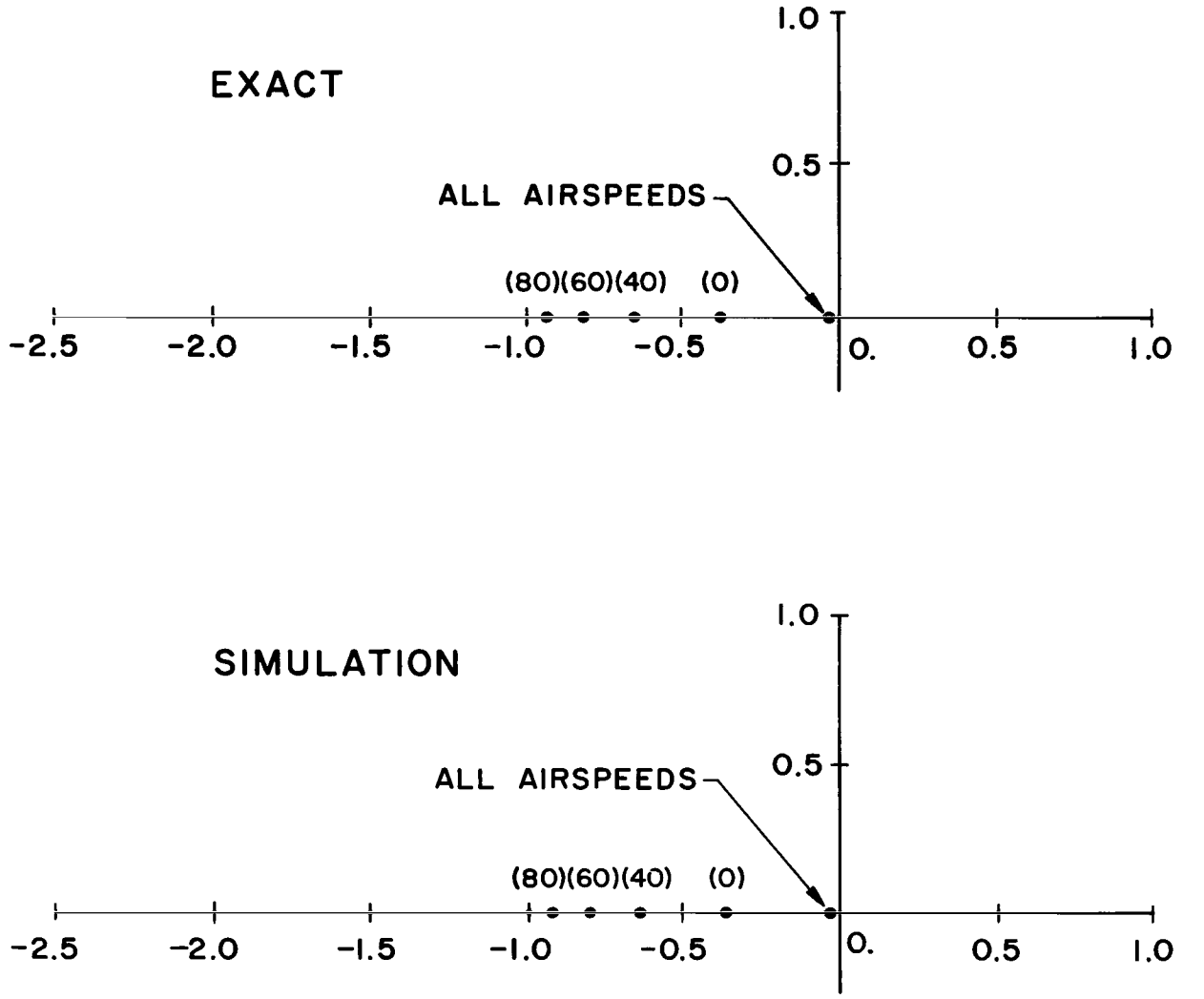

Figure 73.- The roots of the numerator associated with the pitch channel (attitude) of the CH-46C helicopter as a function of air speed in knots

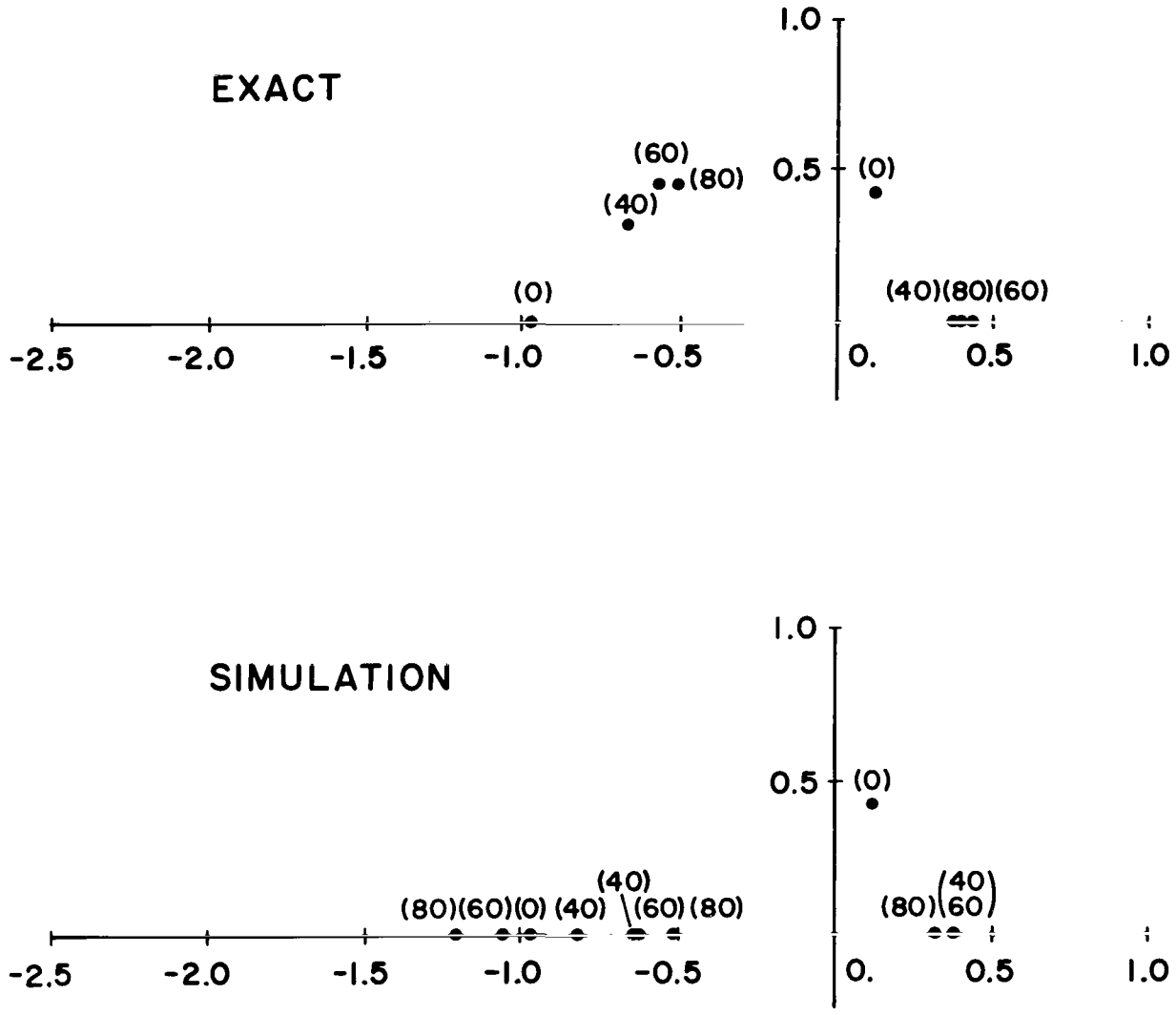

Figure 74.- The roots of the numerator associated with the power channel (vertical velocity) of the CH-46C helicopter as a function of air speed in knots

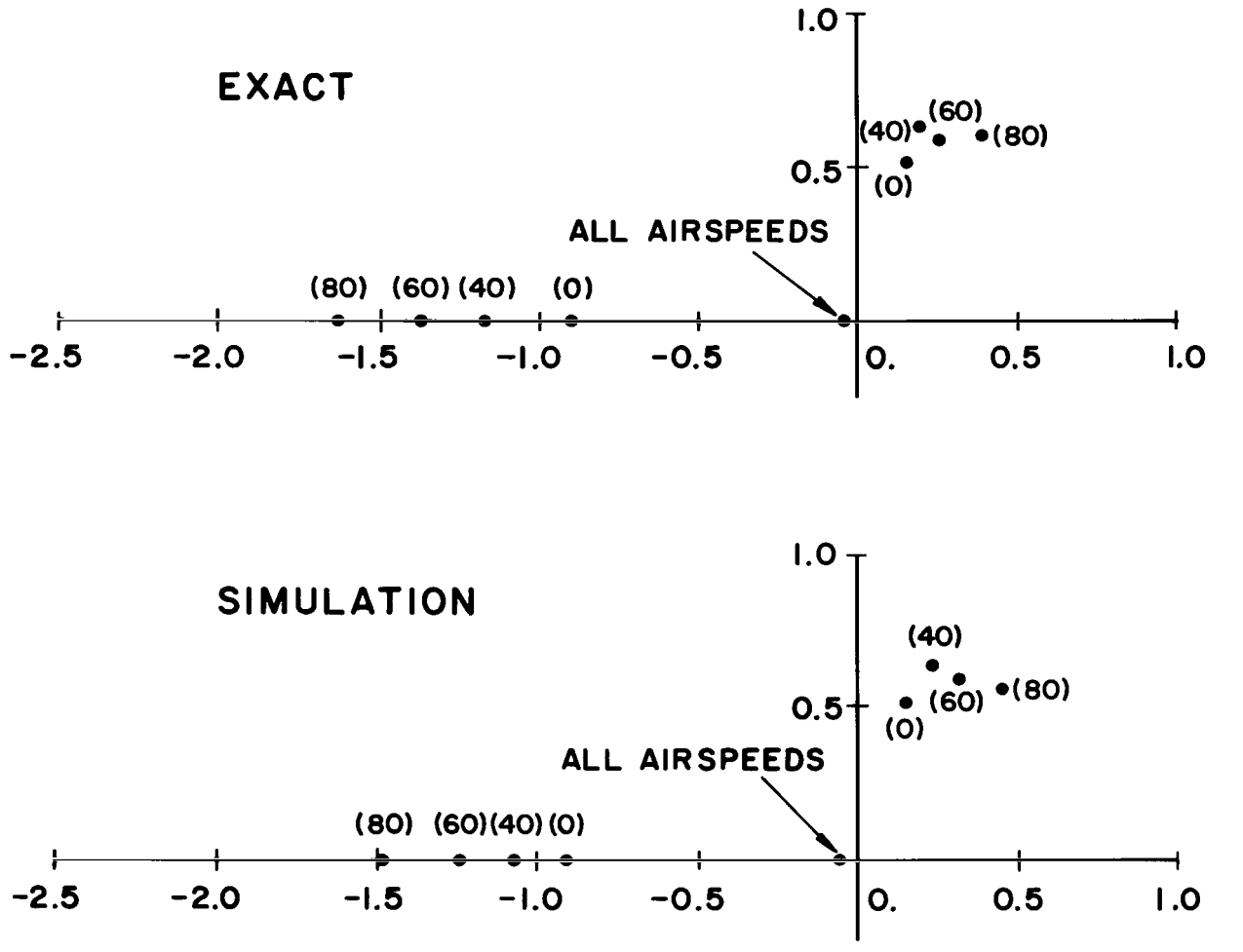

Figure 75.- The roots of the denominator associated with the lateral motions of the CH-46C helicopter as a function of air speed in knots

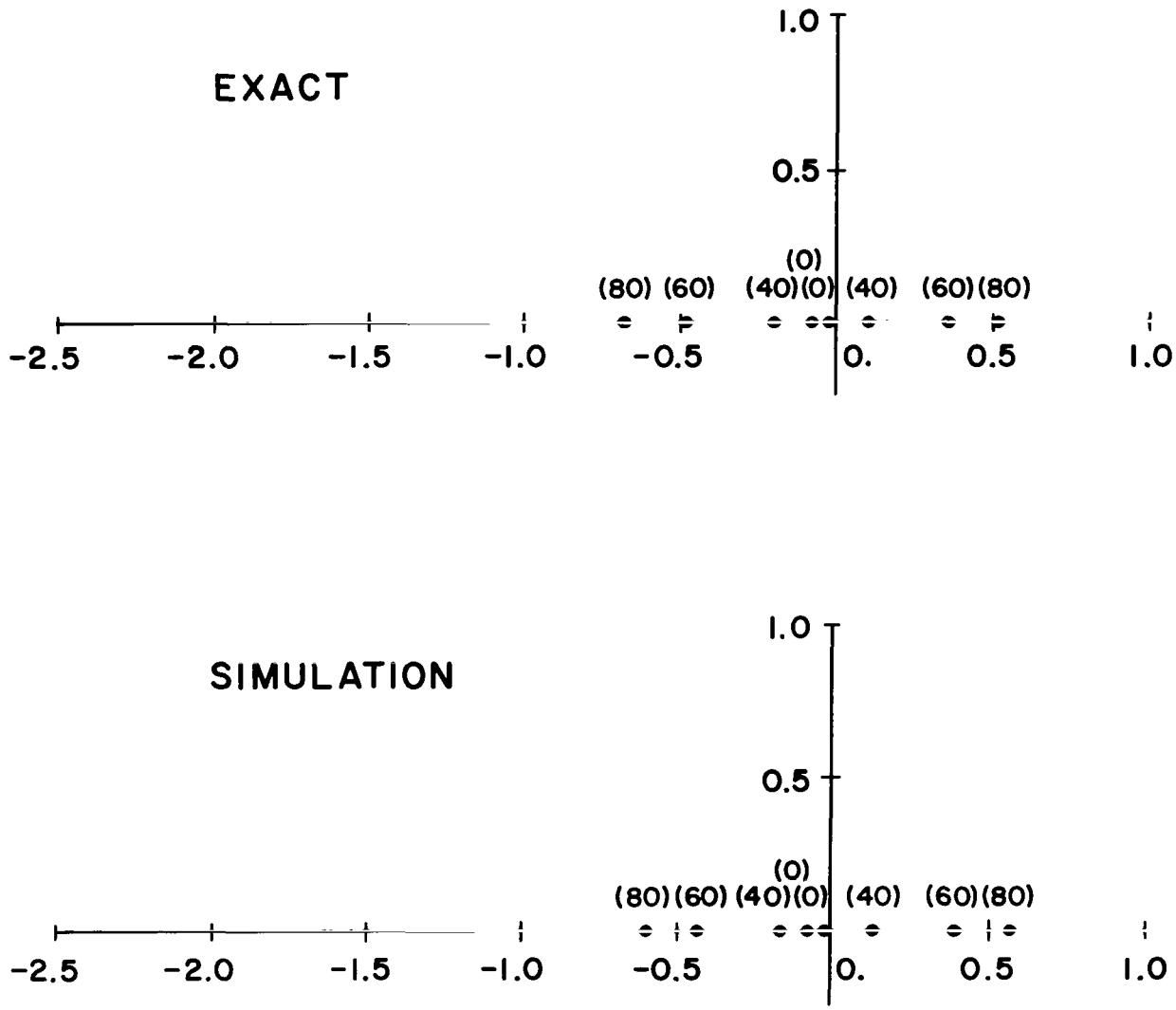

Figure 76.- The roots of the numerator associated with the roll channel (attitude) of the CH-46C helicopter as a function of air speed in knots

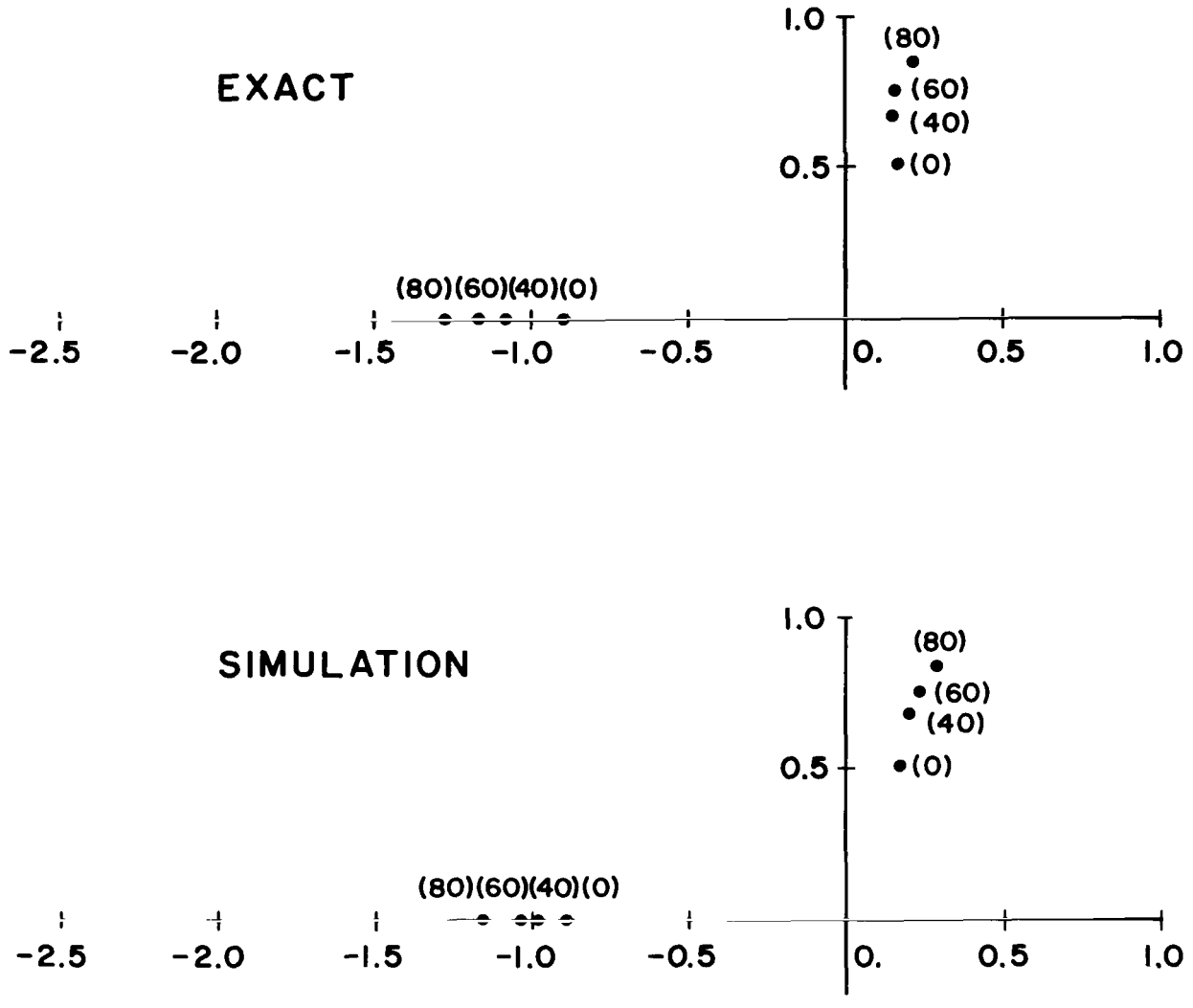

Figure 77.- The roots of the numerator associated with the yaw channel (yaw rate) of the CH-46C helicopter as a function of air speed in knots

Euler Angle Equations.- The following equations used body rates to generate Euler angles.

$$\dot{\Theta} = Q \cos \Phi - R \sin \Phi$$

$$\dot{\Psi} = Q \frac{\sin \Phi}{\cos \Theta} + R \frac{\cos \Phi}{\cos \Theta}$$

$$\dot{\Phi} = P + \dot{\Psi} \sin \Theta$$

(14)

The value of these variables at the beginning of each approach were

$$\Theta_{IC} = \Theta_{TR}(U_{IC})$$

$$\Psi_{IC} = \Psi_{O}$$

$$\Phi_{IC} = O$$

(15)

Vertical Heading (VH) – Coordinate System Velocity Equations.- The following equations resolved the body referenced velocities through Φ and Θ to give what was called VH-coordinate velocities.

$$V_X^h = U \cos \Theta + V \sin \Phi \sin \Theta + W \cos \Phi \sin \Theta$$

$$V_Y^h = V \cos \Phi - W \sin \Phi$$

$$V_Z^h = -U \sin \Theta + V \sin \Phi \cos \Theta + W \cos \Phi \cos \Theta$$

(16)

Approach Navigation Frame (ANF) – Coordinate System Velocity Equations.- The following equations resolved the VH-coordinate velocities through Ψ to give the ANF – coordinate velocities.

$$V_X = V_X^h \cos \Psi - V_Y^h \sin \Psi$$

$$V_Y = V_X^h \sin \Psi + V_Y^h \cos \Psi$$

$$V_Z = V_Z^h$$

(17)

DIGITAL COMPUTER PROGRAM

The digital program had the tasks of setting up the simulator for each run, simulating the digital flight control system, generating gusts, and reducing the data generated during each approach.

The simulation set up prior to each approach was carried out by means of the typewriter I/O device. The setup consisted of specifying:

(1) The flight control mode that was to be flown during the next approach (e.g., Attitude II without Flight Director Commands).

(2) The state of the helicopter at which the approach was to begin (i.e., X_{IC}, Y_{IC}, Z_{IC}, $(V_x^h)_{IC}$, $(V_z^h)_{IC}$, and Ψ_{IC}). The rates, P_{IC}, Q_{IC}, and R_{IC}, were zero at approach initiation.

(3) The direction of the mean wind vector in the ANF coordinate system.

(4) Any changes with respect to the nominal control system gains, trajectory characteristics, or wind characteristics. This option was particularly convenient during the verification of the linear analysis and in establishing the final form of the flight control system and of the mission.

At this point, the helicopter was commanded to fly to the specified initial conditions with a modified automatic control system. This procedure automatically established the initial conditions on the associated integrators and function generators in the analog computer. After the helicopter reached the starting condition, the pilot would begin the approach with the specified control system. At the completion of the mission, the simulator entered the set-up mode once again.

In order to simulate a sample data flight control system, the digital program was structured such that it consisted of an idle loop and one major subroutine in which the flight control computations were carried out. Upon completion of this subroutine, the program remained in the idle loop until a timing pulse was received from the clock in the analog computer. The interval between pulses (32 msec) represented the sampling period.

In order to exercise the landing system modes, it was necessary to simulate winds. The model chosen was simple but

sufficient for the purpose of the experiment. Model parameters were taken from reference 12. The wind axis system was defined with the X axis along the mean wind vector, the Y axis in the plane of the local horizontal, and the Z axis down the local vertical. The wind model consisted of a mean-wind vector plus gusts along the wind axis. The gusts were assumed uncorrelated and consisted of zero-mean white Gaussian noise passed through a simple first-order filter. A mean-wind amplitude of 20 fps was chosen. This led to standard deviations for the X, Y, and Z wind axes gusts of 2.3, 1.6, and 1.0 fps, respectively. A filter time constant of 1.5 sec was chosen for each axis.

In the simulation, the direction of the mean-wind vector could be varied from run to run while its amplitude was kept fixed. The total winds were then resolved from wind axes to body axes. The winds were added to the inertial velocities and passed through the stability derivatives to generate the forces and moments. A sample of the standard winds described above is shown in Figure 78. The derivation of the noise model is given in Appendix C.

The digital computer reduced the performance data from each run. To establish system performance, the mission was divided into four phases, Localizer Track, ILS Beam Track, Flare, and Terminal Approach. During each phase, the digital computer recorded data consisting of the initial state, the absolute maximum deviation of certain variables from their nominal values, and, in certain cases, the root-mean-square values of certain deviations. At the end of each approach, a normalized performance index involving seventeen of these data points was calculated and printed out along with the data associated with each phase. A typical printout is shown in Figure 79.

The form of the performance index was

$$P.I. = \frac{1}{17} \sum_{i=1}^{17} \frac{\left(E_{(i)} - ENOM_{(i)}\right)_{MAX}}{EMAX_{(i)}} \qquad (18)$$

where E represents each variable; ENOM represents the nominal value of each variable and EMAX represents the maximum allowable deviation of each variable from its nominal. Each of these terms was used in two ways to determine system performance. To establish the basic acceptability of each of the candidate control systems each of the terms associated with maximum absolute excursions from nominal (i.e., excluding the root-mean-squared terms) were looked at individually. If any term exceeded unity, the system was considered to have failed to meet the minimum performance specifications during that approach. The overall percentage of failed approaches to the total number of approaches made with a

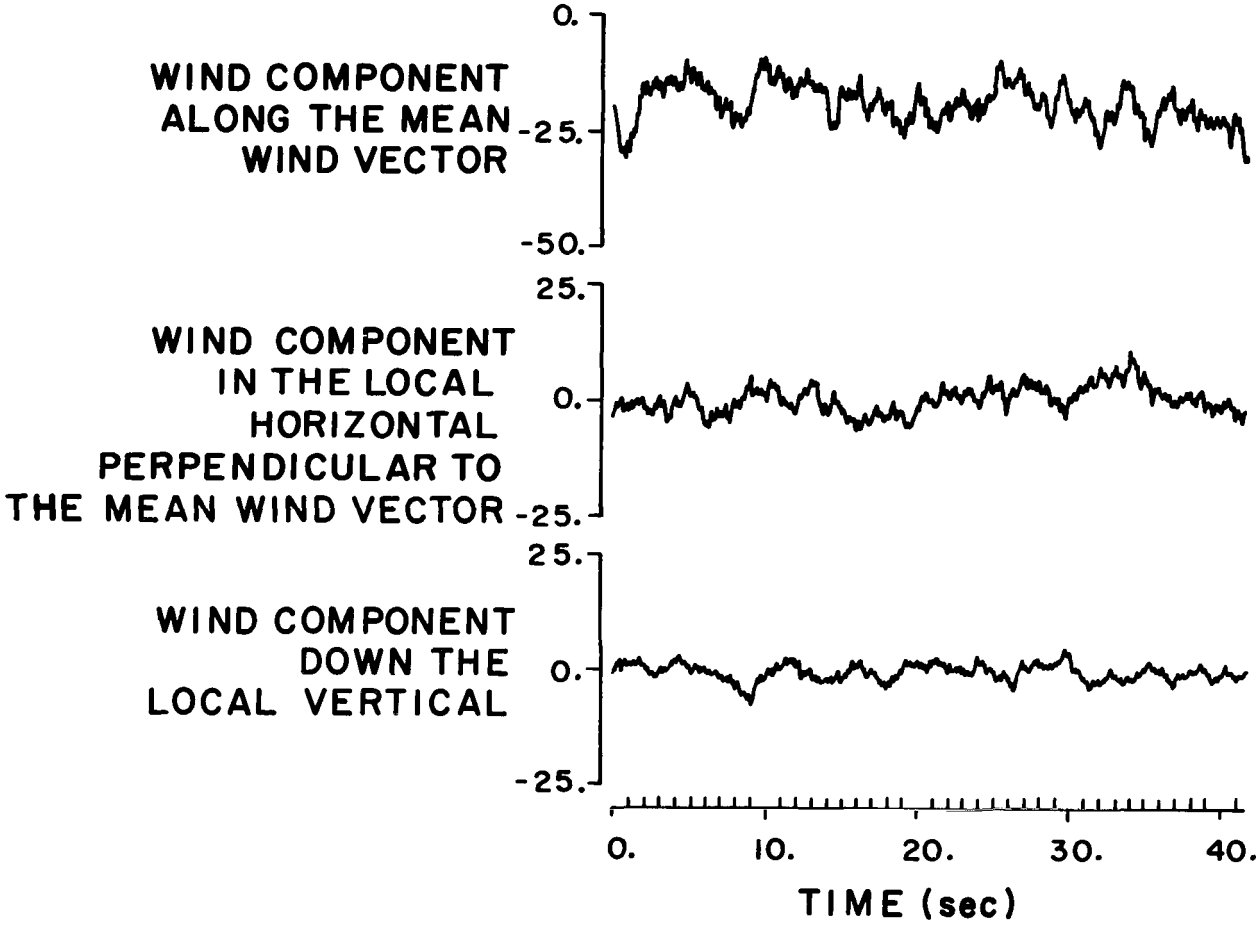

Figure 78.- Example of the wind used in the simulation

MULTI-MODE HELICOPTER FLIGHT CONTROL SYSTEM

INITIAL STATE

X=-0.10000E 05
Y= 0.00000E 00
Z=-0.80000E 03
VLOCE= 0.00000E 00
VX= 0.70982E 02
VY=-0.31373E 00
VZ= 0.48828E-01
AS= 0.87495E 02
AX=-0.14771E 01
AY= 0.61035E-02
AZ=-0.32080E 02
PHI= 0.85205E-03
THETA= 0.49632E-01
PSI=-0.16508E 00
BETA=-0.29996E-02
P=-0.21301E-03
Q=-0.42603E-3
R= 0.10651E-02

X=-0.59981E 04
Y=-0.21082E 00
Z=-0.59739E 03
VLOCE= 0.30663E-04
GSE= 0.98547E-04
VX= 0.70592E 02
VY= 0.11985E 00
VZ= 0.73120E 01
AS= 0.95564E 02
AX= 0.21973E 00
AY= 0.24414E 00
AZ=-0.31024E 02
PHI= 0.57513E-02
THETA= 0.13633E-01
PSI=-0.17531E 00
BETA=-0.51414E-01
P= 0.97986E-02
Q= 0.29609E-01
R= 0.29822E-02

X=-0.15522E 04
Y= 0.61465E-02
Z=-0.14998E 03
VLOCE=-0.19927E-05
GSE=-0.47340E-03
VX= 0.75680E 02
VY= 0.33005E-01
VZ= 0.76782E 01
AS= 0.86042E 02
AX=-0.40283E 00
AY= 0.67139E 00
AZ=-0.31354E 02
PHI=-0.46864E-02
THETA= 0.18106E-01
PSI=-0.17510E 00
BETA= 0.18160E-01
P= 0.63904E-02
Q= 0.48993E-02
R= 0.10225E-01

X=-0.99742E 02
Y= 0.13989E 00
Z=-0.51894E 02
VX= 0.15445E 02
VY= 0.52847E-02
VZ= 0.61035E 00
AS= 0.31159E 02
AX=-0.41382E 01
AY=-0.61035E-02
AZ=-0.32898E 02
PHI=-0.74554E-02
THETA= 0.12610E 00
PSI=-0.38981E 00
BETA=-0.44465E-01
P= 0.10438E-01
Q=-0.63904E-03
R= 0.21301E-02
BEARING= 0.34215E-03
BEARING DESIRED=-0.13089E-02
WORKLOAD TIME = 0.00000E 00

MAXIMUM VALUES

LOCALIZER TRACK

ABYS= 0.89879E 00
ABSDZ= 0.12609E 01
ABSVLOCE= 0.11850E-03
ABSDVX= 0.13387E 01
ABSVY= 0.37041E 00
ABSVZ= 0.79468E 01
ABSDAS= 0.12634E 02
-AX= 0.16479E 01
ABSAY= 0.26062E 01
ABSAZ= 0.35132E 02
ABSPHI= 0.19384E-01
THETAPOS= 0.52188E-01
THETANEG= 0.49419E-01
ABSPSI= 0.21599E 00
ABSBETA= 0.14227E 00
ABSP= 0.45159E-01
ABSQ= 0.29609E-01
ABSR= 0.38555E-01
TT= 0.56608E 02
PLOCE= 0.41210E-04
PVEL= 0.48783E 00
PAS= 0.43343E 01

ILS BEAM TRACK

ABSY= 0.66576E 00
ABSVLOCE= 0.17733E-03
ABSGSE= 0.55401E-03
ABSDVX= 0.97023E 00
ABSVY= 0.42948E 00
ABSVZ= 0.90088E 01
ABSDAS= 0.11487E 02
-AX= 0.13184E 01
ABSAY= 0.18738E 01
ABSAZ= 0.35608E 02
ABSPHI= 0.22579E-01
THETAPOS= 0.39620E-01
THETANEG= 0.12568E-01
ABSPHI= 0.20407E 00
ABSBETA= 0.97461E-01
ABSP= 0.34082E-01
ABSQ= 0.30248E-01
ABSR= 0.29183E-01
TT= 0.62464E 02
PLOCE= 0.12157E-03
PGSE= 0.34178E-03
PVEL= 0.81904E 00
PAS= 0.10746E 02

FLARE

ABSY= 0.25910E 01
Z=-0.51913E 02
ABSVLOCE= 0.16214E-02
ABSVY= 0.54204E 00
ABSVZ= 0.78125E 01
-AX= 0.43579E 01
ABSAY= 0.14465E 01
ABSAZ= 0.35675E 02
ABSPHI= 0.38981E-01
THETAPOS= 0.15848E 00
THETANEG=-0.18106E-01
ABSPSI= 0.39088E 00
ABSBETA= 0.17584E 00
ABSP= 0.35786E-01
ABSQ= 0.41964E-01
ABSR= 0.32378E-01
TT= 0.43200E 02
PLOCE= 0.12592E-02

TERMINAL APPROACH [RANGE=100.FT]

CRITERIA FUNCTION

LOCALIZER TRACK	ILS MEAN TRACK	FLARE	TERMINAL APPROACH
ABSDZMAX/100.= 0.12609E-01	ABSGSEMAX/.035= 0.15829E-01	ABS[ZMIN+50.]/20.= 0.95664E-01	ABSY/100.= 0.13089E-02
ABSLOCEMAX/.1= 0.11850E-02	ABSLOCEMAX/.1= 0.17733E-02	ABSLOCEMAX/.1= 0.16214E-01	ABS[Z+50.]/20.= 0.94688E-01
PLOCE/.05= 0.82419E-03	PLOCE/.05= 0.24313E-2	PLOCE/.05= 0.25184E-01	ABS[VX-16.]/16.= 0.34664E-01
PVEL/20.= 0.24391E-01	PGSE/.018= 0.18988E-01		ABSBEARE/[PI/6]= 0.31549E-02
	PVEL/20.= 0.40952E-01		ABSVZ/3.= 0.20345E 00

[SUMMATION OF THE TERMS /17.= 0.34901-01

Figure 79.- Example of the digital performance data printed out at the termination of each simulated approach

particular flight control system determined its acceptibility as an operational system. The Performance Index (P.I.) is a qualitative measure of over-all system performance which was used to rank the seven candidate control systems with respect to performance. It is not to be considered, in any sense, an absolute scale.

The details of the P.I. can best be understood in the context of the nominal simulated mission. The division between the four phases of the mission was based on basic shifts in the set of guidance parameters that the pilot controls during the approach. During each phase, the associated terms in the P.I., when possible, consisted of these same guidance parameters, Table III. During the following description of how the P.I. relates to the mission, reference may be made to Figure 1, which is a diagram of the mission, and to the section entitled Low-Visibility Mission, in which the simulated mission is established and discussed. The Localizer Track phase was initiated at a range of 10,000 ft, an altitude of 800 ft, a ground speed of 42 kts (70 fps), zero rate of descent, headed into the mean wind, aligned with the localizer, and approaching the glide slope intercept point. The pilot initially was concerned with maintaining altitude, ground speed, and localizer track. Consequently, for this phase to be considered acceptable, the P.I. required that the altitude be maintained between 700 and 900 ft, that the ground speed root-mean-square deviation from 70 fps be less than 20 fps, and that the localizer deviation be within ± 0.1 rad (i.e., full-scale localizer sensitivity), and that the associated localizer root-mean-square deviation be less than 0.05 rad (i.e., half-scale localizer sensitivity). Somewhere between the range of 9000 and 8000 ft, the pilot would normally switch from his altitude hold task and commence to capture the glide slope. For this reason, the calculation of the associated altitude term in the P.I. was terminated at 9000 ft of range. In addition to assuming that glide slope capture would be initiated at some range less than 9000 ft, it was further assumed that glide slope capture would be completed by the time the helicopter was at 6000 ft of range. Since the helicopter can acceptably approach the glide slope at an altitude of 700 ft, 1000 ft of range beginning at the 7000-ft glide slope intercept range was allowed for the intercept maneuver.

At 6000 ft, the calculation of those terms associated with the Localizer Track were replaced by those of the ILS Beam Track. During this phase, the pilot would maintain the localizer, glide slope, and ground speed. The P.I. terms again monitored the deviations of these three parameters. The glide slope deviation from 0.1 radian was to be kept within ± .035 rad (2 deg) which again was the full-scale glide slope sensitivity. As the helicopter approached the flare/deceleration altitude of 150 ft, the pilot would progressively transfer his attention from main-

TABLE III.- GUIDANCE PARAMETERS

Phase of Mission	Parameter	Nominal Value	Perf. Index Parameter	Max. Allow. Deviation
Localizer Track (From range 10,000 ft to range 6,000 ft)	Altitude (terminated at range 9,000 ft)	800 ft	Max. Error	± 100.ft
	Localizer	0.rad	Max. Error RMS Error	± .1 rad .05 rad
	Ground Speed	70.fps	RMS Error	20.fps
ILS Beam Track (From range 6,000 ft to alt. 150 ft)	Glide Slope (Term. at alt. 200 ft)	.1 rad	Max. Error RMS Error	± .035 rad .018 rad
	Localizer	0. rad	Max. Error RMS Error	± .1 rad .05 rad
	Ground Speed	70. fps	RMS Error	20.fps
Flare (From alt. 150 ft to range 100 ft)	Altitude	50. ft (after flare)	Lowest Pt	± 20.ft
	Localizer	0. rad	Max. Error RMS Error	± .1 rad .05 rad
Terminal Approach (From range 100 ft to touchdown)	Altitude (at range 100 ft)	50.ft	Error	± 20.ft
	Lateral Pos. (at range 100 ft)	0.ft	Error	± 100.ft
	Course (at range 100 ft)	Aligned with center of pad	Error	± 30.deg
	Ground Speed (at range 100 ft)	16.fps	Error	± 16.fps
	Vertical Vel. (at range 100 ft)	0.fps	Error	± 3.fps

taining the glide slope to monitoring the radar altimeter in order to coordinate his stick responses with altitude. Consequently, the calculation of the glide slope terms was terminated at 200 ft of altitude. The Flare Phase was entered at 150 ft at which the pilot commenced to decelerate to a ground speed of 10 kts (16 fps) and to flare to an altitude of 50 ft while maintaining the localizer track. The pilot then maintained a ground speed of 10 kts, an altitude of 50 ft, and localizer track until a range of 100 ft. During the flare to the 50-ft altitude and subsequent altitude hold, safety considerations dictated that the helicopter should never drop below 30 ft. This established a lower altitude limit on flare. To establish an upper limit, a symmetric, although minimal, requirement would be that the helicopter must drop below 70 ft at some point. The associated altitude term in the P.I. represented these two conditions. At the range of 100 ft, the Flare Phase terminated and the Terminal Approach phase was entered. At this range, it was assumed that the pilot would be able to switch to VFR for the final approach and touchdown, even in the worst weather conditions. Consequently, the simulated approach was terminated at this range; and the associated terms in the P.I. attempted to establish if the state of the helicopter at flare termination (i.e., breakout) would permit the pilot a high probability of completing the final approach and touchdown smoothly, without the need for abrupt maneuvers. For breakout to be considered successful, the helicopter's terminal altitude had to be between 30 and 70 ft, lateral position had to be less than ± 100 ft, course had to be within ± 30 deg of being aligned with the center of the pad, and the ground speed had to be less than 20 kts. One additional constraint was that the vertical velocity be less than 3 fps. This may seem overly restrictive, but it was found that whenever a flight control system repeatedly failed this test, the pilot's collective stick movement was excessive and that his ability to maintain a constant vertical velocity and altitude was unacceptable.

EXPERIMENT

The objective of the experiment was to determine the relative performance of the various landing modes. To do this six subjects flew a standard sequence of landing missions while the performance was recorded. The subjects consisted of four instrument-qualified pilots and two engineers with simulator experience. A summary profile on each of the six subjects used in the experiment is presented in Table IV. Subjects 1 and 2 were engineers with no flight experience. They both had worked on the system development and understood the mission thoroughly. Each test sequence was run in two consecutive days. The first day was considered training and qualification on each mode. On the second day the production runs were made.

TABLE IV.- BACKGROUND OF EACH TEST SUBJECT

IFR Certification		1	2	3	4	5	6
Fixed Wing	When Last Certified	Never	Never	Current	1968	Current	Current
	Duration of Certification			8 yrs	8 yrs	3 yrs	18 yrs
Rotary Wing	When Last Certified	Never	Never	Never	1968	Never	Current
	Duration of Certification				8 yrs		8 yrs
IFR Instructor Certification							
Fixed Wing	When Last Certified	Never	Never	Current	Current	Current	Never
	Duration of Certification			7 yrs	3 yrs	2 yrs	
Rotary Wing	When Last Certified	Never	Never	Never	Current	Never	Never
	Duration of Certification				3 yrs		
VFR Instructor Certification							
Fixed Wing	When Last Certified	Never	Never	Current	Current	Current	Never
	Duration of Certification			7 yrs	6 yrs	4 yrs	
Rotary Wing	When Last Certified	Never	Never	Current	Current	Never	Never
	Duration of Certification			4 yrs	6 yrs		
IFR Experience							
Fixed Wing		0 hrs	0 hrs	150 hrs	200 hrs	200 hrs	200 hrs
Rotary Wing		0 hrs	0 hrs	0 hrs	150 hrs	0 hrs	200 hrs
VFR Experience							
Fixed Wing		0 hrs	0 hrs	1300 hrs	1000 hrs	1300 hrs	5000 hrs
Rotary Wing		0 hrs	0 hrs	60 hrs	2500 hrs	0 hrs	1000 hrs
Simulation Experience							
Fixed Based Simulators		25 hrs	25 hrs	50 hrs	125 hrs	120 hrs	250 hrs
Moving Based Simulators		0 hrs	0 hrs	30 hrs	25 hrs	130 hrs	50 hrs

The first day of running the subject generally reported after lunch. At that time, a standard description of the program objective, the mission and the landing modes was given the subject. Next, the subject was seated in the cockpit and familiarized with the instruments with respect to the mission. Then, to be sure, the mission was understood a fully-automatic mission was flown while another verbal description of the mission was made. At this point, the subject began a standard training sequence.

The training runs began with the easiest mode to fly, and progressed to the most difficult. The mode order was:

(1) Velocity Command with FDI

(2) Velocity Command without FDI

(3) Attitude Command II with FDI

(4) Attitude Command II without FDI

(5) Attitude Command I with FDI

(6) Attitude Command I without FDI

For each mode but the last, the subject was considered qualified on that mode when either two successful runs in a row were made or eight runs were made. The second provision of eight runs was made due to the time constraint. In general, pilots were only available for an afternoon and the next day. When the subject had qualified, two additional runs were made and then the subject went on to the next mode. For the last and most difficult mode only two out of four in a row were required for qualification. Subjects were given the option of a ten-minute break between each mode. The training sequence was generally completed within four hours.

The production runs were made on the second day. For the production runs, the order of the modes was different for each subject to average out the effect of order on the data. Each mode was run until the subject requalified and then production runs were made. Five runs were made for each of the FDI modes and eight runs were made for modes without the FDI. The number of runs selected was based on the time constraint. The five/eight ratio was chosen since the variance of the FDI runs was much smaller than those without FDI and therefore more runs without FDI were desired. Subjects were given the option of a ten-minute break between modes and lunch was taken between the third and fourth mode. The production sequence was generally completed within seven hours including an hour for lunch.

In addition to taking the performance data, the pilot was also asked the following question after finishing each mode (i.e., the mode just flown). "Would you fly this system for the defined mission in an operational environment?" The answers were to be simply, yes, no, or marginal.

RESULTS

The results of the experiment are shown for each subject in Figures 80 through 85. These data represent only those runs made on the second day after the training had been completed. In each figure, the overall performance index is shown for each system. Each individual data point is plotted and beside each the mean is circled and the standard deviation indicated. Below each plot is a table indicating for each system the number of runs made, the number of failures and, for the pilot subjects, the answer to the question: "Would you fly this system for the defined mission in an operational environment?"

The composite results are shown in Figure 86. The means of each subjects performance index are plotted and beside them the composite mean is circled and the standard deviation of the individual means is indicated. Below the plot is a table indicating for each system the total number of runs made and the total number of failures. A summary of the pilot's answers to the question cited above is also included.

As was expected, the relative performance of the automatic system is best. In the absence of electronic failure and sensing problems, an automatic system can be easily designed with only bandwidth considerations. As the level of pilot participation increases, the performance of the system decreases. This is due to the bandwidth limitations of the pilot. With the FDI, however, this decrease in performance is significantly reduced. This indicates that the FDI information source permits the pilot to operate at higher bandwidth than raw data sources.

In addition to relative performance, an attempt was made to judge absolute acceptability of each system based on the percentage of approaches that failed to meet the minimum performance specifications. To be considered an acceptable operational system 90 percent of the approaches made with a system had to be successful. The 90 percent figure was chosen based on current FAA Category-II system certification requirements as cited in reference 13. With this criterion the Attitude-I control system was unacceptable both with and without the FDI. All other systems were acceptable. These results correlated well with the pilots rating of the modes. All pilots rated both Attitude-I systems unacceptable or marginal while rating all other systems acceptable.

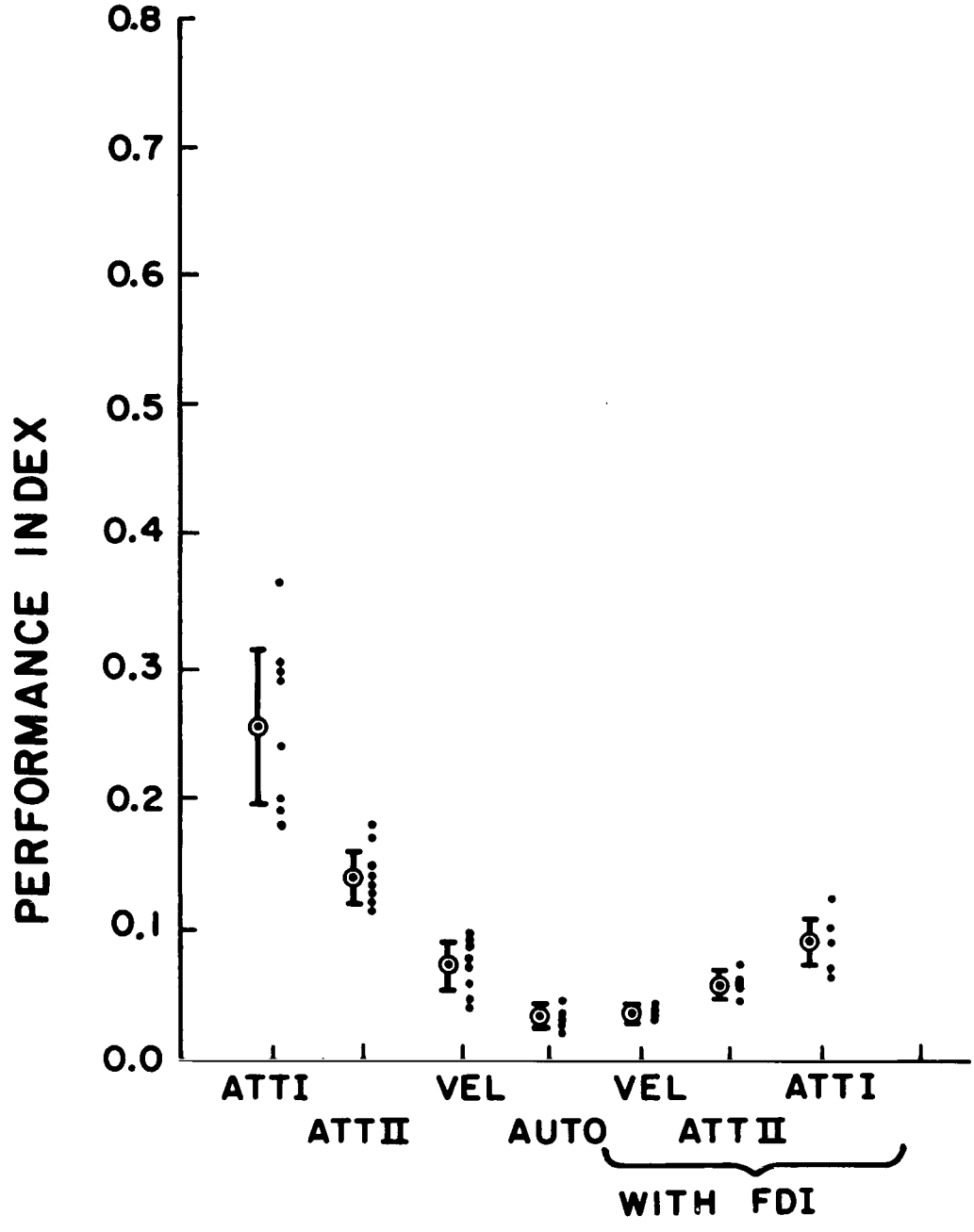

NUMBER OF RUNS	8	8	8	5	5	5	5
NUMBER OF FAILS	1	0	0		0	0	0

Figure 80.- Results of the experiment-Subject 1

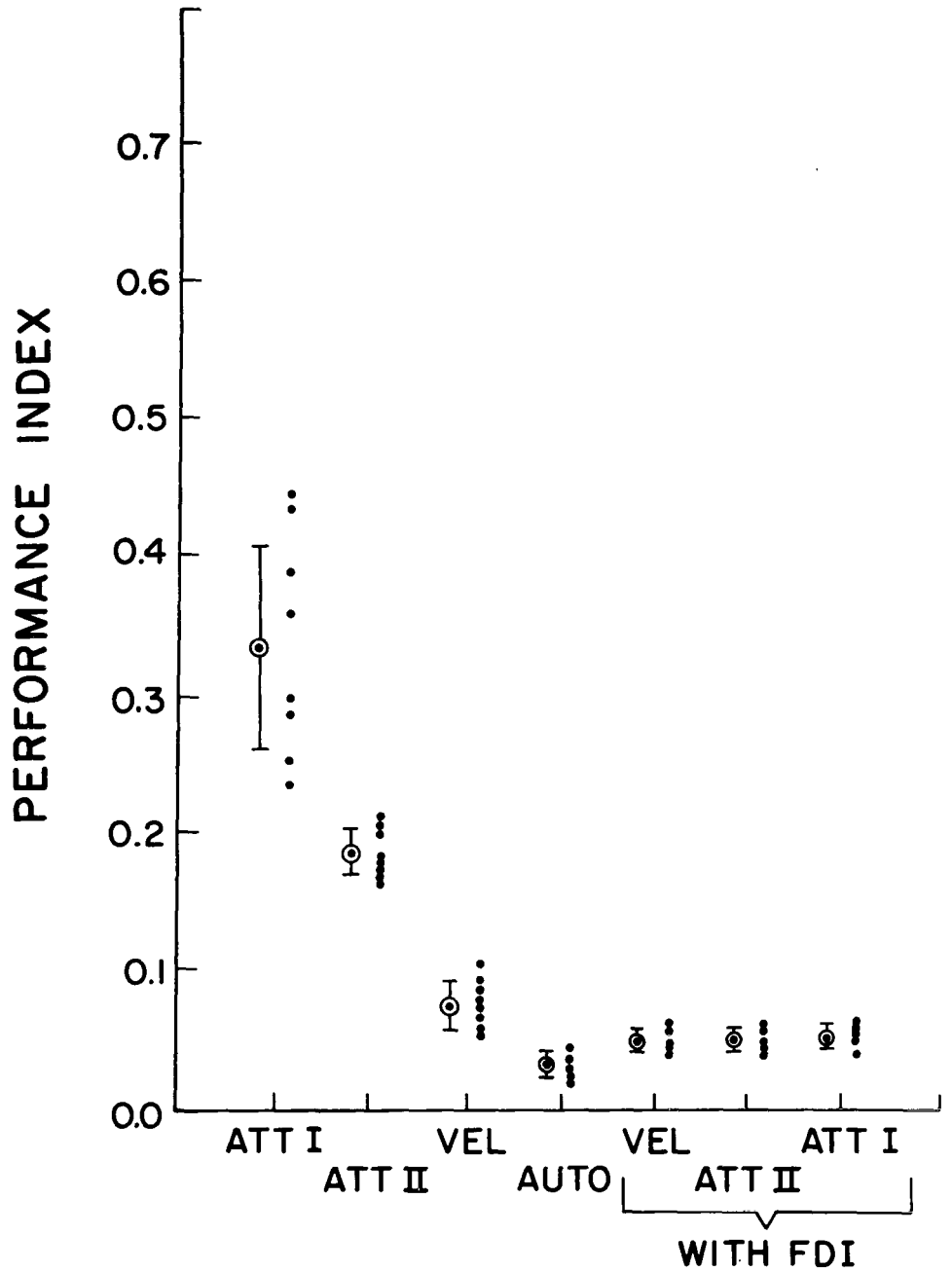

NUMBER OF RUNS	8	8	8	5	5	5	5
NUMBER OF FAILS	3	0	0		0	0	0

Figure 81.- Results of the experiment-Subject 2

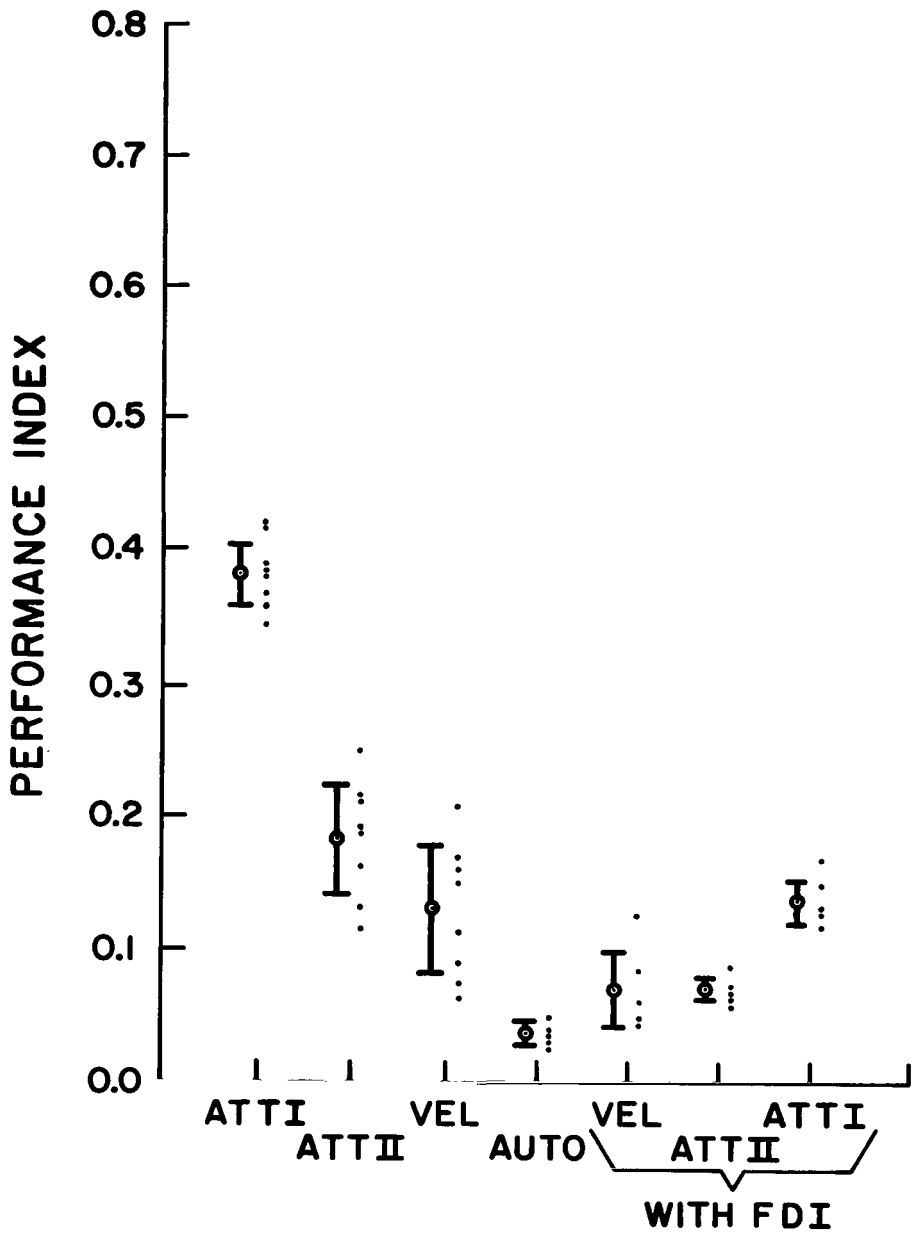

NUMBER OF RUNS	8	8	8	5	5	5	5
NUMBER OF FAILS	7	0	0		0	0	2
ANSWER TO QUESTION	NO	YES	YES		YES	YES	NO

Figure 82.- Results of the experiment-Subject 3

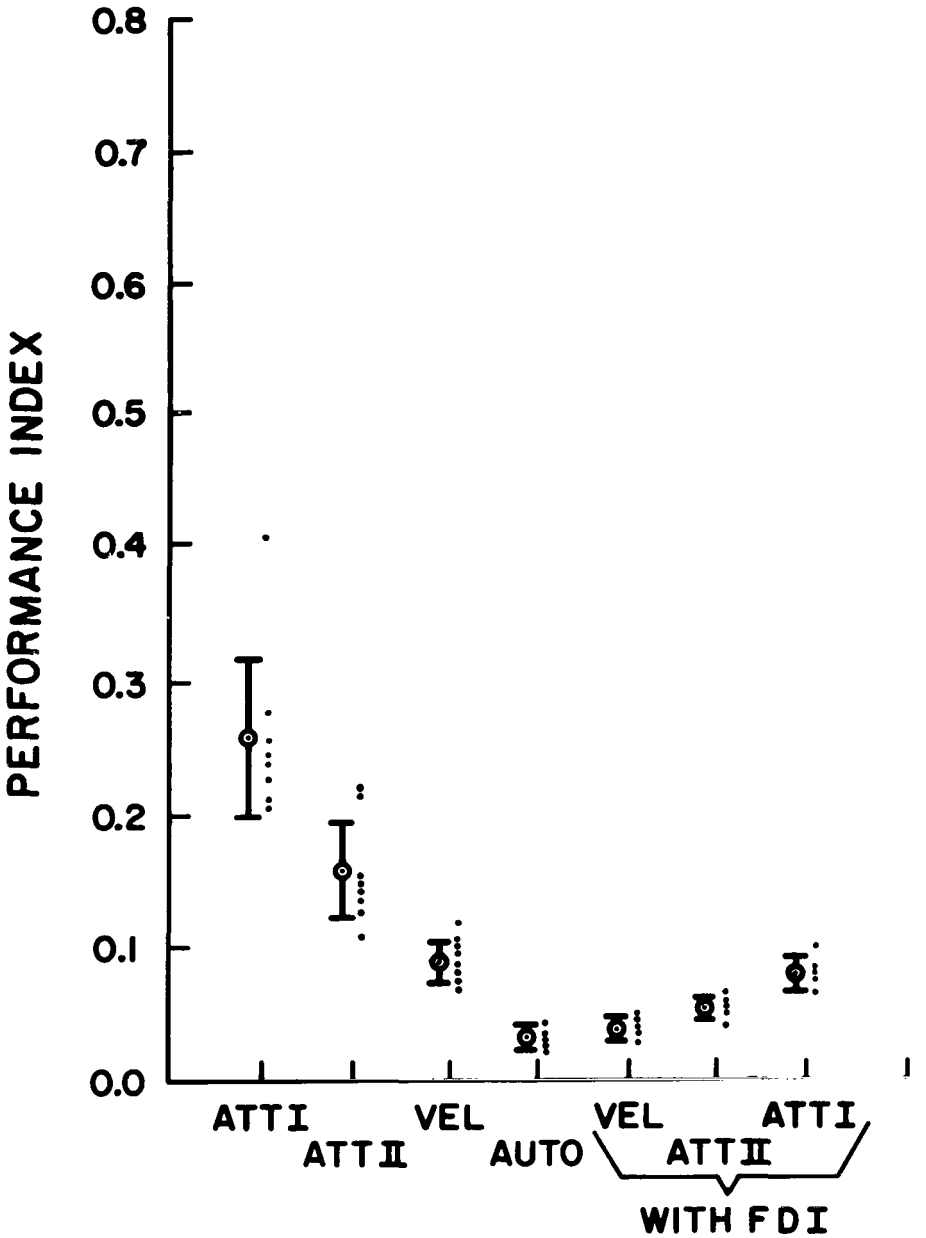

NUMBER OF RUNS	8	8	8	5	5	5	5
NUMBER OF FAILS	1	0	0		0	0	0
ANSWER TO QUESTION	NO	YES	YES		YES	YES	MARG

Figure 83.- Results of the experiment-Subject 4

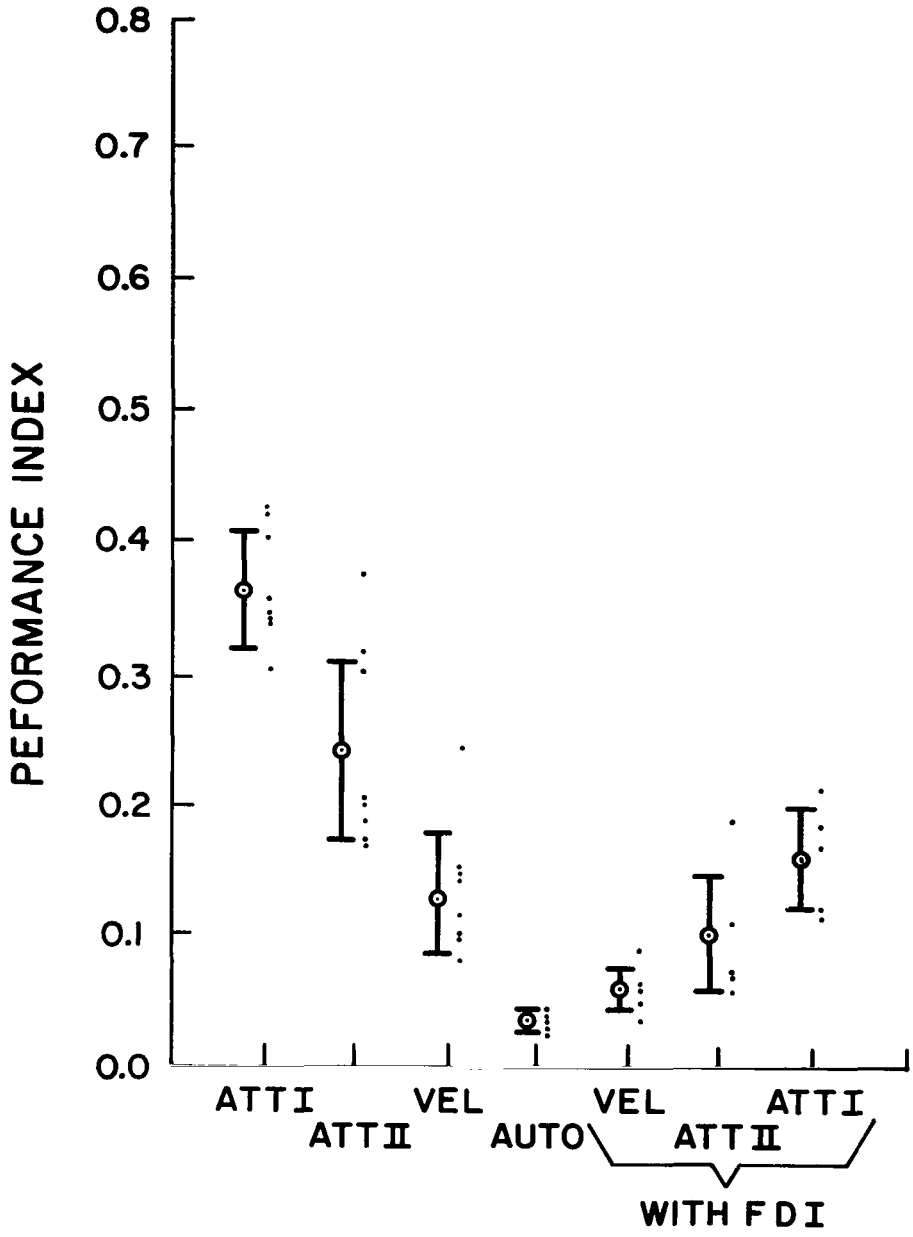

NUMBER OF RUNS	8	8	8	5	5	5	5
NUMBER OF FAILS	5	0	1		0	0	2
ANSWER TO QUESTION	MARG.	YES	YES		YES	YES	MARG.

Figure 84.- Results of the experiment-Subject 5

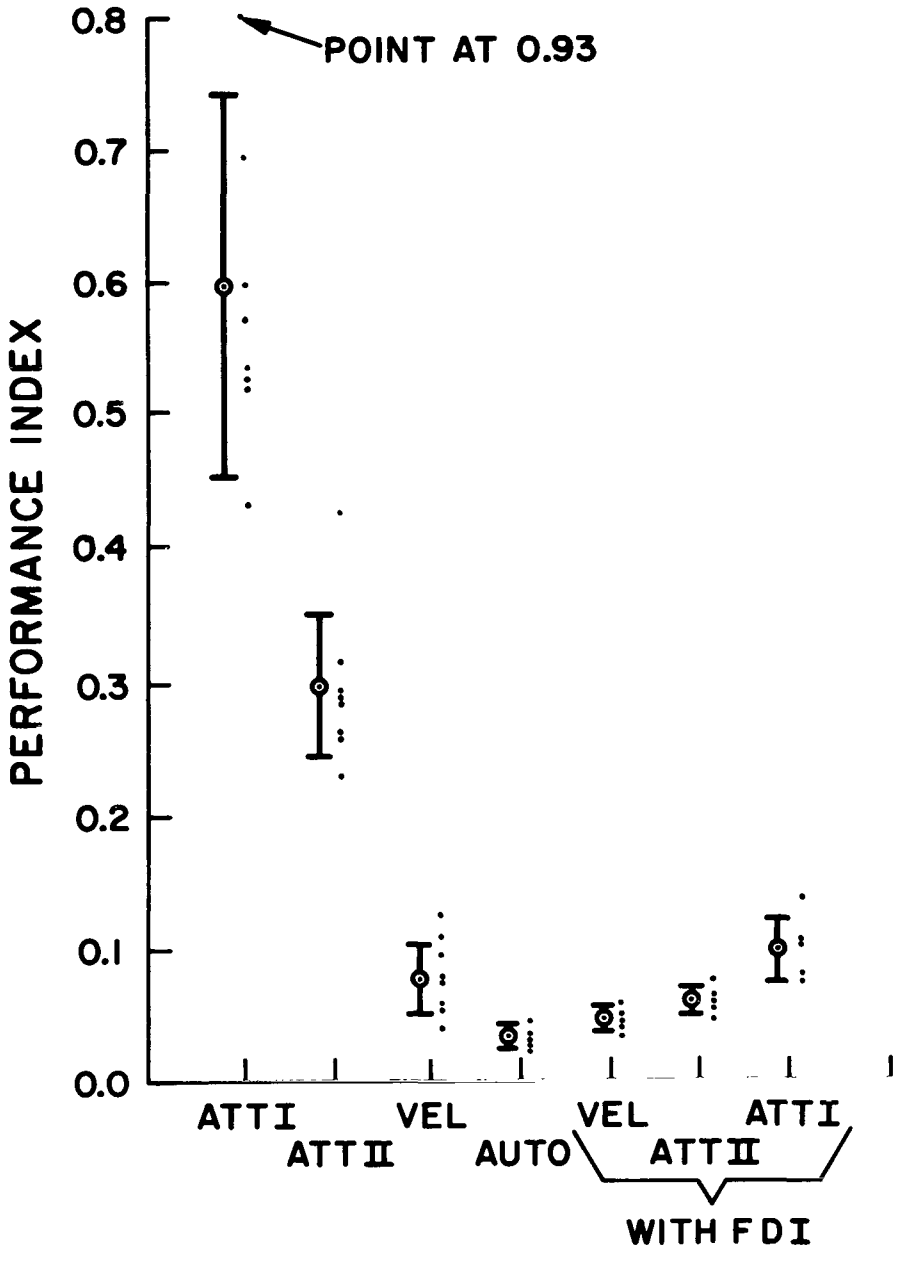

NUMBER OF RUNS	8	8	8	5	5	5	5
NUMBER OF FAILS	8	4	0		0	0	0
ANSWER TO QUESTION	NO	YES	YES		YES	YES	NO

Figure 85.- Results of the experiment-Subject 6

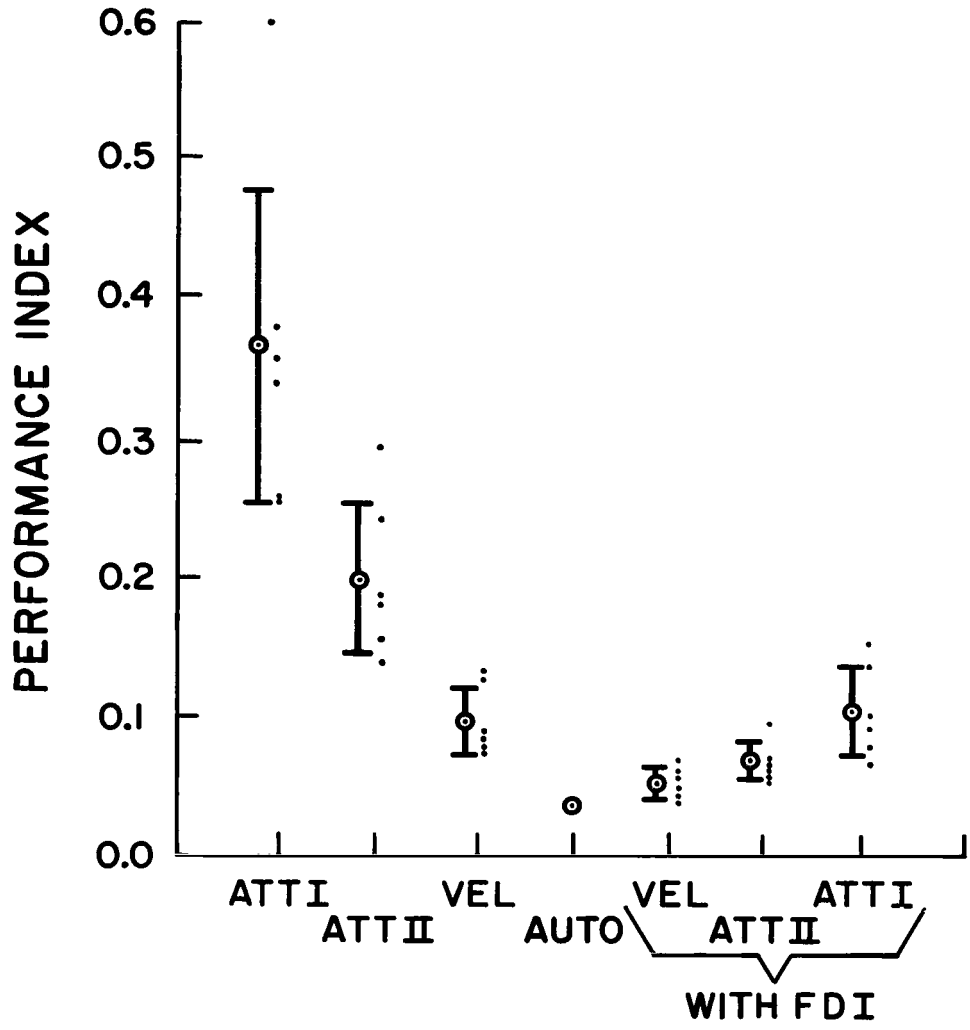

TOTAL NUMBER OF RUNS		48	48	48	5	30	30	30
TOTAL NUMBER OF FAILS		26	4	1		0	0	4
ANSWER TO QUESTION	YES	0	4	4		4	4	0
	MARG.	1	0	0		0	0	2
	NO	3	0	0		0	0	2

Figure 86.- Composite results of the experiment

In investigating the reason for the failure of both Attitude-I systems, the pilot workload must be considered. In the Attitude-I systems, the general comment of the pilots was that the workload was high. Since this was not the case with Attitude II and, since the Attitude-II system was acceptable, it can be deduced that the prime cause for the high workload of Attitude I was the unaugmented vertical axis. The coupling of pitch and collective inputs, the nonlinear collective trim (i.e., power required curve), and the effect of vertical gusts without augmentation made the vertical axis of Attitude I very difficult to fly. This is dramatically evident in the number of failures sustained in Attitude I with raw information sources. The effect of the FDI was to assist the pilot in flying the vertical axis but the workload remained high and the pilot was still unable to consistently remain within specified acceptable performance. In addition, the subject was forced to "tunnel" on the FDI (i.e., concentrate solely on the FDI) for this system and act solely as a servo. The high workload and the associated "tunneling" on the FDI led to the low pilot rating on this system.

In considering the standard deviation of the various runs associated with each subject, it is seen that, in general, the lower the bandwidth required of the subject, the smaller the standard deviation. This is because as less action is required of the subject, less experience with each system is required to produce a consistent set of runs. In considering the standard deviation of the means presented in the composite, again, the lower the bandwidth required of the subject the smaller the standard deviation. This is because as less action is required of the subject, less general experience and innate talent is required to produce a consistent set of runs. These results on standard deviation are important with respect to training. They indicate that the lower the bandwidth required of the subject by a system, the lower the amount of training required to obtain proficiency with that system.

Finally, each system was considered for the localizer track and ILS beam track phases of the mission alone. Such a mission would assume visual breakout while the helicopter is on the ILS beam at 150 ft of altitude. For this reduced mission, every run for every mode met the minimum performance specifications (i.e., all failures in the data occurred in the flare and deceleration maneuver). Therefore, all modes are considered acceptable operationally to 150 ft of altitude. This was to be expected, since such missions are currently flown with simple attitude rate damper systems.

CONCLUSIONS

A fixed-base simulation evaluation of various low-visibility landing systems for helicopters has been made. The objective was to provide performance data for use in making trade-off studies required in selecting an operational system. Based upon the simulation, the following conclusions are made:

(1) All systems considered are operationally acceptable for a straight-in 6-degree glide slope and localizer mission with visual breakout prior to 150 ft of altitude.

(2) For the total low-visibility mission with visual breakout prior to 100 ft of range, the attitude command mode with an unaugmented vertical axis (i.e., Attitude Mode I) is operationally unacceptable with raw information sources or with a flight director indicator (FDI). All other systems are operationally acceptable for the total low-visibility mission.

(3) For the total low-visibility mission, augmentation of the vertical axis to provide a tight Rate of Descent Command system is essential for an acceptable system.

(4) There is a substantial improvement in performance of the Velocity Command Mode over the attitude mode with vertical axis augmentation (i.e., Attitude Mode II).

(5) The Automatic System has the best performance.

(6) An FDI improves the performance of each of the three control modes. This is done, however, at the expense of "tunneling" on the FDI with resultant loss of knowledge of system status.

(7) The lower the bandwidth required of the subject by a mode, the less the amount of training required to obtain proficiency with that mode.

APPENDIX A

The flight control modes were defined by considering the complexity of the sensors and computations which would be required to implement each mode in operation. The sensors and associated filters were only hypothesized. They were not studied in depth nor were they simulated.

First, three sets of basic sensors and associated instruments were defined as follows:

VFR Flight Sensors and Instruments

Barometric Altimeter (Displayed)

Barometric Rate of Descent (Displayed)

Indicated Airspeed (Displayed)

Three Angular Rate Gyros (for Stabilization)

Sideslip Sensor (for Stabilization)

IFR Flight Sensors and Instruments

Vertical Gyro (Displayed via Attitude Indicator)

Directional Gyro (Displayed)

Landing Sensors and Instruments

Glide Path and Localizer (Displayed)

Range and Range Rate (Displayed)

Radar Altimeter (Displayed)

From these sensors the flight control modes were defined as follows.

Attitude Mode I - Would use the information from the VFR and the IFR sensors.

Attitude Mode II - Would use the information from the VFR sensors, the IFR sensors, and, in addition, require at least a set of three body-mounted accelerometers. The accelerometer data would be used to blend with the barometric altimeter to derive a good vertical velocity estimate. A hypothesized filter is shown in Figure A-1.

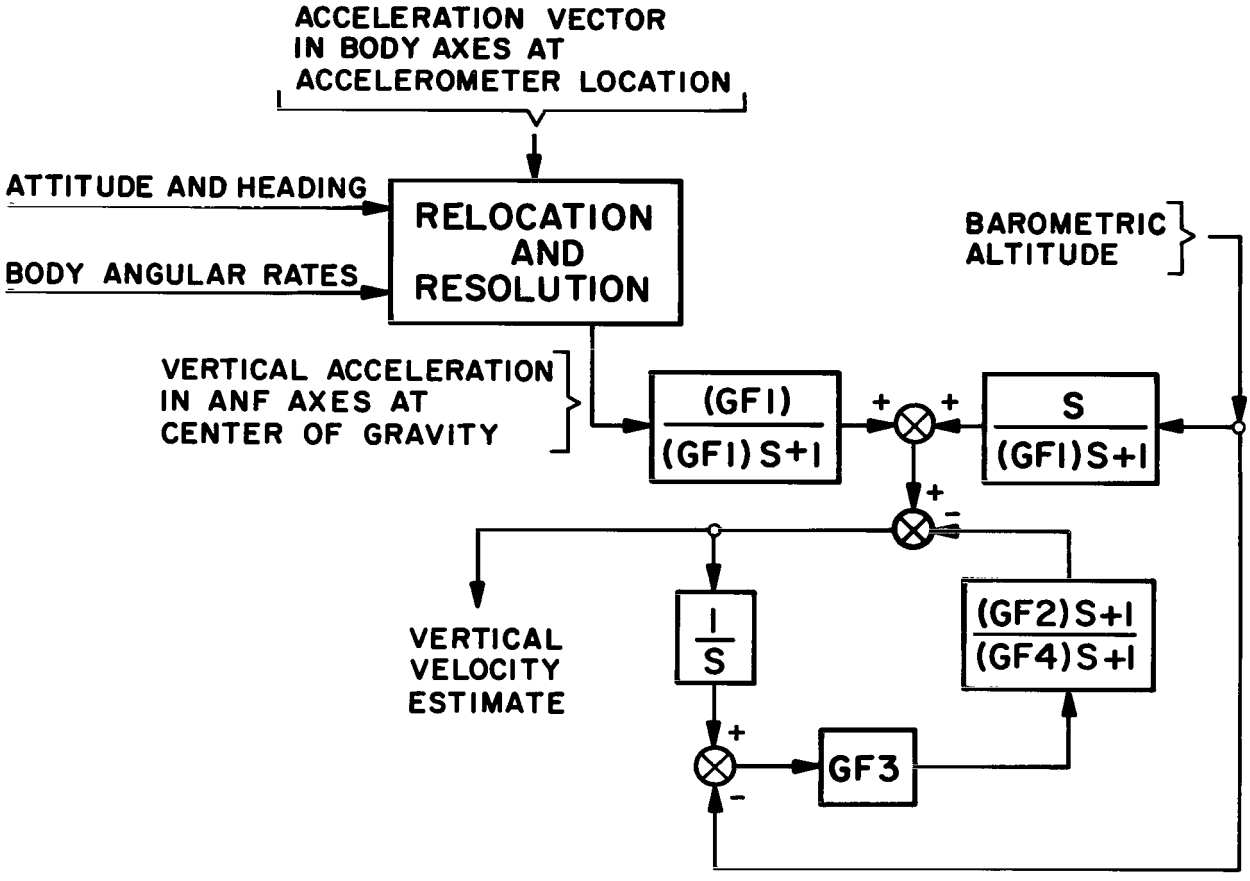

Figure A-1.- Hypothesized vertical velocity filter

Velocity Mode - Would use the information from the VFR sensors, the IFR sensors, the accelerometers, and the landing sensors. The accelerometer data would be used to blend with the landing sources to derive good V_x and V_y information. The filters could be similar to that for the vertical velocity.

Automatic Mode - Would use the same information as the velocity mode.

APPENDIX B

The stability and control derivatives for Flight Condition 1 are listed in Tables B-I and B-II for the longitudinal and lateral-directional modes, respectively. The operating conditions are:

Gross Weight	13,400 lbs
Center-of-Gravity Position	Normal
I_{xx}	9,203 slug ft^2
I_{yy}	75,914 slug ft^2
I_{zz}	71,786 slug ft^2
J_{xz}	-7,114 slug ft^2
Rate of Descent	0 ft/min
Altitude	Sea Level

TABLE B-I.- LONGITUDINAL STABILITY DERIVATIVES AT FLIGHT CONDITION I

Forward Velocity	kts	0	20	40	60	80	100	120	140
Forward Velocity	ft/sec	0.0	33.76	67.52	101.28	135.04	168.80	202.56	236.32
α_{TR}	deg	0.0	8.13709	6.54894	4.67298	2.31058	1.40310	-2.27505	-6.6963
θ_{TR}	deg	9.30627	8.19834	6.62235	4.75227	2.32294	1.43387	-2.26671	-6.6331
X_u/m	$\frac{ft/sec^2}{ft/sec}$	-.02540	-.00181	-.02156	-.03604	-.04642	-.05579	-.06456	-.07206
X_w/m	$\frac{ft/sec^2}{ft/sec}$	.05449	.06818	.08255	.08944	.08548	.10343	.08523	.05666
X_q/m	$\frac{ft/sec^2}{rad/sec}$	.60185	.74915	.87508	.84957	.73079	1.24872	.77601	.25183
$X_{\delta e}/m$	$\frac{ft/sec^2}{in}$	.17696	.13988	.12312	.14237	.16406	-.05165	-.03776	-.01954
$X_{\delta c}/m$	$\frac{ft/sec^2}{in}$	1.20482	.97467	.87948	.80253	.68335	.88200	.72040	.48341
Z_u/m	$\frac{ft/sec^2}{ft/sec}$	.06009	-.12594	-.08296	-.02192	.01396	.06077	.06546	.04980
Z_w/m	$\frac{ft/sec^2}{ft/sec}$	-.36933	-.48399	-.63639	-.80152	-.92055	-1.00063	-1.04552	-1.10516
Z_q/m	$\frac{ft/sec^2}{rad/sec}$	-.71511	-1.16872	-1.77844	-1.81400	-1.81986	-2.22039	-2.25955	-2.47935
$Z_{\delta e}/m$	$\frac{ft/sec^2}{in}$	-.00407	.21188	.51943	.56820	.52527	.46341	.41480	.36743
$Z_{\delta c}/m$	$\frac{ft/sec^2}{in}$	-7.43006	-7.23138	-7.65410	-8.52446	-9.49005	-10.2660	-11.0874	-11.7111
M_u/I_{yy}	$\frac{rad/sec^2}{ft/sec}$	.00656	.00645	-.00587	-.00670	-.00582	-.00185	-.00120	-.00089
M_w/I_{yy}	$\frac{rad/sec^2}{ft/sec}$	-.00285	.00978	.01630	.01363	.01154	.00956	.00774	.00691
M_q/I_{yy}	$\frac{rad/sec^2}{rad/sec}$	-.73173	-.96002	-1.31158	-1.45996	-1.52219	-1.62003	-1.59067	-1.51570
$M_{\delta e}/I_{yy}$	$\frac{rad/sec^2}{in}$	.35447	.35364	.40144	.45022	.48135	.51572	.53335	.54565
$M_{\delta c}/I_{yy}$	$\frac{rad/sec^2}{in}$	-.04765	-.04252	.04556	.06776	.06725	.04707	.03948	.03505
$\delta_{e_{TR}}$	in	.66523	-.06503	-.23516	.28888	.77817	-.06119	.16392	.34298
$\delta_{c_{TR}}$	in	5.01959	4.47346	3.73135	3.51111	3.84917	4.67777	6.04983	8.02025

TABLE B-II.- LATERAL STABILITY DERIVATIVES AT FLIGHT CONDITION I

Forward Velocity	kts	0	20	40	60	80	100	120	140
Forward Velocity	ft/sec	0.0	33.76	67.52	101.28	135.04	168.80	202.56	236.32
Y_v/m	$\frac{ft/sec^2}{ft/sec}$	-.026638	-.05408	-.07986	-.11823	-.15121	-.18040	-.19766	-.23442
Y_p/m	$\frac{ft/sec^2}{rad/sec}$	-.76514	-.95618	-1.15981	-1.24824	-1.23341	-1.02295	-.76619	-.29372
Y_r/m	$\frac{ft/sec^2}{rad/sec}$	-.12517	-.18179	-.20082	-.12813	-.05819	.13380	.12514	.22125
$Y_{\delta a}/m$	$\frac{ft/sec^2}{in}$	.99794	.99700	.97673	.96426	.96955	.97123	1.01613	1.10225
$Y_{\delta r}/m$	$\frac{ft/sec^2}{in}$	.14652	.13634	.11652	.10583	.09849	.11641	.13883	.15262
L_v/I_{xx}	$\frac{rad/sec^2}{ft/sec}$	-.00778	-.01305	-.01388	-.01720	-.02442	-.03188	-.04724	-.05080
L_p/I_{xx}	$\frac{rad/sec^2}{rad/sec}$	-.50730	-.57483	-.64045	-.65271	-.62549	-.52243	-.41134	-.23476
L_r/I_{xx}	$\frac{rad/sec^2}{rad/sec}$	-.02297	-.04571	-.05943	-.02270	.01172	.09531	.11659	.19955
$L_{\delta a}/I_{xx}$	$\frac{rad/sec^2}{in}$	.46536	.46558	.45954	.45575	.45805	.45820	.47354	.50528
$L_{\delta r}/I_{xx}$	$\frac{rad/sec^2}{in}$	-.12638	-.13036	-.13422	-.13544	-.13910	-.13256	-.13248	-.14433
N_v/I_{zz}	$\frac{rad/sec^2}{ft/sec}$	.00013	.00037	-.00123	-.00290	-.00415	-.00536	-.00377	-.00060
N_p/I_{zz}	$\frac{rad/sec^2}{rad/sec}$	-.01831	-.02076	-.02598	-.03947	-.05344	-.06864	-.07797	-.07471
N_r/I_{zz}	$\frac{rad/sec^2}{rad/sec}$	-.05847	-.05450	-.04597	-.05020	-.05438	-.05078	-.08642	-.12617
$N_{\delta a}/I_{zz}$	$\frac{rad/sec^2}{in}$	.03001	.02923	.02764	.02663	.02633	.02696	.02857	.02970
$N_{\delta r}/I_{zz}$	$\frac{rad/sec^2}{in}$	.17584	.17578	.17261	.17032	.17141	.17146	.17933	.19536
$\delta_{a_{TR}}$	in	.12983	.08462	.09191	.13466	.17931	.29754	.44154	.49785
$\delta_{r_{TR}}$	in	-.17764	-.04701	-.08508	-.33705	-.61293	-.75397	-1.04713	-1.14123

APPENDIX C

The formal presentation of the wind model follows. Given the differential equation:

$$\dot{\Gamma} = -\beta_n \Gamma + \sigma_n \beta_n \sqrt{2}\, \zeta_n \tag{C1}$$

where $\beta_n > 0$ and ζ_n is white noise with a spectral density equal to one. It can easily be shown that the steady-state auto-correlation function is:

$$E(\Gamma(t)\Gamma(t+\tau)) = \sigma_n^2 \beta_n e^{-\beta_n |\tau|} \tag{C2}$$

If one wishes Γ to have a variance, ρ_n, and a correlation time, α_n, then:

$$\begin{aligned} \beta_n &= 1/\alpha_n \\ \sigma_n &= \sqrt{\alpha_n \rho_n} \end{aligned} \tag{C3}$$

To approximate this process on a digital computer, Eq. (C1) was time discretized and a white, gaussian-distributed sequence $[\zeta_n^n]$ was generated to provide a piecewise constant approximation to $\zeta_n(t)$. Under the assumption that the product of the discretization interval, Δ_n, and of β_n is small compared to unity, Eq. (C1) becomes:

$$\Gamma^{n+1} = (1-\Delta_n \beta_n)\Gamma^n + \sigma_n \beta_n \sqrt{2}\, \Delta_n \zeta_n^n \tag{C4}$$

where superscripts indicate time instants. Since $\zeta_n(t)$ is the formal derivative of a Wiener process, its integral must possess the same statistical properties as the Wiener process, that is:

$$\begin{aligned} \varepsilon\left(\int_0^t \zeta_n(\sigma)\, d\sigma\right) &= 0 \\ \varepsilon\left(\left[\int_0^t \zeta_n(\sigma)\, d\sigma\right]^2\right) &= |t| \end{aligned} \tag{C5}$$

The sequence $[\zeta_n^n]$ must be chosen such that

$$\varepsilon\left[\int_0^t \zeta_n^n \, d\sigma\right]^2 = \varepsilon\left[\sum_{i=1}^{t/\Delta_n} \sum_{j=1}^{t/\Delta_n} \zeta_n^i \, \zeta_n^j \, \Delta_n^2\right] = |t| \tag{C6}$$

Since $[\zeta_n^n]$ is white, equation (C6) becomes

$$\varepsilon\left[\int_0^t \zeta^n \, d\sigma\right]^2 = \text{var } (\zeta_n^2) \; \Delta_n \; |t| \tag{C7}$$

Upon comparing Eq. (C7) with Eq. (C6), it is found that

$$\text{VAR } (\zeta_n^n) = 1/\Delta_n \tag{C8}$$

is required to provide the desired noise sequence. Defining $[\zeta_n^n] = [\eta_n^n/\sqrt{\Delta_n}]$ where $[\eta_n^n]$ is a white, gaussianly distributed random sequence with zero mean and unit variance, causes Eq. (C4) to become

$$\Gamma^{n+1} = (1-\Delta_n\beta_n)\Gamma^n + \sigma_n\beta_n \sqrt{2\Delta_n} \; \eta_n^n \tag{C9}$$

The sequence (η_n^n) is generated by summing twelve samples from a normalized, uniform distribution in (0, 1) and then by subtracting off the mean value of the sum. The Central Limit Theorem states that the distribution of these sums will be approximately gaussian. The uniform distribution was generated by using a multiplicative, congruential random number generator tailored to the SDS 9300, which has a word length of 24 bits. The $[\eta_n^n]$ is given by

$$\Xi_{i+1}^n = 2899 * \Xi_i^n \pmod{2^{23}}$$

$$\text{with } \Xi_1^0 = 7$$

$$\eta^n = \sum_{i=1}^{12} 2^{-23} \, \Xi_i^n - 6 \qquad n = 0,1,2,\cdots$$

REFERENCES

1. Gracey, W., Sommer, R.W., Tibbs, D.F.: Evaluation of Cross-Pointer-Type Instrument Display in Landing Approaches with a Helicopter. NASA TN D-3677, Nov. 1966.

2. Garren, J.F., Kelly, J.R., Sommer, R.W.: VTOL Flight Investigation to Develop a Decelerating Instrument Approach Capability. Presented at the 1969 SAE National Aeronautics and Space Engineering and Manufacturing Meeting, SAE Report No. 690693, 1969.

3. Johnson, H.B., Oliver, F.J.B.: The Development and Testing of an Experimental Flight Director for Helicopters, Royal Aircraft Establishment Technical Note. IEE 11, Dec. 1962.

4. Bondurant, R.A.: VTOL IFR In-Flight Simulation. Proc. of the Twentieth National Aerospace Electronics Conference, sponsored by the IEEE, May 1968.

5. Advanced Flight Control System Concepts for VTOL Aircraft. TRECOM Technical Report 64-50, Oct. 1964.

6. Reeder, J.P.: V/STOL Aircraft Operation in the Terminal Area. Conference on Aircraft Operating Problems, NASA Langley Research Center, May 10-12, 1965, NASA SP-83.

7. Reeder, J.P.: The Impact of V/STOL Aircraft on Instrument Weather Operations. AGARD Report 485, Oct. 1964.

8. Litchford, G.B., Saganowich, J.T.: Helicopter Landing Systems. IEEE International Convention Record, vol. 15, 1967.

9. Computer Recommendations for an Automatic Approach and Landing System for V/STOL Aircraft. Vol. II: Equations, NASA CR 86174, June 1968.

10. Military Specification: Helicopter Flying and Ground Handling Qualities, General Requirements for MIL-H-8501A; Sept. 7, 1961.

11. Morrall, J.C.: The Role of the Pilot in All-Weather Operation. Royal Aircraft Establishment/England, Tech. Memo. BLEU 123, June 1966.

12. Skelton, G.B.: Investigation of the Effects of Gusts on V/STOL Craft in Transition and Hover. AFFDL-TR-68-83, March 1968.

13. Halaby, N.E.: All-Weather Operations-Progress and Challenges. Astronautics and Aeronautics, May 1968.

NASA-Langley, 1971 — 2 C-119